J Nanopart Res (2018) 20: 160
https://doi.org/10.1007/s11051-018-4235-1

REVIEW

Recent advances on Fe- and Mn-based cathode materials for lithium and sodium ion batteries

Xiaobo Zhu · Tongen Lin · Eric Manning · Yuancheng Zhang · Mengmeng Yu · Bin Zuo · Lianzhou Wang

Received: 18 January 2018 / Accepted: 23 April 2018 / Published online: 11 June 2018
© Springer Science+Business Media B.V., part of Springer Nature 2018

Abstract The ever-growing market of electrochemical energy storage impels the advances on cost-effective and environmentally friendly battery chemistries. Lithium-ion batteries (LIBs) are currently the most critical energy storage devices for a variety of applications, while sodium-ion batteries (SIBs) are expected to complement LIBs in large-scale applications. In respect to their constituent components, the cathode part is the most significant sector regarding weight fraction and cost. Therefore, the development of cathode materials based on Earth's abundant elements (Fe and Mn) largely determines the prospects of the batteries. Herein, we offer a comprehensive review of the up-to-date advances on Fe- and Mn-based cathode materials for LIBs and SIBs, highlighting some promising candidates, such as Li- and Mn-rich layered oxides, $LiNi_{0.5}Mn_{1.5}O_4$, $LiFe_{1-x}Mn_xPO_4$, $Na_xFe_yMn_{1-y}O_2$, $Na_4MnFe_2(PO_4)(P_2O_7)$, and Prussian blue analogs. Also, challenges and prospects are discussed to direct the possible development of cost-effective and high-performance cathode materials for future rechargeable batteries.

Keywords Cathode materials · Iron-based · Manganese-based · Lithium ion batteries · Sodium ion batteries · Energy storage

This article is part of the topical collection:
20th Anniversary Issue: From the editors

Nicola Pinna, Executive Editor, Mike Roco, Editor-in-Chief

X. Zhu · T. Lin · E. Manning · L. Wang (✉)
Nanomaterials Centre, School of Chemical Engineering and Australian Institute for Bioengineering and Nanotechnology, The University of Queensland, QLD, Brisbane 4072, Australia
e-mail: l.wang@uq.edu.au

E. Manning
Faculty of Engineering, University of Alberta, Edmonton, AB T6G 2R3, Canada

Y. Zhang · M. Yu · B. Zuo
Shandong Baoli Biomass Energy Corporate, Changan Group, Huanghe Road, Dongying 257067, People's Republic of China

Introduction

The demand for electrical energy storage is increasing exponentially along with the advancement of technologies and our ambition for clean and sustainable development. As a state-of-the-art energy storage system, lithium-ion batteries (LIBs) continue to power consumer electronics and are increasingly used in defense, automotive, and aerospace applications owing to their high energy density (Larcher and Tarascon 2015; Thackeray et al. 2012). Such penetration also raises the concern of lithium shortage. In this context, sodium-ion batteries (SIBs) have entered the spotlight due to having similar electrochemistry and a higher global abundance of Na (Slater et al. 2013; Yabuuchi et al. 2014b). Though it is hard for them to compete with LIBs in compact applications due to reduced energy density, SIBs are deemed as the most promising complements to LIBs for large-scale electrical storage applications (Palomares et al. 2012).

A typical LIB is an enclosed device consisting of a cathode, an anode, a separator, and an electrolyte. In respect to the manufacturing cost of a LIB (Fig. 1a), the cathode part accounts for the most significant share, 36% of the total cost, due to the high content of material required and costly constitution (Kim et al. 2014). Most cathode materials are compounds containing extractable Li and multivalent transition metal (TM) ions. For example, $LiCoO_2$ (LCO) is the first commercially successful cathode material and still the most commonly used one (Mizushima et al. 1980; Nitta et al. 2015), in which both Li and Co are non-abundant and expensive. However, the expense of the Co precursors is significantly higher than Li ones. Thus, switching from Li to Na is only expected to afford a 3.6 % cost reduction of cathode materials in the case of SIBs. Therefore, to improve the affordability and sustainability of the rechargeable batteries, it is essential to develop low-cost cathode materials incorporating earth abundant TM elements, preferably Fe and Mn (Fig. 1b, c), which primarily determine the scope and prospect of the rechargeable batteries (Larcher and Tarascon 2015).

Although both LIBs and SIBs should be directed to lower cost and higher performance, given the different application scenarios and development phases of LIBs and SIBs, the challenges existing in them still varies. In LIBs, Mn-based spinel $LiMn_2O_4$ (LMO) and Fe-based polyanionic $LiFePO_4$ (LFP) are progressively replacing LCO in some areas. However, both of them are restricted by lower galvanometric and volumetric energy densities compared with LCO (Zheng et al. 2017). Consequently, LFP and LMO are not capable of weight or size-sensitive applications including advanced portable devices and electrical vehicles (EVs). Therefore, a critical criterion for the development of future Fe- and Mn-based cathodes for LIBs is to achieve comparable or even higher energy densities. The energy density of cathode material is determined collectively by its Li storage capacity and discharge potential. In this regard, some high-capacity and high-voltage materials such as Li- and Mn-rich oxides, $LiNi_{0.5}Mn_{1.5}O_4$, and $LiFe_{1-x}Mn_xPO_4$ have attracted more attention. Meanwhile, candidates should also meet the requirements of rate capability, lifespan, and safety for practical applications.

Taking advantage of abundant Na sources, SIBs hold the promise to support large-scale energy storage applications, which is critical in harnessing intermittent renewable energies such as solar and wind power. An essential step to realizing large-scale SIB applications is the quest of suitable electrode materials that meet the long-term stability requirement and can deliver and accept large amounts of energy quickly. However, the radii of Na^+ (0.102 nm) is much larger compared to that of Li^+ (0.076 nm), posing considerable challenges of sluggish ion mobility and volumetric change of the hosts (Dai et al. 2017; Yabuuchi et al. 2014b). Direct analogs from LIB cathodes often result in continuous structural change and inferior kinetics (Berthelot et al. 2010; Tripathi et al. 2013). Therefore, many efforts have been made on crystal-structure engineering, nanostructuring, hybridization, etc. For example, the combinations of different polyanion groups such as $Na_4MnFe_2(PO_4)(P_2O_7)$ create new open crystal frameworks with feasible paths for Na^+ diffusion (Kim et al. 2016a).

Herein, this review summarizes the research advances on Fe- and Mn-based cathode materials for LIBs and SIBs, respectively, which are categorized into oxides, polyanion compounds, and hexacyanometalates (for SIBs). With a grasp of the inherent properties and up-to-date achievements of these candidates, especially high-energy LIB cathode candidates and highly stable SIB cathodes, we further discuss the impendent challenges and prospects in this field and put forward some insights into the opportunity of Fe- and Mn-based cathode materials. We hope that this review can inform readers of the rationality and priority of Fe- and Mn-based cathode materials as candidates for future LIBs and SIBs, and call for further efforts to fulfill this goal.

Fe- and Mn-based oxides as LIB cathodes

The introduction of LCO cathode has empowered the commercialization of the first LIB. LCO also guides the investigation of a family of α-$NaFeO_2$-type layered oxides $LiMO_2$, where M can be a TM or a mixture of several (Chen et al. 2016). As shown in Fig. 2a, they have a rhombohedral structure with a space group of R-3m, in which the M-O octahedral slabs and Li-O octahedral layers follow O3 stacking along the *c* axis. Though LCO has a high theoretical capacity of 282 mAh g^{-1}, the structure will undergo an irreversible phase transition when more than half of the Li ions are removed (Xia et al. 2007). Moreover, LCO also suffers from safety issues due to its thermal instability at the highly charged states (MacNeil et al. 2002). Therefore, motivation exists for Co to be replaced by abundant, inexpensive, and non-toxic transition metals.

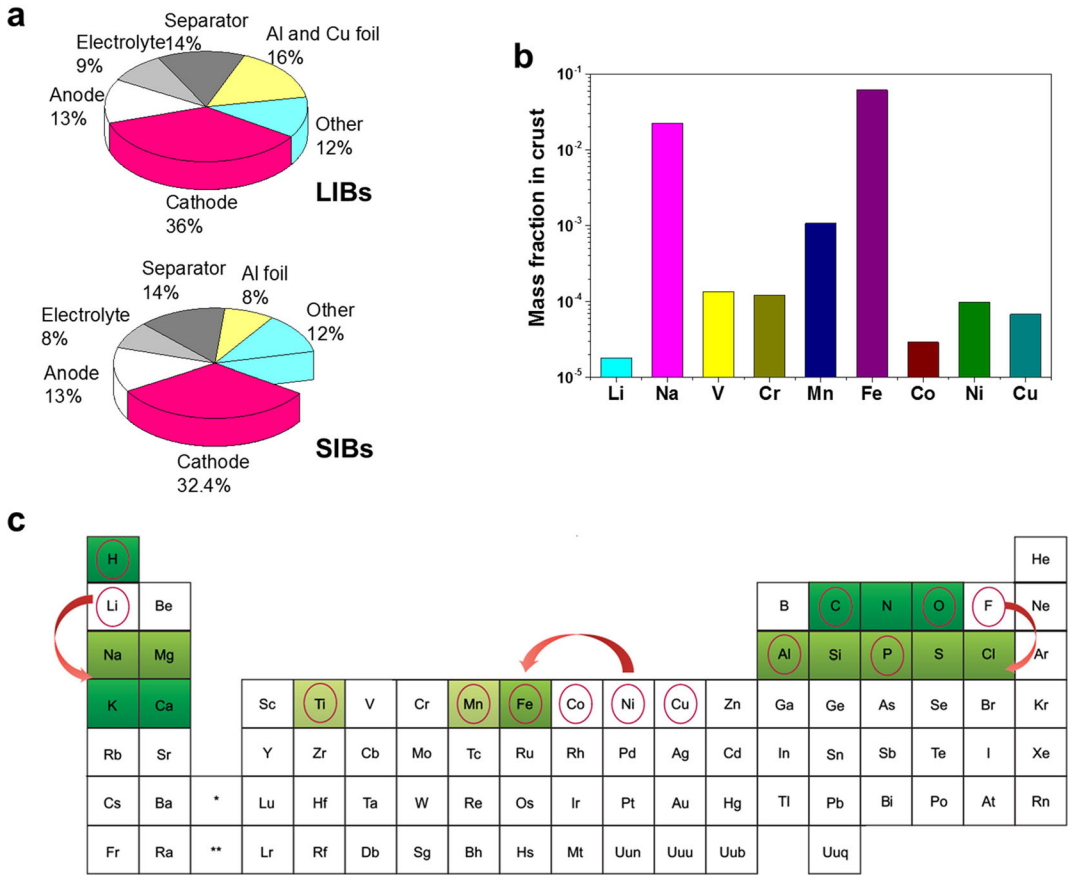

Fig. 1 **a** Constitutional costs for manufacturing a typical LIB and SIB. Values are from ref. (Kim et al. 2014). **b** Abundances of metal elementals involved in standard cathode materials. Values are taken from ref. (Nitta et al. 2015). **c** Sustainable (naturally recycled) elementals (shown in green) in the periodic table, in which main elements of current LIBs are circled in red. Reproduced from ref. (Larcher and Tarascon 2015)

$LiMnO_2$

After the success of LCO, researchers have made significant efforts to investigate the Mn-based structural analog of LCO (Fuchs and Kemmler-Sack 1994; Rossouw et al. 1993). However, layered O3-type $LiMnO_2$ is challenging to prepare due to its thermodynamic instability (Armstrong and Bruce 1996). Moreover, as the Mn ions in $LiMnO_2$ all present as Mn^{3+}, which is susceptible to Jahn–Teller distortion, rendering structural change and the disproportionation reaction to soluble Mn^{2+}. Such issues also haunt the thermodynamically favorable orthorhombic $LiMnO_2$ (Croguennec et al. 1997a; Davidson et al. 1995; He et al. 2010; Liu et al. 2007; Xiao et al. 2009). Therefore, to make cost-effective and environmentally friendly layered oxides, most of the research interest has been shifted to multi-metal constitution such as $LiNi_xMn_{1-x}O_2$ (Rossen et al. 1992) and $LiNi_xMn_yCo_{1-x-y}O_2$ (Shaju et al. 2002; Tsutomu and Yoshinari 2001) (NMC). For example, the existence of low valance Ni (Ni^{2+}) can reduce the proportion of Mn^{3+}. The synergistic contributions of various metals guarantee improved electrochemical performance, leading to the successful commercialization of NMC.

Mn-substituted $LiNi_xMn_{1-x}O_2$ has been initially designed to address the issues in $LiNiO_2$ (Chen et al. 2014; Ohzuku et al. 1993), which is hard to prepare due to the difficulties in controlling stoichiometry, Li/Ni ordering, and the oxidation state of Ni (Nitta et al. 1995; Rossen et al. 1992). In 2001, Ohzuku et al. prepared the isometric $LiNi_{0.5}Mn_{0.5}O_2$ cathode which maintained a discharge capacity of 150 mAh g^{-1} after 30 cycles. However, the binary $LiNi_{0.5}Mn_{0.5}O_2$ still suffers from problematic preparation and cation disordering that results in obstructive Li diffusion. In 2006, Kang et al. reported

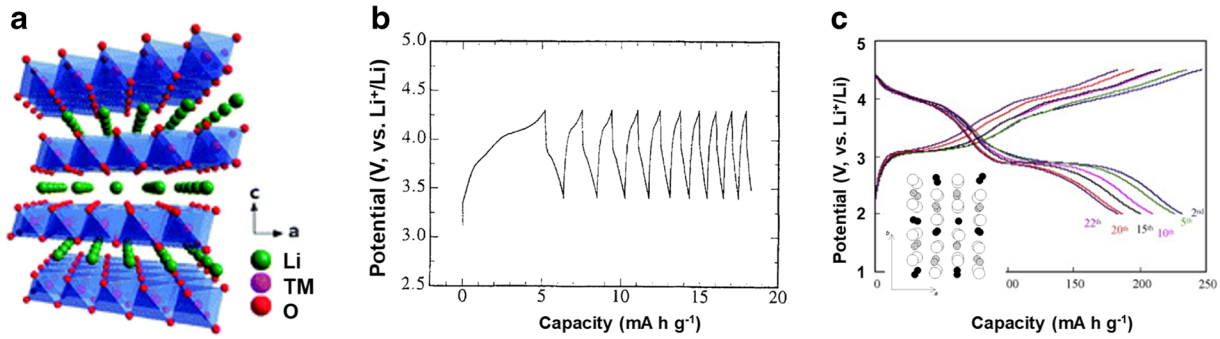

Fig. 2 **a** Crystal structure of layered $LiMO_2$. Reproduced from ref. (Chen et al. 2016) with permission. **b** Cycling profile of layered $LiMnO_2$. Reproduced from ref. (Armstrong and Bruce 1996) with permission. **c** Structural illustration and voltage profiles of orthorhombic $LiMnO_2$. Reproduced from ref. (Croguennec et al. 1997b) and ref. (He et al. 2010) with permissions

the use of an ion-exchange process to prepare high-quality $LiNi_{0.5}Mn_{0.5}O_2$ with very low little intralayer disordering, which could maintain a capacity of ~ 180 mAh g^{-1} even at a high rate of 6 °C (Kang et al. 2006). However, the extra cost from the method prevents it from practical application.

Meanwhile, researchers investigated the co-substitution of Co and Mn for better structural stability. In 2001, Ohzuku et al. reported the isometric $LiNi_{1/3}Mn_{1/3}Co_{1/3}O_2$ (NMC111) cathode, which demonstrated a rechargeable capacity of 150 mAh g^{-1} in 3.5–4.2 V or 200 mAh g^{-1} in 3.5–5.0 V (Tsutomu and Yoshinari 2001). The appreciable capacity and cycling stability of NMC soon attracted considerable interest from the science community as well as industry. It is widely recognized that high Ni content in the layered NMC as the active redox species contributes to a higher capacity but at the expense of safety and difficult preparation. High Mn content existing as inactive Mn^{4+} enhances the structural stability, and high Co content improves the rate performance and processing ability. As the NMC materials still consume Ni and Co largely, the next-generation cathodes should be Ni and Co poor or free materials.

$LiFeO_2$

In principle, the structure of $LiMO_2$ is dependent on the size of the M cation (Shirane et al. 1995). When Co is substituted by similarly smaller M cations, such as V^{3+}, Cr^{3+}, Ni^{3+}, the layered rock-salt structure can be easily preserved, whereas the same structure can hardly be inherited when accommodating Fe^{3+} with much larger size. In fact, the structural complexity of $LiFeO_2$ is much higher than other $LiMO_2$. Around ten phases of $LiFeO_2$ have been reported under different preparation conditions (Catti and Montero-Campillo 2011). Those include disordered rock salt α phase and its derivate (Tabuchi et al. 1995), layered O3 phase (Shirane et al. 1995), corrugated layered phase (orthorhombic), goethite-type (orthorhombic) (Sakurai et al. 1997), β-$NaFeO_2$-type (orthorhombic) (Armstrong et al. 2008), and hollandite-type (tetragonal) (Matsumura et al. 2002).

The electrochemical performance of $LiFeO_2$ is strongly related to the crystal structure, which decides the Li^+ pathway during the reaction. For example, bulk α-$LiFeO_2$ obtained by solid state reaction is found to be electrochemically inactive as the iron ions block the Li pathway in the disordered structure (Li et al. 2011). However, the reactivity problem has been solved by tailoring the particles into nanoscale. As a result, α-$LiFeO_2$ with particle size over 50 nm demonstrates a discharge capacity up to 150 mAh g^{-1} in the 50th cycle (Morales and Santos-Peña 2007). Another nano-α-$LiFeO_2$ also achieves similar results (Liu et al. 2016b). Carbon modification can further enhance the reactivity, and nanocrystalline porous α-$LiFeO_2$–C composite can deliver 230 mAh g^{-1} at 0.5 °C after 100 cycles (Rahman et al. 2011).

Though electrochemical activities have repeatedly been demonstrated for $LiFeO_2$ with different phases, a critical issue is the abnormal redox reaction. Different from the reversible Li^+ intercalation/deintercalation in LCO on the basis of Co^{3+}/Co^{4+}, $LiFeO_2$ cannot work on the Fe^{3+}/Fe^{4+} redox couple, as the Fe^{3+} 3*d*-orbital is strongly hybridized with the oxygen 2*p* orbital in the $LiFeO_2$, the first delithation process will trigger the oxygen removal instead of the oxidation of Fe^{3+} (Yabuuchi et al. 2012a). Hirayama et al. studied the structure and electrode reactions of layered $LiFeO_2$

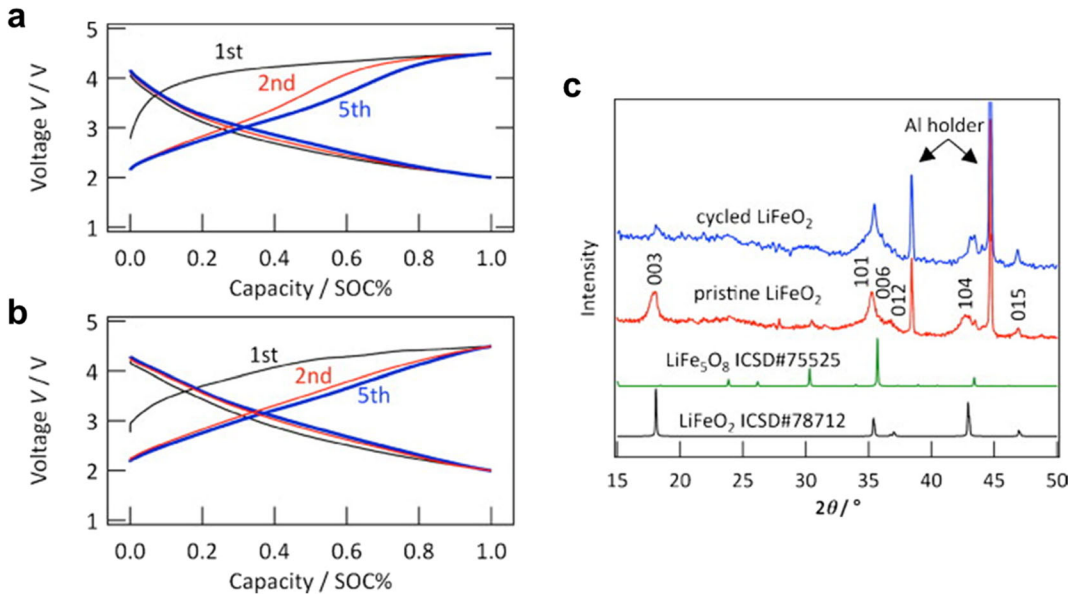

Fig. 3 **a**, **b** Charge/discharge curves of $LiFeO_2$ (**a**) and oxygen-deficient $LiFeO_{2-x}$ (**b**). **c** XRD pattern of cycled O3-type $LiFeO_2$. Reproduced from ref. (Hirayama et al. 2011) with permission

(Hirayama et al. 2011). As shown in Fig. 3, large voltage hysteresis is identified in the first cycle of $LiFeO_2$, and the following profiles are similar with initially reduced $LiFeO_{2-x}$. X-ray diffraction (XRD) patterns also clearly revealed the degradation of the structure. To address the intrinsic redox issue, the possible route is to incorporate other materials to form solid solutions or nanocomposites. For example, $LiFeO_2$-Li_2MnO_3 solid solution ($Li_{1+x}(Fe_yMn_{1-y})_{1-x}O_2$) with optimized Fe content ($0.2 < y < 0.4$) is found to show high initial discharge capacity (240–300 mAh g^{-1}) under 40 mA g^{-1} (Tabuchi et al. 2010).

Li_2MnO_3-based oxides

With the low-cost constitution and very high deliverable capacities exceeding 250 mAh g^{-1}, Li_2MnO_3-based layered oxides are considered as one of the most promising cathode candidates for next-generation LIBs (Thackeray et al. 2007; Yabuuchi et al. 2011). Bare Li_2MnO_3 possesses a layered structure that can be represented in conventional-layered $LiMO_2$ notation as $Li(Li_{1/3}Mn_{2/3})O_2$, in which Li^+ has substituted 1/3 of the Mn ions in the transition metal layers. Such composition change also results in a symmetry of monoclinic C2/m, and all the Mn are oxidized to the more stable valance of 4+. Commonly, the Li_2MnO_3 is incorporated with traditional layered $LiMO_2$ to form a class of Li- and Mn-rich layered oxides (LMRs), which is deemed as either a single-phase solid solution (Jarvis et al. 2012; Koga et al. 2012; Shukla et al. 2015) expressed as $Li(Li_{1/3-2x/3}M_xMn_{2/3-x/3})O_2$ or a structurally integrated $xLi_2MnO_3{\cdot}(1\text{-}x)LiMO_2$ composite (Amalraj et al. 2013; Gu et al. 2013; Thackeray et al. 2007; Yu et al. 2013). To our best knowledge, the crystal structure may vary in different samples, depending on the preparation method, constitution, etc. Apart from the disputes on the structure model, it is widely acknowledged that a range of technical challenges including large initial irreversible capacity, voltage and capacity decay, and poor rate capability must be solved before their application (Fig. 4).

The electrochemical properties of LMRs are highly associated with a unique activation behavior. The typical first charge profile involves several steps (Erickson et al. 2017). Below 4.4 V is a Li extraction from the Li-layer, which requires oxidizable TM ions such as Ni^{2+} and Co^{3+}. Next is the activation of initially inactive Li_2MnO_3, during which the removal of Li+ from the TM layers is accompanied with the oxidation of O^{2-}, leading to the formation of oxygen vacancies and structural change (Armstrong et al. 2006). Synchrotron XRD patterns disclosed the loss of in-plane superstructure peaks, indicating the irreversible structural change, which answers the voltage hysteresis and large initial irreversible capacity (Gent et al. 2017). Wang's group reported the critical role in the activation process. For a low Ni-doped LMR

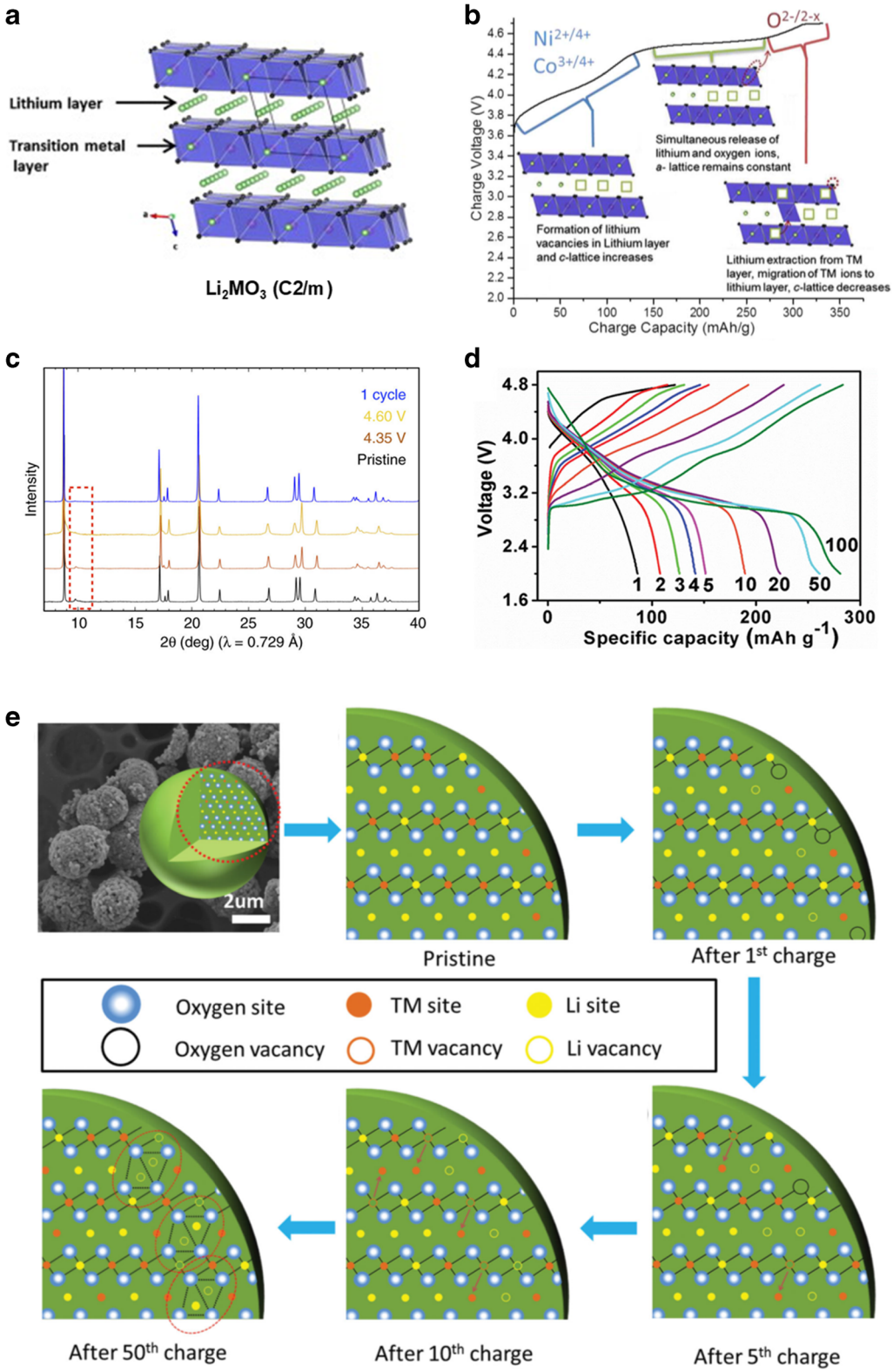
a
Lithium layer
Transition metal layer
Li2MO3 (C2/m)
b
Ni2+/4+
Co3+/4+
O2-/2-x
Charge Voltage (V)
Charge Capacity (mAh/g)
Simultaneous release of lithium and oxygen ions, a- lattice remains constant
Formation of lithium vacancies in Lithium layer and c-lattice increases
Lithium extraction from TM layer, migration of TM ions to lithium layer, c-lattice decreases
c
1 cycle
4.60 V
4.35 V
Pristine
Intensity
2θ (deg) (λ = 0.729 Å)
d
Voltage (V)
Specific capacity (mAh g-1)
1 2 3 4 5 10 20 50 100
e
2um
Pristine
After 1st charge
Oxygen site
Oxygen vacancy
TM site
TM vacancy
Li site
Li vacancy
After 5th charge
After 10th charge
After 50th charge

◀ **Fig. 4** **a** Crystal structure of monoclinic Li_2MO_3. Reproduced from ref. (Mohanty et al. 2013) with permission. **b** Charge voltage profile of a model LMR, $0.35LiMn_2O_3{\cdot}0.65LiMn_{0.45}Ni_{0.35}Co_{0.20}O_2$ with the illustration of structure evolution. Reproduced from ref. (Erickson et al. 2017) with permission. **c** Synchrotron XRD patterns over the first cycle showing the loss of in-plane superstructure peaks. Reproduced from ref. (Gent et al. 2017) with permission. **d**, **e** Our previous results and understandings of the activation process on the basis of $Li_{1.87}Mn_{0.94}Ni_{0.19}O_3$. Reproduced from ref. (Ye et al. 2015a) with permission

material, $Li_{1.87}Mn_{0.94}Ni_{0.19}O_3$, the Li_2MnO_3 activation process took dozens of cycles (Fig. 1d). By combining the electrochemical measurements with material characterisation including in-situ XRD and high-angle annular-dark-field scanning transmission electron microscopy (HAADF-STEM) observation, it was unveiled that the oxygen release reaction is completed in first five cycles while the Li and TM ions from TM layers migrate gradually to the Li layers, leading to a stepwise capacity increase (Ye et al. 2015a). The stepwise capacity increase can also be controlled by tuning the Ni or Co doping, which also profoundly influences the rate capability and cycling performance (Ye et al. 2014a, b, 2015b). Our studies shed light on the compositional design for high-performance LMRs.

As a promising cathode candidate that has been under the spotlight in past years, extensive work has been conducted to understand the local crystal structure, structural evolution, electrochemical behavior of LMRs, and to engineer the electrode materials for better performance. The history and progress have also been summarized elsewhere (Erickson et al. 2017; Hy et al. 2016; Manthiram et al. 2016; Zheng et al. 2017). In the pursuit of commercial application, the major obstacles including voltage and capacity decay over cycling, initial irreversible capacity, poor rate capability, and low volumetric energy density still need to be overcome.

$LiMn_2O_4$

Spinel $LiMn_2O_4$ is another classic cathode material for LIBs, of which Thackeray et al. have studied the lithium insertion/deinsertion properties since the 1980s (Thackeray et al. 1983, 1984). Different from the layered structure, Li ions in the spinel structure occupy 1/8 tetrahedral sites, and the MnO_6 octahedrons form a three-dimensional (3D) framework, leaving vacant tetrahedral and octahedral interstitial sites for the highly efficient diffusion of Li^+ (Fig. 5a). Even though the low concentration of Li ions in the spinel body (Li/Mn = 1:2) results in only half of the theoretical specific capacity (146 mAh g^{-1}) of layered $LiMO_2$, attributing to the low-cost, stable, and kinetic Mn-based 3D spinel framework, $LiMn_2O_4$ has progressively substituted LCO in some large-scale and high-power applications. Another pronounced feature from the spinel configuration is the flat working voltage plateau at 4.0 V. In contrast, layered structured cathodes display sloping potential profiles and significantly lower potentials based on the same Mn^{3+}/Mn^{4+} redox couple. As an explanation, the 3D spinel framework experiences negligible structural distortion during the insertion/deinsertion of Li ions, thereby displaying an almost constant electrochemical potential due to the consistent site energy. However, the layered structures are greatly distorted, resulting in the gradual change in site energy and hence sloping potential profiles for the insertion of Li-ions. The Li ions in the spinel structure are located in the tetrahedrons, experiencing less repulsive forces from the local environment compared with the Li ions in the octahedrons of layered oxides, and the reduced site energy contributes to a higher potential (Liu et al. 2016a).

Apart from the relatively low energy density, the other most claimed issue is the limited cycle life of $LiMn_2O_4$ due to Mn ions' dissolution, especially under elevated temperatures (Jang et al. 1996; Xia et al. 1997). Previously, the cause of the degradation was ascribed to the dissolution of Mn^{2+} ions, originating from the disproportionation of Mn^{3+} ions $LiMn_2O_4$ ($2Mn^{3+} \leftrightarrows Mn^{2+} + Mn^{4+}$) (Gummow et al. 1994; Jang et al. 1996; Xia et al. 1997). However, a recent combined analysis of electron paramagnetic resonance and inductively coupled plasma spectroscopy data disclosed that Mn^{3+} is the dominant dissolved Mn cation in $LiPF_6$-based organic electrolytes, and the Mn^{3+} can stably exist in the electrolyte instead of suffering disproportionation (Banerjee et al. 2017). Even though the metal dissolution is not negligible and haunts all the metal oxides, the practical cycling performance depends on its microstructure and physico-chemical properties. In general, hierarchical microstructures are considered as optimal choices, which can shorten the ion diffusion pathway compared with bulk materials. Meanwhile, in contrast to nanosized particles, the primary micron particles can be densely packed for high volumetric energy density and show better structural integrity over repeated charge/discharge cycles (Zhou et al. 2017). For example, as shown in Fig. 5b–e, Lee et al. recently reported densely

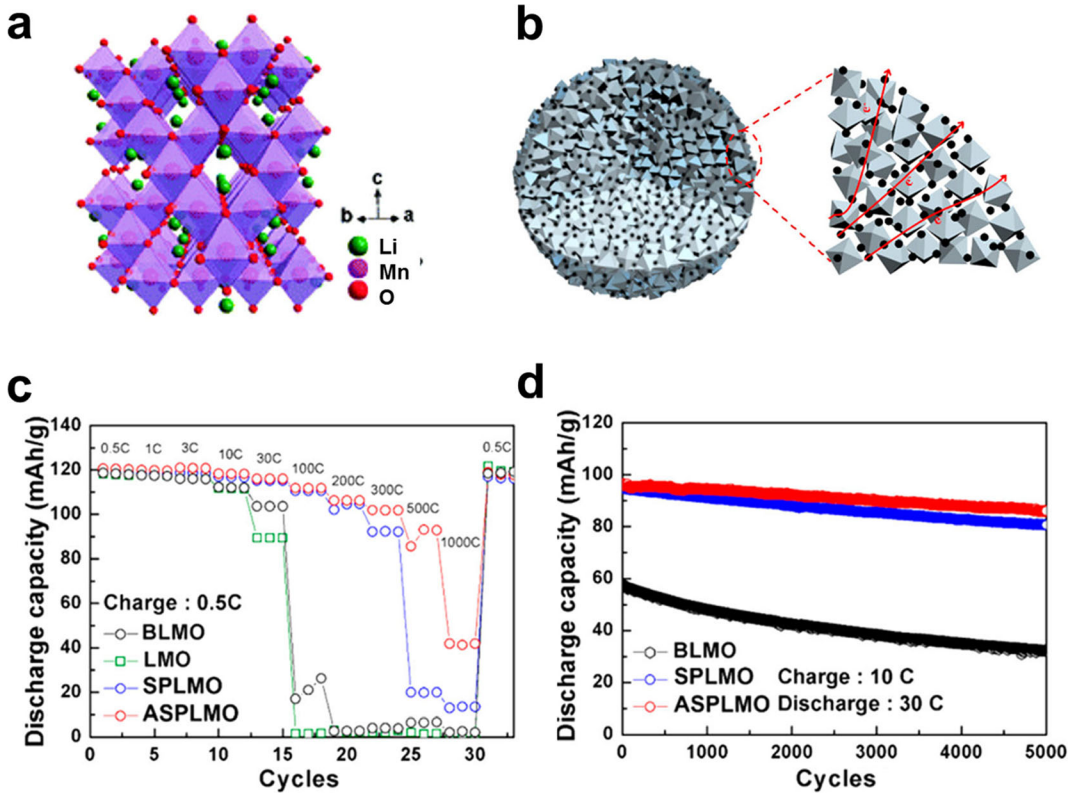

Fig. 5 **a** Crystal structure of spinel $LiMn_2O_4$. Reproduced from ref. (Chen et al. 2016) with permission. **b**–**e** Schematic diagram of the composites and the corresponding electrochemical performance. Reproduced from ref. (Lee et al. 2017) with permission

packed composites composed of carbon coated nanosized $Li_{1.015}Al_{0.06}Mn_{1.925}O_4$, maintained 84.5% of the initial capacity over 5000 cycles (Lee et al. 2017).

$LiNi_{0.5}Mn_{1.5}O_4$

Substitution of Mn in $LiMn_2O_4$ by low-valance metal ions (Co^{3+} (Kawai et al. 1998), Cr^{3+} (Sigala et al. 1995), Ni^{2+} (Zhong et al. 1997), Fe^{3+} (Amine et al. 1997), Cu^{2+} (Ein-Eli et al. 1998), etc.) was initially designed to enhance the cycling stability by elevating the valance of Mn ions. Among the doped spinels, $LiNi_{0.5}Mn_{1.5}O_4$ (LNMO) surprisingly displays one dominant plateau at around 4.7 V along with good electrochemical activity, thus presenting it as the most attractive spinel cathode for high-energy and high-power densities (Ohzuku et al. 1999). The massive substitution of Mn by 1/4 Ni adds complexity to the spinel structure, which is divided into two different symmetries: Fd-3m and $P4_332$. The former one is isostructural to $LiMn_2O_4$ with Ni and Mn ions randomly distributed in the 16d octahedral sites, named the disordered phase. The later one has distinct 4a and 12d sites to accommodate Ni and Mn ions, known as an ordered phase (Kim et al. 2004; Liu et al. 2012a). It is accepted that oxygen stoichiometry plays a leading role to determine the phase. In an oxygen-stoichiometric LNMO, all the Mn ions are Mn^{4+} and inclined to occupy distinct sites with Ni^{2+}. The existence of oxygen vacancies can bring about a fraction of the Mn^{3+} ions, leading to a Ni/Mn disordered phase (Kim et al. 2004; Wang et al. 2011b). Many reports have shown the disordered LNMO to have better electrochemical performance due to the more efficient Li^+ diffusion and better conductivity of Mn^{3+} (Jin et al. 2012; Kim et al. 2004; Wang et al. 2011b; Xiao et al. 2012). However, it also plausible to achieve high rate performance on the basis of an ordered phase (Ma et al. 2010; Zhang et al. 2013b). Therefore, more experimental and computational studies are required to understand the correlation between electrochemical performance and structural properties better.

Previously, with the aid of high-resolution transmission electron microscope (HR-TEM) imaging and energy-dispersive X-ray spectroscopy (EDS) elemental scanning, we observed minor $P4_332$ phase on the edge

of Fd-3m body coupled with the different Mn/Ni ratio in the naturally cooled sample (Fig. 6c). As shown in Fig. 6d, both the samples delivered favorable rate and cycling performances. The role of the crystal phase may be eclipsed by other factors (Zhu et al. 2014a). The physical morphology of LNMO which profoundly influences its performance (Yang et al. 2013; Yi et al. 2016; Zhang et al. 2013a; Zhou et al. 2012; Zhu et al. 2014b). In another study, we designed two types of porous LNMO microspheres, and it was surprisingly found that pore diameter shows a profound influence toward the rate capability. The LNMO microspheres with larger pores achieved a discharge capacity of 101.7 mAh g^{-1} even at 50 °C (Zhu et al. 2014b). This would inspire the design of high-performance cathode materials via refined control of physical parameters.

Perhaps the biggest barrier preventing LNMO from the practical application is the lack of long-cycling reliability. LNMO was initially introduced to prolong the cyclability of primary $LiMn_2O_4$ spinel. However, the exploitation of high-potential Ni^{2+}/Ni^{4+} redox leads to adverse cycling performance, as it is largely below the highest occupied molecular orbital (HOMO) of current electrolytes. Some investigators suggested the Mn^{4+} in the ordered phase can stabilise the electrode for long cycles (Zhang et al. 2013b). However, this hypothesis was not supported by any experimental and computational evidences. On the contrary, Talyosef et al. identified the dissolution of manganese and nickel and reduction of Mn^{2+} and Ni^{2+} on the lithium counter electrode by electrolyte and electrode analyses (Talyosef et al. 2005). X-ray absorption and optical fluorescence spectroscopy and imaging analyses conducted by Jarry et al. also confirmed the formation of fluorescent Ni^{2+} and $Mn^{2+/3+}$ complexes with β-diketonate ligands and Ni^{2+} and Mn^{3+} oxalates and carbonates, accompanying the oxidation of electrolyte (Jarry et al. 2015). The problematic Ni^{2+}/Ni^{4+} redox is also reflected in the electrochemical process. Song et al. investigated a series of spinel cathodes with compositions of $LiNi_{0.5-x}Mn_{1.5+x}O_4$ ($x = 0$, 0.05, and 0.08) and found the removal of the Ni^{4+}/Ni^{2+} redox reactions from the surface stabilizes the electrochemical performance at 55 °C. Doping with alien ions and surface coating are widely used strategies to improve the cyclability of cathode materials, which have also been extensively studied on LNMO. In general, elemental doping aims at improving the electronic conductivity of LNMO by altering the conduction band of the whole bulk, whereas the goal of the surface coating is to reduce the side reactions by creating artificial electrode/electrolyte interfaces. A wide variety of doping elementals (e.g., Na^+, Mg^{2+}, Cu^{2+}, Zn^{2+}, Al^{3+}, Cr^{3+}, Co^{3+}, Ti^{4+}, F^-) and coating layers (e.g., carbon, Ag, ZnO, CuO, Al_2O_3, TiO_2, ZrO_2, Li_3PO_4, Al_3PO_4, $LiFePO_4$) have been exerted on LNMO and proved effective for enhanced stability, which have been summarised elsewhere (Xu et al. 2017b; Yi et al. 2016; Yi et al. 2011). However, it should be noted that there is a lack of long cycling results (over 1000 cycles). As pristine LNMO can also stand for hundreds of cycles (Zhang et al. 2013b), the modifications will only be attractive if substantial improvements are achieved with an acceptable extra cost on materials and processing. This may rely on the introduction of new strategies or techniques. Apart from electrode engineering, the development of better electrolytes may provide a more effective solution. As shown in Fig. 6e, f, Li et al. reported the use of the lithium phosphorus oxynitride solid electrolyte, which enables exceptional capacity retention of 90% over 10,000 cycles (Li et al. 2015b). Such high capacity retention demonstrates the critical role of the solid electrolyte in supporting high-voltage batteries.

Fe- and Mn-based polyanion compounds as LIB cathodes

Represented by $LiFePO_4$, polyanion cathode materials are typically 3D structured compounds constructed by corner- and/or edge-shared M-O and X-O (X = P, S, As, Mo, or W) polyhedrons. These frameworks afford much better structural stability toward lithium (de)insertion compared with layered oxides, and the covalently bonded oxygen atoms prevent the oxygen loss that haunts lithium metal oxides. Also, the strong X-O bond can pull some charge density out of M–O bonds, and as a result, the M-O bond exhibits increased ionicity, leading to higher redox potential as a result of the inductive effect (Gong and Yang 2011; Masquelier and Croguennec 2013).

Fe- and Mn-based phosphates

Olivine $LiFePO_4$ (LFP) is the most successful polyanion cathode material, attributing to its low-cost and non-toxic constitution, appreciable capacity (*ca.* 170 mAh g^{-1}) and excellent thermal and

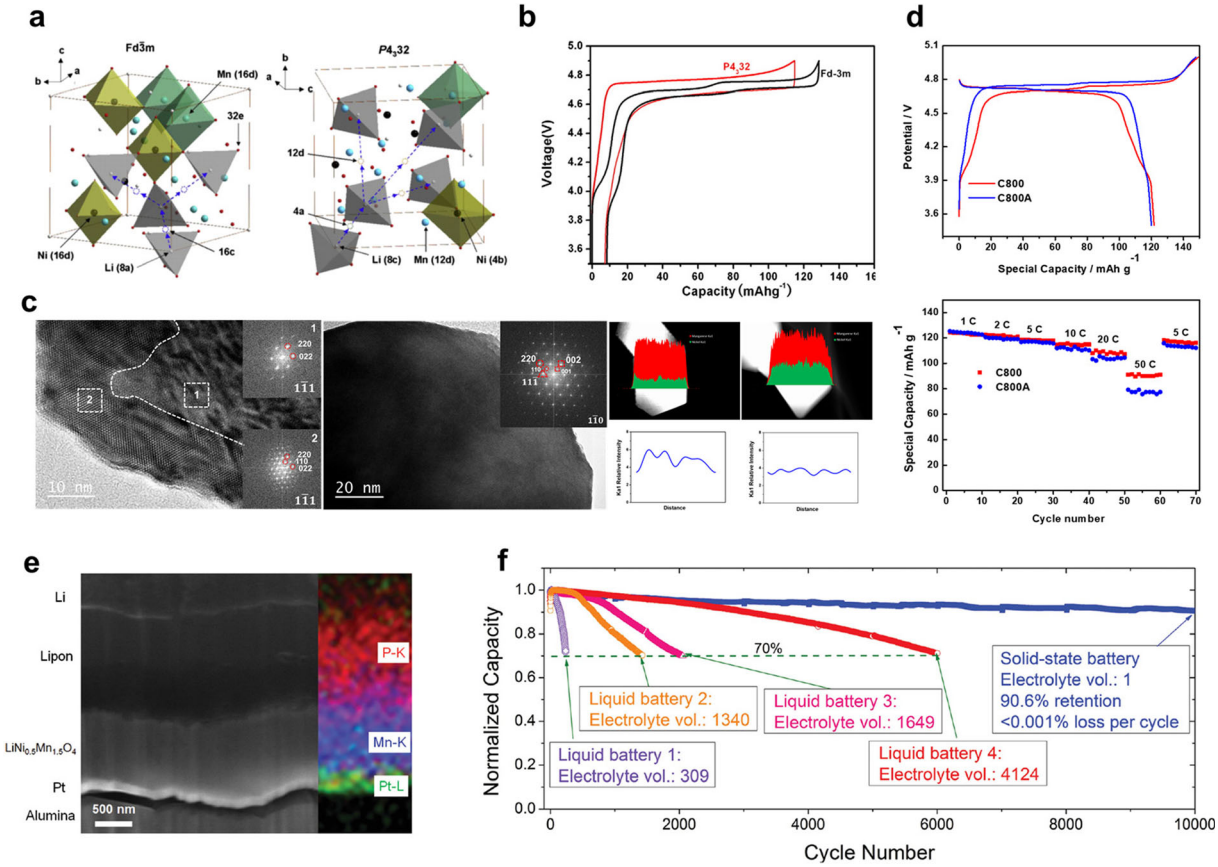

Fig. 6 **a** Comparison of the two structural configurations in LNMO. Reproduced from ref. (Liu et al. 2012a) with permission. **b** Typical charge/discharge curves of LNMO with the two phases. Reproduced from ref. (Wang et al. 2011b) with permission. **c**, **d** Structural characteristics and electrochemical properties on the basis of our prepared samples. **e**, **f** Outstanding capacity retention achieved by using lithium phosphorus oxynitride solid electrolyte. Reproduced from ref. (Li et al. 2015b) with permission

structural stability. The key drawbacks of $LiFePO_4$ are inferior electric conductivity (*ca.* 10^{-9} S cm^{-1}), the selective one-dimensional (1D) lithium pathway (Fig. 7a), and low gravimetric and volumetric energy densities. Intensive studies in the last 20 years have effectively addressed the kinetic issues by size tailoring, crystal facet controlling, bulk doping, and surface conducting modification. In light of the 1D lithium ion pathway along [010], constructing nanostructures, especially 2D nanosheets with exposed (010) facets and shortened diffusion length, is an effective solution (Zhao et al. 2014). Surface modification with conductive layers, mainly carbonaceous materials, is widely used to improve the conductivity. However, common procedures easily result in uneven and/or incompact coating layers due to the lack of affinity between the two substances. Constructing high-quality coating layers requires new feasible strategies. For example, Paolella et al. reported the use of $LiPF_6$ treatment to make LFP nanocrystals hydrophilic, thereby enabling carbon coating uniformly (Paolella et al. 2014). Compared with surface modification, the improvement made by tuning fundamental crystal chemistry is more appealing, as it is a uniform melioration of the lattice electronic and/or ionic conductivity without the penalty of energy densities from inactive additives. For example, Chung et al. combined cation non-stoichiometry with solid-solution doping to dramatically improve the electronic conductivity of LFP to $> 10^{-2}$ S cm^{-1}, resulting in markedly improved rate capability (Chung et al. 2002). As shown in Fig. 7b, Kang et al. also reported enhanced fast charging capability by an off-stoichiometric $LiFe_{0.9}P_{0.95}O_{4-\delta}$ (Kang and Ceder 2009). Recently, Naoi et al. achieved ultrafast charge/discharge of up to

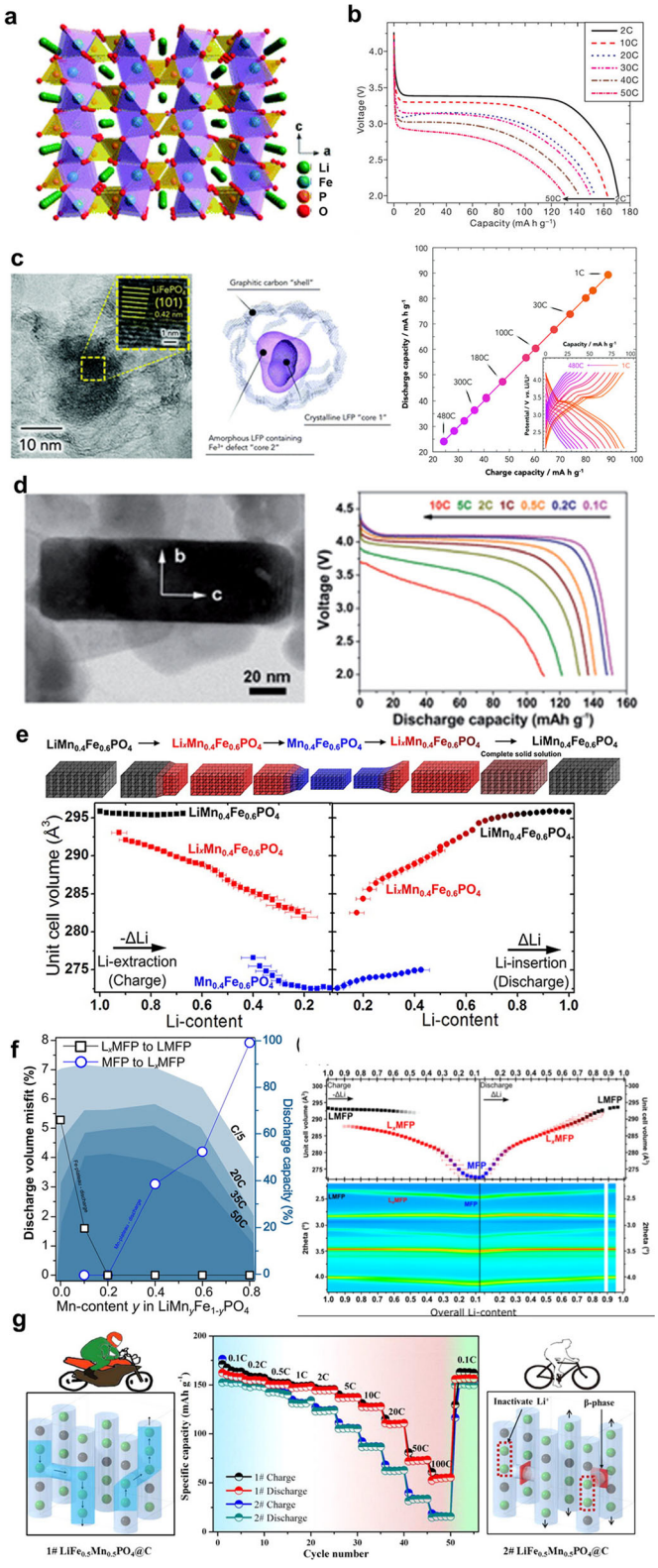

Fig. 7 **a** Crystal structure of spinel $LiMn_2O_4$. Reproduced from ref. (Chen et al. 2016) with permission. **b** High-rate discharge capability of $LiFe_{0.9}P_{0.95}O_{4-\delta}$. Reproduced from ref. (Kang and Ceder 2009) with permission. **c** Structural and electrochemical properties of a core-shell LFP nanocomposites. Reproduced from ref. (Naoi et al. 2016) with permission. **d** Morphology and discharge curves of LMO nanoparticles. Reproduced with permission (Hong et al. 2015). **e** Phase transformation diagram of $LiMn_{0.6}Fe_{0.4}PO_4$ over the extraction/insertion of Li ions. Reproduced from ref. (Ravnsbæk et al. 2014) with permission. **f** Phase transformation strain as a function of the Mn content in LFMP, and a special case of $LiMn_{0.2}Fe_{0.8}PO_4$ with no misfit strain. Reproduced from ref. (Ravnsbæk et al. 2016) with permission. **g** $LiMn_{0.5}Fe_{0.5}PO_4$ nanocrystals with different Fe-Li antisite defects showing distinct rate performance. Reproduced from ref. (Hu et al. 2017) with permission

480 °C by developing ultra-small core-shell nanocomposites (Naoi et al. 2016). The charge/discharge curves are dominated by the sloping pseudocapacitive behavior (Fig. 7c), and the rate capability is generated at the large expense of energy density.

The gravimetric and volumetric energy densities are restricted from the essential redox reaction and atom density in the crystal structure. Even though the inductive effect from the PO_4^{3-} elevates the Fe^{2+}/Fe^{3+} redox to 3.4 V, much higher than that in $LiFeO_2$, it is still considerably lower than 4 V-class $LiCoO_2$ and $LiMn_2O_4$. In the pursuit of high energy density, there is motivation to replace Fe with other transition metals, mainly Mn, Co, Ni to attain higher potentials. Among them, Co and Ni are not abundant elements, and the very high potentials of $LiCoPO_4$ and $LiNiPO_4$ at 4.8 and 5.1 V inhibit the research due to severe side reactions with commonly used electrolytes. $LiMnPO_4$ (LMP), on the other hand, is environmentally friendly and operates at a moderately high potential of 4.1 V, which enables a theoretical energy density of 697 W h kg^{-1}, 20% higher than that of LFP. However, the pathway for switching from Fe to Mn is unsatisfactory due to the sluggish kinetics of LMP (Delacourt et al. 2004). The origin of the depressed kinetics is ascribed to the small polaronic conductivity of Jahn–Teller active Mn^{3+} (Martha et al. 2009b). It not only leads to extremely low electronic (< 10^{-10} S cm^{-1}) and lithium ion conductivities (< 10^{-16} cm^2 s^{-1}), but also triggers the large lattice misfit between the delithiated and lithiated phases (6.5% volume misfit for LFP, 11.6% for LMP), resulting in inferior boundary mobility (Chen et al. 2011; Delacourt et al. 2005; Li et al. 2002; Meethong et al. 2008; Nie et al. 2010; Norberg and Kostecki 2012; Ong et al. 2011; Zhou et al. 2004). In search of better kinetics, many attempts have been reported on confining particle size and/or conductive modification (Barpanda et al. 2011; Guo et al. 2014a; Hong et al. 2015; Oh et al. 2010; Pivko et al. 2012; Qin et al. 2012; Wang et al. 2017; Yoo et al. 2011). As shown in Fig. 7d, Hong et al. prepared carbon-coated LMP nanorods, which showcased a high reversible capacity of 168 and 110 mAh g^{-1} at 0.05 and 10 °C, respectively, and capacity retention of 94.5% after 100 cycles at 0.5 °C (Hong et al. 2015).

Another effective approach to boost the kinetics of LMP is Fe-substitution. The as-formed $LiFe_{1-x}Mn_xPO_4$ solid solutions (LFMP) combines the dynamics of LFP and high energy density of LMP, and they are considered as the second-generation olivine cathode materials, which have received much attention from investigators (Kim et al. 2016b; Li et al. 2013; Martha et al. 2009a; Wang et al. 2011a; Yan et al. 2015; Yang et al. 2015c). Yamada et al. (Yamada et al. 2001) and Ravnsbæk et al. (Ravnsbæk et al. 2014) disclosed a different phase transformation mechanism of $LiMn_{0.6}Fe_{0.4}PO_4$ over the extraction/insertion of Li ions, which possesses an extended solid-solution region, different from the two-phase mechanism of LFP (Fig. 7e). Ravnsbæk et al. further investigated the phase transformation strain as a function of the Mn content in LFMP, and disclosed a direct negative influence of volume misfit toward electrode kinetics. Figure 7f demonstrates that $LiMn_{0.2}Fe_{0.8}PO_4$ with no misfit strain showed the best rate capability (Ravnsbæk et al. 2016). A range of in-situ electrochemical and material analyses conducted on Mn-rich LFMP ($LiMn_{0.8}Fe_{0.2}PO_4$) revealed that the Mn redox reaction is the kinetic bottleneck of LFMP, which triggers the poor apparent Li^+ diffusivity (Wi et al. 2017a, b). However, current studies on achieving the appreciable performance of LFMP still focused on nanostructuring and carbon modification, which raise the concern of low volumetric density and increased costs. For example, Kim et al. synthesized reduced graphene oxide (rGO)-modified $LiMn_{0.75}Fe_{0.25}PO_4$ microspheres, which showed 161 and 90 mAh g^{-1} at 0.05 and 60 °C, respectively. The claimed "high" tap density (1.1 g cm^{-3}), far lower than the practical standard of ca. 3 g cm^{-3}. Pan et al. reported $LiMn_{0.5}Fe_{0.5}PO_4$ nanocrystals with tuned Fe-Li antisite defects which also showed impressive rate capacities (Fig. 7g) (Hu et al. 2017). Therefore, the future successes of LMP and LFMP still await the achievements of reasonable kinetics without the compromise of volumetric energy density and processing cost.

Apart from the olivine-type structure, the lithium metal phosphates can also exist as NASICON, anti-NASICON, alluaudite, pyrophosphate, tavorite, and even amorphous phases with varied composition (Masquelier and Croguennec 2013). However, these phases largely eclipsed by $LiMn_xFe_{1-x}PO_4$ regarding practical energy (capacity and potential) density and power density.

Fe- and Mn-based silicates

Encouraged by the success of phosphate, other polyanion compounds are successively explored to function as cathode materials for LIBs. Particularly, lithium

silicates Li_2MSiO_4 are very attractive as they potentially afford a two-electron reaction with a theoretical capacity of 332 mAh g^{-1}. The structures are composed of tetragonally packed oxygen ions (a distorted form of *hcp*), in which the cations (Li^+, M^{2+} and Si^{4+}) occupy half of the tetrahedral sites (Nytén et al. 2005). The various cationic arrangements and structural distortions create a rich polymorphism, including monoclinic and orthorhombic structures (Islam et al. 2011). Li_2FeSiO_4 was introduced as a LIB cathode by Nytén et al. in 2005 (Nytén et al. 2005). At that time, it was regarded as a one-electron reaction electrode, given the difficulties of Fe^{3+}/Fe^{4+}. It was then found that even Fe^{4+} can be stable in tetrahedral coordination, which is difficult for Mn^{4+} and Co^{4+} (Arroyo-de Dompablo et al. 2006).

The slow Li reaction kinetics are due to the frustrated ion migration in the complex lattices as well as the separated M redox centers, resulting in extremely low electronic conductivity (~ 5×10^{-16} S cm^{-1} for Li_2MnSiO_4 and ~ 6×10^{-14} S cm^{-1} for Li_2FeSiO_4) (Dominko 2008). Also, the Li conductivity is very low due to high diffusion activation energy, which is approximately 1.0 eV determined by theoretical calculations and experimental studies (Armstrong et al. 2011; Fisher et al. 2013; Kokalj et al. 2007), much higher concerning that of LFP (0.3 eV) (Sun et al. 2012). Although the accurate understanding of the ion transfer mechanism remains an ongoing task, researchers have made considerable efforts in advancing the synthesis of these promising cathode materials with satisfactory performance (Ding et al. 2016; He and Manthiram 2014; Li et al. 2016; Muraliganth et al. 2010; Pei et al. 2016; Ramar and Balaya 2016; Rangappa et al. 2012; Yang et al. 2015b; Zhang et al. 2015b). Similar to the cases of phosphates, the strategy is focused on tunning the size, shape, and electronic structure by varying the synthetic approach and experimental conditions, summarised by two recent reviews (Cheng et al. 2017; Ni et al. 2017). For example, Pan et al. reported the achievement of better performing Li_2FeSiO_4 nanocrystals by Ti(IV) doping (Yang et al. 2016). However, the realization of reversible two-electron reactions in silicates is still difficult, and the average potential is quite low (below 3 V) within a large window, which is therefore not suitable for the application.

Fe- and Mn-based borates

Lithium metal borates entered into researchers' sight in 2001, because the polyanion group BO_3^{3-} is the lightest one, ensuring a high theoretical capacity of ~ 220 mAh g^{-1} (Legagneur et al. 2001). However, the early practice only realized the reversible capacity of ~ 8 mAh g^{-1} at C/250, suggesting deficient electrochemical activity. Until 2010, Yamada et al. obtained an attractive capacity of 200 mAh g^{-1} by introducing Ketjen black and vapor grown carbon fibers to increase its electrical conductivity (Yamada et al. 2010). They also pointed out the moisture sensitivity of this material, of which the surface degradation happens after exposure to air. Considering the appreciable electrical conductivity of $LiFeBO_3$ (reported to be 3.9×10^{-7} S cm^{-1}) together with the negligible volume change of ~ 2%, the inferior performance may be due to the constricted Li^+ mobility in the lattice. $LiMBO_3$ is most commonly reported to crystallize in the monoclinic space group *C*2/c ($LiMnBO_3$ also exists as a hexagonal form) (Bo et al. 2014; Kim et al. 2011; Tao et al. 2014). The structure is composed of chains of edge-sharing FeO_5 trigonal bipyramids along [−101] direction, which are linked by BO_3 groups to form a 3D network. Also, edge-sharing LiO_4 tetrahedrons along [001] direction result in zigzag one-dimensional (1D) Li diffusion tunnels, but as disclosed by first-principles calculations, the easily formed Li-M antisite can block the 1D Li diffusion path (Kim et al. 2015c; Seo et al. 2011). The prospect of borates is largely compromised by problematic kinetics, sample preservation, and low operating potential, which cannot be simply alleviated by common modifications (Fig. 8e) (Chen et al. 2015; Dong et al. 2017).

Fe- and Mn-based oxides as SIB cathodes

Sodium metal oxides have been intensively studied as SIB cathodes, which mimic the lithium metal oxides, but the considerably different physico-chemical properties (e.g., ionic size, electron configuration) renders some disparities on the crystal chemistry. First, the vast Na^+ can hardly be hosted in tetrahedral sites. Therefore, there are no isostructural spinel cathodes for SIBs. Second, layered sodium metal oxides (Na_xMO_2) have a richer polymorphism due to the varied Na-O coordination and oxygen stacking rules. Figure 9a shows the crystal structures of the most common polymorphs, O3 and P2, which are present in layered Na_xMO_2 (Yabuuchi et al. 2012a). The notions were introduced by Delmas et al. (Delmas et al. 1980), where the O or P stands for the octahedral (O) or a prismatic (P) sites accommodating Na^+ ions. The number *n* (*n* = 1, 2, 3, etc.) represents

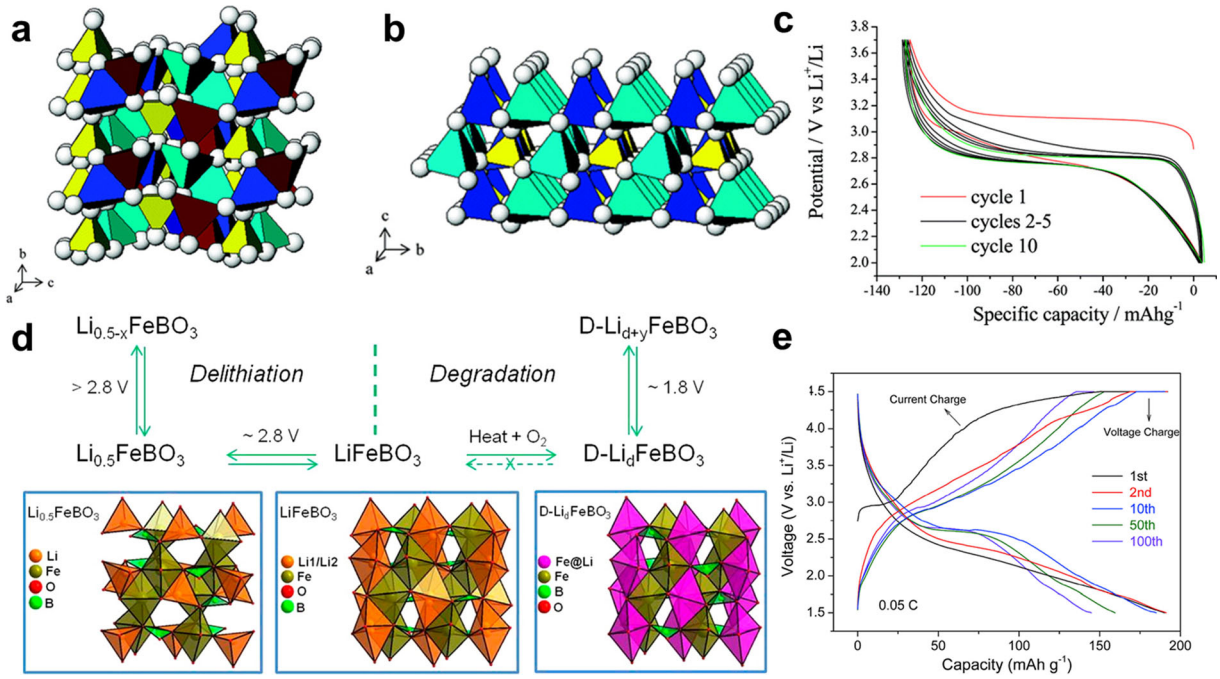

Fig. 8 **a**, **b** Crystal structures of $P2_1/n$ Li_2FeSiO_4 (**a**), which transforms into $Pmn2_1$ Li_2FeSiO_4 (**b**). **c** Typical charge/discharge curves of Li_2FeSiO_4. Reproduced from ref. (Armstrong et al. 2011) with permission. **d** Structural transformation routes of $LiFeBO_3$ during delithiation and degradation. Reproduced from ref. (Bo et al. 2014) with permission. **e** Charge/discharge profiles of mesoporous LiFeBO3/C hollow spheres. Reproduced from ref. (Chen et al. 2015) with permission

the Na ion octahedral or prismatic layers contained in each unit cell, and a prime symbol (′) is added to indicate a monoclinic distortion. In the synthesis of layered oxides, the resultant structure is decided by many factors, especially the sintering temperature and composition (Lei et al. 2014). In general, sodium-rich oxides with x approaching 1 are inclined to crystallize into the O3 structure, whereas P2 phase forms in the broader range of Na-deficient composition.

Though sodium ions are low-cost charge carriers, many layered oxides still rely on redox centers that are scarce and/or may be toxic transition metal elements such as cobalt (Berthelot et al. 2010), nickel (Han et al. 2014), and chromium (Komaba et al. 2010). The advantage of SIBs is therefore largely compromised regarding cost and sustainability. In this context, Fe and Mn-based oxides are of more research interest.

$NaFeO_2$

$NaFeO_2$ has been reported to have two polymorphs: hexagonal α-$NaFeO_2$ and orthorhombic β-$NaFeO_2$ (Kikkawa et al. 1985). The former one is the prototype of layered oxides, opening the era of LIB chemistry. An early study only realized removal of 0.1 Na using chemical oxidizer (Kikkawa et al. 1985). By coupling with Li foil into a battery, Takeda et al. reported the electrochemical desodiation of α-$NaFeO_2$ into monoclinic $Na_{0.5}FeO_2$, suggesting its possibility to function as a cathode for SIBs (Takeda et al. 1994). The first demonstration of α-$NaFeO_2$ working as a SIB cathode was in 2006 by Okada et al., where α-$NaFeO_2$ showed a flat plateau at 3.3 V with a capacity of 80 mAh g^{-1} (Okada et al. 2006). Differing from $LiFeO_2$, reversible Fe^{3+}/Fe^{4+} redox couple has been realized in the electrochemical cycling of α-$NaFeO_2$. Later studies revealed the critical role of the cut-off voltage in the electrode performance of α-$NaFeO_2$ in the sodium cells. When a cut-off voltage was raised over 3.5 V, the cathode experienced irreversible structural transition coupled with significant capacity decay (Yabuuchi et al. 2012b). The fade of the electrode after heavy removal of Na^+ should also be related to increasing amount of highly active Fe^{4+}. A recent study disclosed the chemical instability of Fe^{4+} in batteries which spontaneously oxidized the electrolyte to reduce back to Fe^{3+} at charged state (Lee et al. 2015). α-$NaFeO_2$

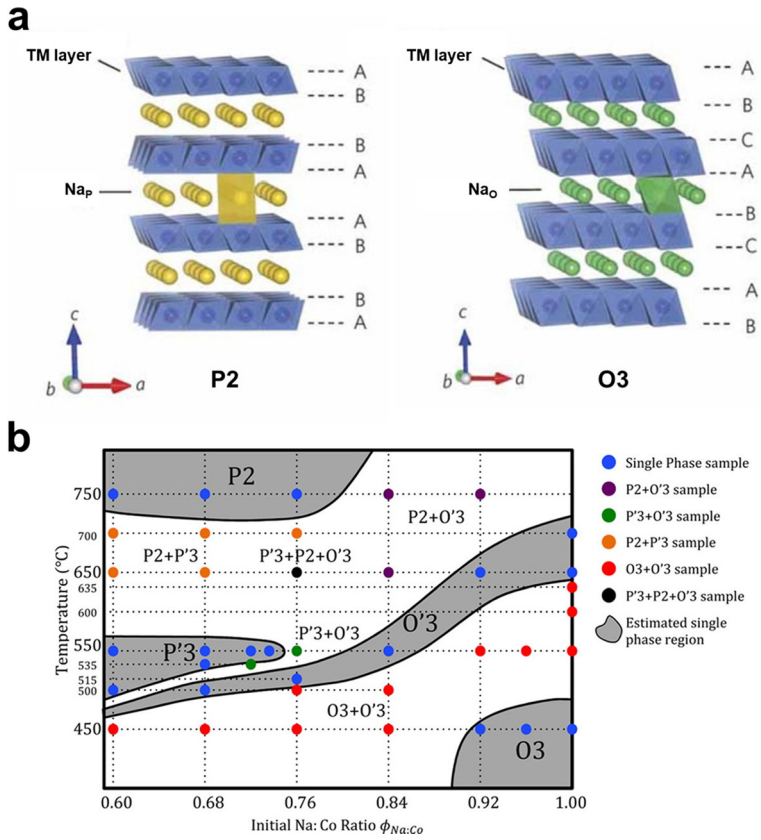

Fig. 9 **a** Structural comparison of P2-type and O3-type Na_xMO_2. Reproduced from ref. (Yabuuchi et al. 2012a) with permission. **b** Synthesis phase diagram of Na_xCoO_2 as a function of the Na/Co ratio from precursors and heating temperature. Reproduced from ref. (Lei et al. 2014) with permission

was also found to show an additional advantage of good thermal stability. As reported by Zhao et al. (Zhao et al. 2013), the highly charged $Na_{0.58}FeO_2$ powder decomposed thermally at a temperature higher than 300 °C, and $NaFeO_2$ showed better thermal stability in the electrolyte than LCO in LIBs. The development of $NaFeO_2$ is restricted by the low reversible capacity of 80–100 mAh g^{-1} and the inferior cycling performance (Fig. 10).

Na_xMnO_2

Na_xMnO_2 has a variety of polymorphs, which can be divided into two large groups: 2D layered structures consisting of slabs of edge-sharing MO_6 octahedra at high x (e.g., $Na_{2/3}MnO_2$, $NaMnO_2$) and 3D tunnel-like structures at low x (e.g., $Na_{0.2}MnO_2$, $Na_{0.4}MnO_2$, $Na_{0.44}MnO_2$) (Clément et al. 2015; Parant et al. 1971). For $NaMnO_2$, monoclinic α-$NaMnO_2$ (O′3 structure) and orthorhombic β-$NaMnO_2$ (consisting of zig-zag layers) show high specific capacities. However, similar to the case of its lithium counterpart, Na_xMnO_2 is subjected to severe capacity decay when cycled in SIBs. As reported by Ceder et al. (Ma et al. 2011), α-$NaMnO_2$ delivered a reversible capacity of 185 mAh g^{-1} at 0.1 °C within in the potential window of 2.0–3.8 V, but only maintained 132 mAh g^{-1} after 20 cycles. In comparison, $NaMnO_2$ consisting of intergrown regions of α-$NaMnO_2$ and β-$NaMnO_2$ domains was found to show a high capacity of ~ 190 and 142 mAh g^{-1} at C/20 and 2 °C, respectively, maintaining 70% after 100 cycles at 2 °C (Billaud et al. 2014a) (Fig. 11).

With the Na/Mn ratio of around 2/3, the distortion of the ideal P2 structure is dependent on the synthesis conditions. Lowering the sintering temperature below 600 °C with a more oxidizing atmosphere stabilizes a higher average Mn oxidation state, producing α-$Na_{0.7}MnO_{2+z}$ ($0.05 \le z \le 0.25$) with a slightly distorted P2 structure. Otherwise, β-$Na_{0.7}MnO_{2+y}$ ($y \le 0.05$) formed at high temperature with an orthorhombically distorted P′2 structure coexisted with α-$NaMnO_2$ (Parant et al. 1971). Paulsen et al. confirmed the substitution of low-valance metals (Co, Li, and Ni) favors the formation of the ideal P2 structure by elevating the oxidation state of Mn and also extends its stable temperature range (Paulsen and Dahn 1999). Later, by using

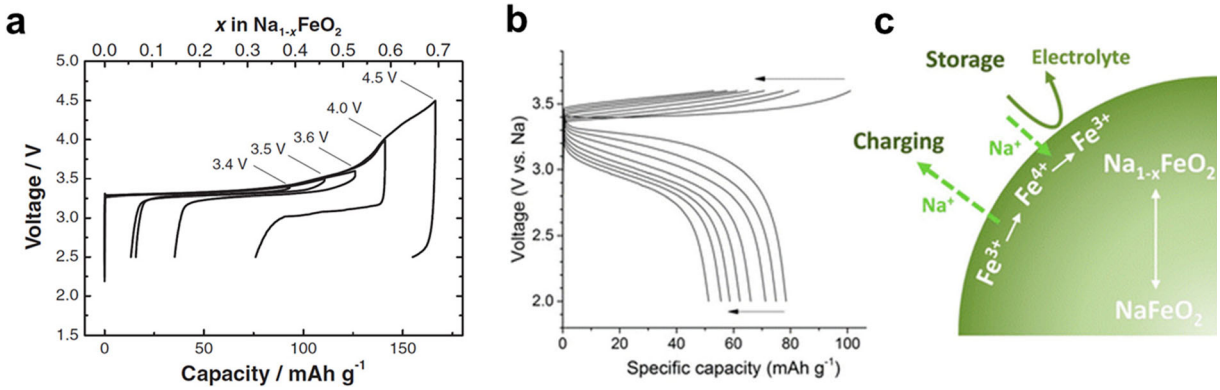

Fig. 10 **a** Initial charge/discharge curves of $NaFeO_2$ on the dependence of different cut-off potentials. Reprinted from ref. (Okada et al. 2006) with permission. **b** Voltage profiles along cycling. **c** A diagram illustrating the electrochemical active Fe^{3+}/Fe^{4+} redox couple. Reproduced from ref. (Lee et al. 2015) with permission

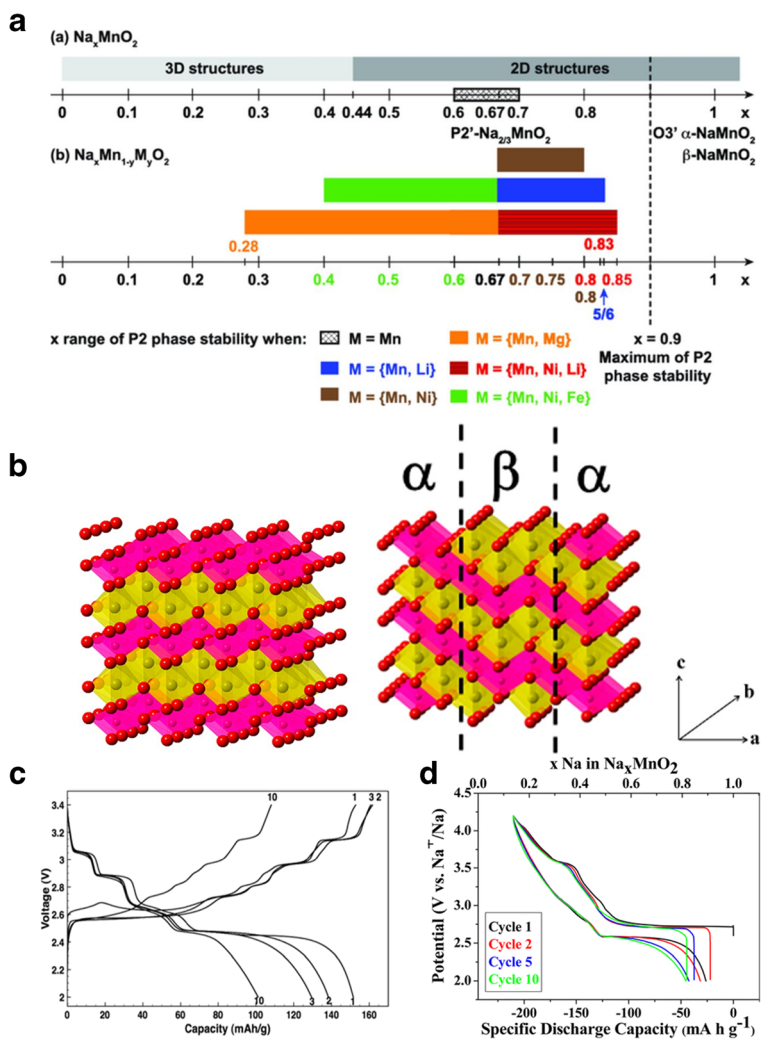

Fig. 11 **a** Stability domain of the different structural types observed for as-synthesized Na_xMnO_2 compounds. Reproduced from ref. (Clément et al. 2015) with permission. **b** Schematic representations of β-$NaMnO_2$ and an intergrowth model between α- and β-$NaMnO_2$. Reproduced from ref. (Billaud et al. 2014a) with permission. **c**, **d** Voltage profiles of α-$NaMnO_2$ and the complex structure. Reproduced from ref. (Ma et al. 2011), (Billaud et al. 2014a) with permissions

a sol-gel method, Caballero et al. reported the synthesis of an undistorted P2-$Na_{0.6}MnO_2$ phase at a high temperature of 800 °C. They further tested the material in SIBs, which delivered *ca.* 140 mAh g^{-1}, but only withstood for 8 cycles. Correspondingly, the active material became amorphous after cycling (Clément et al. 2015). The inferior cycling stability of Na_xMnO_2 is associated with the complex phase transitions caused by the intense Jahn–Teller effect of Mn^{3+}, which reflect as multiple voltage steps during charge and discharge. Therefore, it is a viable strategy to partially substitute the Mn ions by low valency ions to minimize the Jahn–Teller active Mn^{3+}. For example, Billaud et al. introduced a series of Mg-substituted $Na_{2/3}Mn_{1-x}Mg_xO_2$ ($x = 0.05, 0.1, 0.2$) compounds that gave a smoother voltage profile and smaller cell polarisation, leading to enhanced capacity retention (Billaud et al. 2014b). Their further studies unveiled that those achievements are attributed to the more gradual structural changes upon charge and discharge (Clement et al. 2016; Sharma et al. 2015). Similar improvements have also been realized by doping with other cations (de la Llave et al. 2016; Kumakura et al. 2017; Kwon et al. 2017; Luo et al. 2017; Wu et al. 2015; Yabuuchi et al. 2014a). Interestingly, contrary to most efforts made by elevating the Mn valance to suppress the Mn^{3+}, a recent study from Komaba's group showed the high energy density and excellent cycling stability on distorted Mn^{3+}-rich P′2-$Na_{0.7}MnO_2$ (*o*-NMO) (Fig. 12), which exhibited broader P′2 regions when compared with P2-$Na_{0.7}MnO_2$ (*h*-NMO) (Kumakura et al. 2016). These conflicting findings also call for the elucidation of the role of Jahn–Teller distortion and Na/Mn stoichiometry, which may direct the design of future electrodes.

Tunnel $Na_{0.44}MnO_2$ with an orthorhombic structure is another widely studied cathode material for SIBs. As shown in Fig. 13a (He et al. 2016), an open 3D framework is constructed by sheets of edge-sharing MnO_6 and columns of MnO_5 square-pyramids. Three types of Na ion sites exist in the structure, but only Na ions in the large S-shaped tunnels (Na1, Na2) are movable, constituting two kinds of tunnels along [001] for Na diffusion. Full occupation of the Na1 and Na2 sites leads to a formula of $Na_{0.66}MnO_2$. Correspondingly, it has a theoretical capacity of 121 mAh g^{-1}. An early study of the properties of sodium storage based on $Na_{0.44}MnO_2$ prepared by solid-state reaction showed a reversible capacity of only 80 mAh g^{-1} at 0.1 °C and lost 50% of the capacity over 50 cycles with a noticeable cell polarisation increase

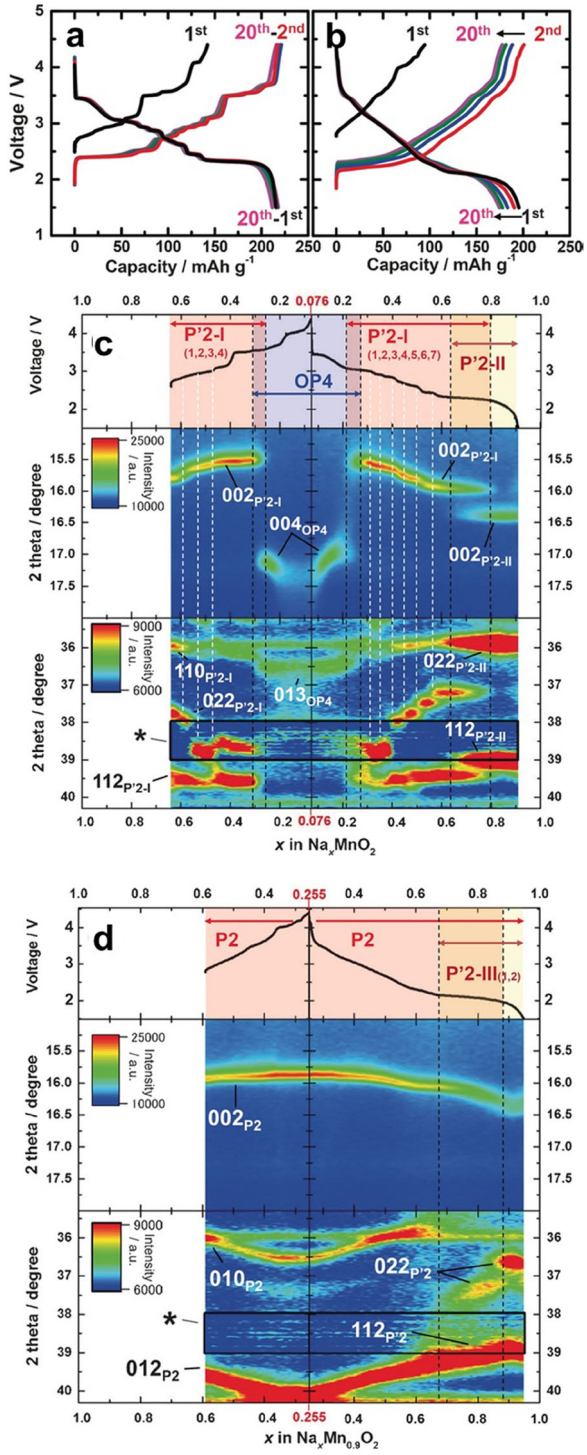

Fig. 12 **a**, **b** Charge-discharge curves of *o*-NMO (**a**) and *h*-NMO (**b**). **c**, **d** Operando XRD patterns of *o*-NMO (**c**) and *h*-NMO (**d**) over initial charge/discharge curves. Reproduced from ref. (Kumakura et al. 2016) with permission

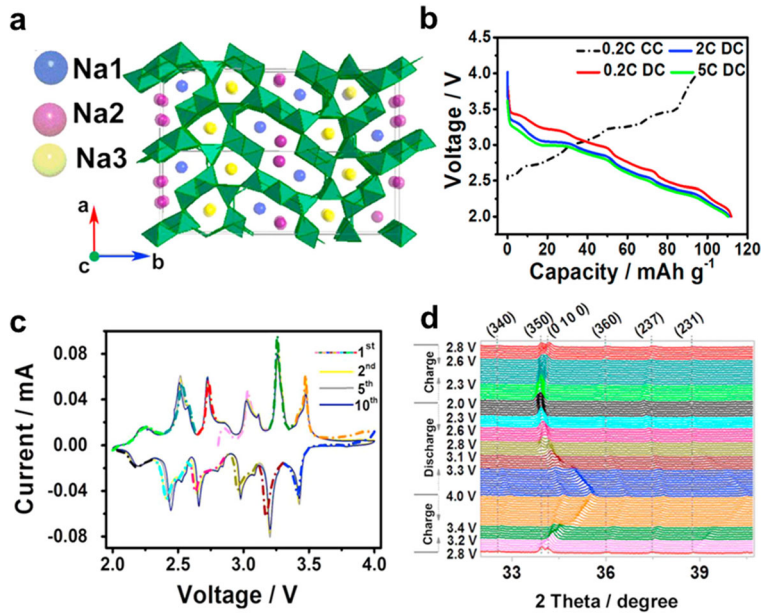

Fig. 13 **a** Schematic representation of the tunnel $Na_{0.44}MnO_2$. **b** Voltage profiles of the monocrystal $Na_{0.44}MnO_2$ nanoplates. **c** Cyclic voltammograms (CVs) of the $Na_{0.44}MnO_2$ electrode between 2.0 and 4.0 V at a scanning rate of 0.1 mV s^{-1}. **d** Corresponding in-situ XRD patterns over the voltage scanning. Reproduced from ref. (He et al. 2016) with permission

(Sauvage et al. 2007). The optimization of preparation method and morphology control contribute to much improved electrochemical performance. For example, single crystalline $Na_{0.44}MnO_2$ nanowires prepared by Cao et al. delivered a capacity of 84.2 mAh g^{-1}, corresponding to 77% capacity retention after 1000 cycles at 0.5 °C (Cao et al. 2011). Dai et al. reported $Na_{0.44}MnO_2$ produced by polyvinylpyrrolidone (PVP)-combustion delivered 99 mAh g^{-1} at a discharging rate of 20 °C and maintained 82.9% of its initial capacity even after 700 cycles at 10 °C (Dai et al. 2015). He et al. prepared $Na_{0.44}MnO_2$ nanoplates by a template-assisted sol-gel method, which discharged 96 mAh g^{-1} at 10 °C and maintains 97.8% capacity after 100 cycles at 0.5 °C (Fig. 13b–d) (He et al. 2016). It is rational to believe that the 3D tunnel is capable of fast and durable sodium extraction and insertion even for thousands of cycles (Liu et al. 2017a). However, its practical application awaits a feasible method to compensate the initial Na deficiency providing that the low energy density is accepted. There are some other emerging sodium manganese oxides, such as the "post-spinel" $NaMn_2O_4$ (tunnel-structure) (Liu et al. 2014), layered $NaMn_3O_5$ (Guo et al. 2014b), and $Na_2Mn_3O_7$ (Adamczyk and Pralong 2017; Zhang et al. 2017).

$Na_xFe_yMn_{1-y}O_2$

Considering the distinct features of the two single metal oxides, it is promising to develop Fe and Mn-mixed $Na_x(Fe_yMn_{1-y})O_2$ which is expected to combine the high potential of $NaFeO_2$ and high capacity of $NaMnO_2$ to target high-energy and cost-effective electrodes. Komaba's group made a critical step by reporting the unprecedented high-performance of P2-$Na_{2/3}Fe_{1/2}Mn_{1/2}O_2$, which delivered a capacity of 190 mAh g^{-1} at 0.05 °C (13 mA g^{-1}). Attributing to the contribution of the reversible high-energy Fe^{3+}/Fe^{4+} redox at above 3.2 V, the energy density of this cathode reached over 500 Wh kg^{-1}. However, only a 30 cycling profile was presented (~ 79% capacity retention) together with poor rate capability. Also, they also presented the O3-$Na_{2/3}Fe_{1/2}Mn_{1/2}O_2$, only receiving an initial capacity of 125 mAh g^{-1} with more serious polarisation (Yabuuchi et al. 2012a). After that, Thorne et al. investigated a serious of $Na_xFe_xMn_{1-x}O_2$ ($0.5 \leq x \leq 1.0$), confirming that the existence of Fe reduced the voltage hysteresis and increased capacity retention over cycling. By restricting the potential window below 4.0 V, more than 90% capacity retention was achieved after 20 cycles (Thorne et al. 2013). They further studied the sodium (de)intercalation behavior of P2-$Na_xMn_{1/2}Fe_{1/2}O_2$ by using operando in situ X-ray powder diffraction, which revealed a larger solid-solution region ($0.35 < x < 0.82$), and an orthorhombic P′2-type structure formed when charged over 4.0 V (Mortemard de Boisse et al. 2014). Recently, Rojo's group carried out a series of studies on Fe-rich $Na_{2/3}Fe_{2/3}Mn_{1/3}O_2$. First, they decoupled the influence from Na/Mn stoichiometry and the structure by preparing P2 and O3 structured oxides on the basis of the

same formula of $Na_{2/3}Fe_{2/3}Mn_{1/3}O_2$. As a result, the O3 structure demonstrated similar electrochemical performance (Gonzalo et al. 2014) or even slightly higher reversible capacity (Han et al. 2015) compared with its P2 counterpart. They further made a direct comparison of phase transitions for two electrodes during charge/discharge by in-situ synchrotron X-ray diffraction, and they showed distinct and rate-dependent structural evolution. Phase change in the P2 phase was limited at 0.4 °C, but amplified at 1 °C. Whereas the O3 electrode behaved inversely. Interestingly, the O3 structure converted partially into a P2-like phase after cycling (Sharma et al. 2016). These results offer new understandings about the Na/Mn stoichiometry-crystal structure-electrochemistry relations.

As the Fe- and Mn-based oxides suffer from the significant capacity drop as well as unsatisfactory rate capability, continuous efforts have been made to mitigate the issues. Low-valance metal substitution is still deemed as an effective strategy. Kim et al. reported the heavily Ni-substituted $NaNi_{1/3}Fe_{1/3}Mn_{1/3}O_2$ as a stable cathode in a SIB full cell with hard carbon, which maintained 100 mAh g^{-1} after 150 cycles at a 0.5 °C rate (75 mA g^{-1}) (Kim et al. 2012a). After that, a range of Ni- (Hasa et al. 2014; Talaie et al. 2015), Co- (Liu et al. 2015a), and Cu-substituted (Li et al. 2015c) oxides have been investigated. These ions not only suppress the ratio of Mn^{3+} but also partially replaced the redox reactions. The deleterious high voltage transition is mitigated by substitution of Fe^{3+} by Mn^{4+}/Ni^{2+}, permitting better cycling performance. (Fig. 14).

Fe- and Mn-based polyanion compounds as SIB cathodes

As discussed above, polyanion compounds feature robust crystal framework with the oxygen atoms covalently bonded by counterions (S, P, Si, etc.), affording favorable structural stability toward lithium (de)insertion. Such merit is more demanded in SIB chemistry, as the movement of the larger Na ions puts forward higher requirement for structural stability. Given the poor cycling stability haunting most of the layered oxides, much interest has shifted to develop polyanion compounds as long-life cathodes for SIBs.

Fe-and Mn-based phosphates

Olivine LFP is the most successful polyanion cathode for LIBs. Unfortunately, its sodium counterpart $NaFePO_4$ (NFP) simply cannot duplicate its success, as the thermodynamically stable phase of NFP is a maricite structure (Bridson et al. 1998), in which Na^+ and Fe^{2+} ions occupy the opposite sites of those in olivine $LiFePO_4$. Due to the absence of Na^+ channels in such atomic configurations (Fig. 11), the maricite structure is therefore electrochemically inactive (Moreau et al. 2010; Zaghib et al. 2011). Metastable olivine NFP is usually synthesized through electrochemical displacement from olivine LFP (Ali et al. 2016; Fang et al. 2015; Moreau et al. 2010; Oh et al. 2012; Zaghib et al. 2011; Zhu et al. 2013). Though the prepared NFP electrodes preserve the microstructures and conductive modifications from the LFPs, their performances are much lower than the original LFP in LIBs, receiving capacities of only around 120 mAh g^{-1} together with deteriorated rate capability. Atomistic simulations conducted in Nazar's group showed the low formation of Na/M antisite defects in the Na-olivine and significant volume change of 15% during the removal of Na^+, which possibly answered the poor performances (Tripathi et al. 2013). Moreover, their costs are even significantly higher than LFP, which are against the purpose of developing SIBs. Therefore, research interest has been shifted to explore other crystal chemistries of NFP. Amorphous α-$FePO_4$,

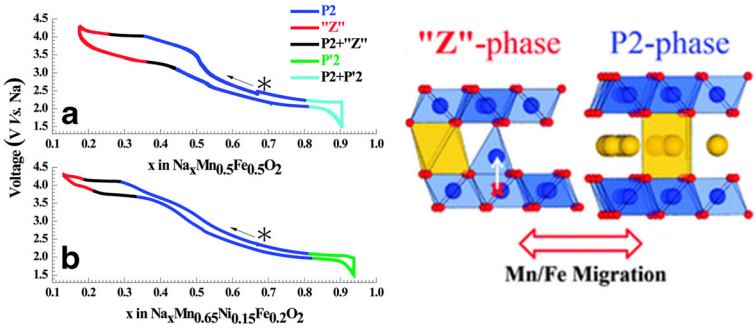

Fig. 14 Phase evolution in $Na_{0.67}Mn_{0.5}Fe_{0.5}O_2$ and Ni-substituted $Na_{0.67}Mn_{0.65}Ni_{0.15}Fe_{0.2}O_2$ over the first cycle, and schematic illustration of Mn/Fe migration into tetrahedral sites in the Na space at high potential. Reproduced from ref. (Talaie et al. 2015) with permission

which is electrochemically active for (de)lithiation, is reinvestigated as a cathode material for SIBs (Fang et al. 2014; Liu et al. 2015b; Liu et al. 2012b). With the nanosized particle and high content of conductive carbon, they can deliver a capacity of up to 160 mAh g^{-1}. The concern of the initial desodiated state was further addressed by Li et al. by the direct preparation of amorphous NFP nanospheres, which showed a capacity of 152 mAh g^{-1} and retained 144.3 mAh g^{-1} after 300 cycles (Li et al. 2015a). Recently, Kang et al. reported an alternative route toward amorphous $NaFePO_4$, which was converted from nanosized maricite after long charging, after that, a reversible capacity of 142 mAh g^{-1} in a potential window of 1.5–4.5 V was achieved (Kim et al. 2015b).

Also, Fe-based phosphates crystalized in other structures have also been investigated as SIB cathodes. Trad et al. reported the electrochemical performance of a "layered" $Na_3Fe_3(PO_4)_4$, where only ~ 80 mAh g^{-1} was discharged at 0.02 °C (Trad et al. 2010b). Huang et al. prepared alluaudite $Na_2Fe_3(PO_4)_3$/CNT composites, delivering a discharge capacity of up to 143 mAh g^{-1} after 50 cycles (Huang et al. 2015b). Very recently, Liu et al. tested the NASICON-type $Na_3Fe_2(PO_4)_3$, which showed a low capacity of 61 mAh g^{-1} and low plateau at 2.5 V, but the capacity retention was excellent, maintaining 93% capacity after 500 cycles at 1 °C (Liu et al. 2017b). Those phases including the amorphous NFP are not competitive compared with olivine LFP in LIB system regarding energy density, power densities, and cycling stability. Considering the abundant polymorphism in the Na-Fe-P-O system, the future success of sodium iron phosphate may rely on the exploration of new structures.

Like NFP, $NaMnPO_4$ (NMP) also crystalized favorably in the maricite phase. However, the olivine phase of NMP is still more stable than olivine NFP. Lee et al. (Lee et al. 2011) and Boyadzhieva et al. (Boyadzhieva et al. 2015) have developed ion-exchange reactions to prepare olivine NMP from $NH_4MnPO_4{\cdot}H_2O$ and $KMnPO_4{\cdot}H_2O$, respectively. The olivine-to-maricite conversion temperatures are respectively 450, 500, and 550 °C for NFP, $NaFe_{0.5}Mn_{0.5}PO_4$, and NMP. To our knowledge, there are no reports on the electrochemical properties of pure NMP up to now, indicating deteriorating reactive activity. Lee et al. showed discharge profile of $NaFe_{0.5}Mn_{0.5}PO_4$ over 3 cycles at C/40, in which a discharge capacity around 90 mAh g^{-1} is obtained (Lee et al. 2011). Besides, Fe- and Mn-mixed alluaudite-type phosphates have been investigated as SIB cathodes (Huang et al. 2015a; Trad et al. 2010a), where the existence of Mn further lowers the limited specific capacity (Fig. 15).

Fe- and Mn-based pyrophosphates

Though pyrophosphates have been eclipsed by LFP in the LIB system due to the large gap of capacities, the pyrophosphates show intrinsically better kinetics when compared to other polyanion materials, including LFP (Furuta et al. 2012; Nishimura et al. 2010). Their sodium analogs, therefore, attract much interest. Barpanda et al. first reported the preparation and electrochemical properties of $Na_2FeP_2O_7$. $Na_2FeP_2O_7$ was preferably crystalized into a triclinic structure (*P*-1), consisting of interconnected FeO_6 octahedral and PO_4 tetrahedral building blocks. Attributing to the large channels within the 3D structure, the unmodified sample showed a reversible capacity of 82 mAh g^{-1} with an impressive rate capability (Barpanda et al. 2012). The *ex-situ* XRD test conducted by Kim et al. revealed that $Na_2FeP_2O_7$ experienced a single-phase reaction at ~ 2.5 V and consecutive two-phase reactions in the higher potential range of 3.0–3.25 V (Kim et al. 2013b). Both $Na_2FeP_2O_7$ and charged $NaFeP_2O_7$ phases exhibited impressive thermal stability up to 500 °C, adding its feasibility to practical applications (Barpanda et al. 2013a; Kim et al. 2013b). The electrochemical performance has been further enhanced by some recent efforts made on the optimization of morphology and conductive modification, such as $Na_2FeP_2O_7$ decorated by carbon nanotubes, reduced graphene oxide-supported $Na_{3.12}Fe_{2.44}(P_2O_7)_2$/C (Song et al. 2017b), and $Na_2FeP_2O_7$ nanoparticles embedded in carbon (Song et al. 2017a).

Along with the success of $Na_2FeP_2O_7$, its Mn analog $Na_2MnP_2O_7$ has also been investigated. Unlike most Mn-based cathode materials suffering from sluggish kinetics, Park et al. found the unexpected high activity of micron-sized $Na_2MnP_2O_7$, which exhibited a reversible capacity of 90 mAh g^{-1} with an elevated plateau at ~ 3.8 V. First-principles calculations revealed that the impressive kinetics were attributed mainly to the corner-sharing crystal structure in triclinic $Na_2MnP_2O_7$, permitting locally flexible accommodation of Jahn–Teller distortions of Mn^{3+} (Park et al. 2013). After that, Barpanda et al. reported the new polymorph of β-$Na_2MnP_2O_7$ (triclinic *P*1), which was also electrochemically active

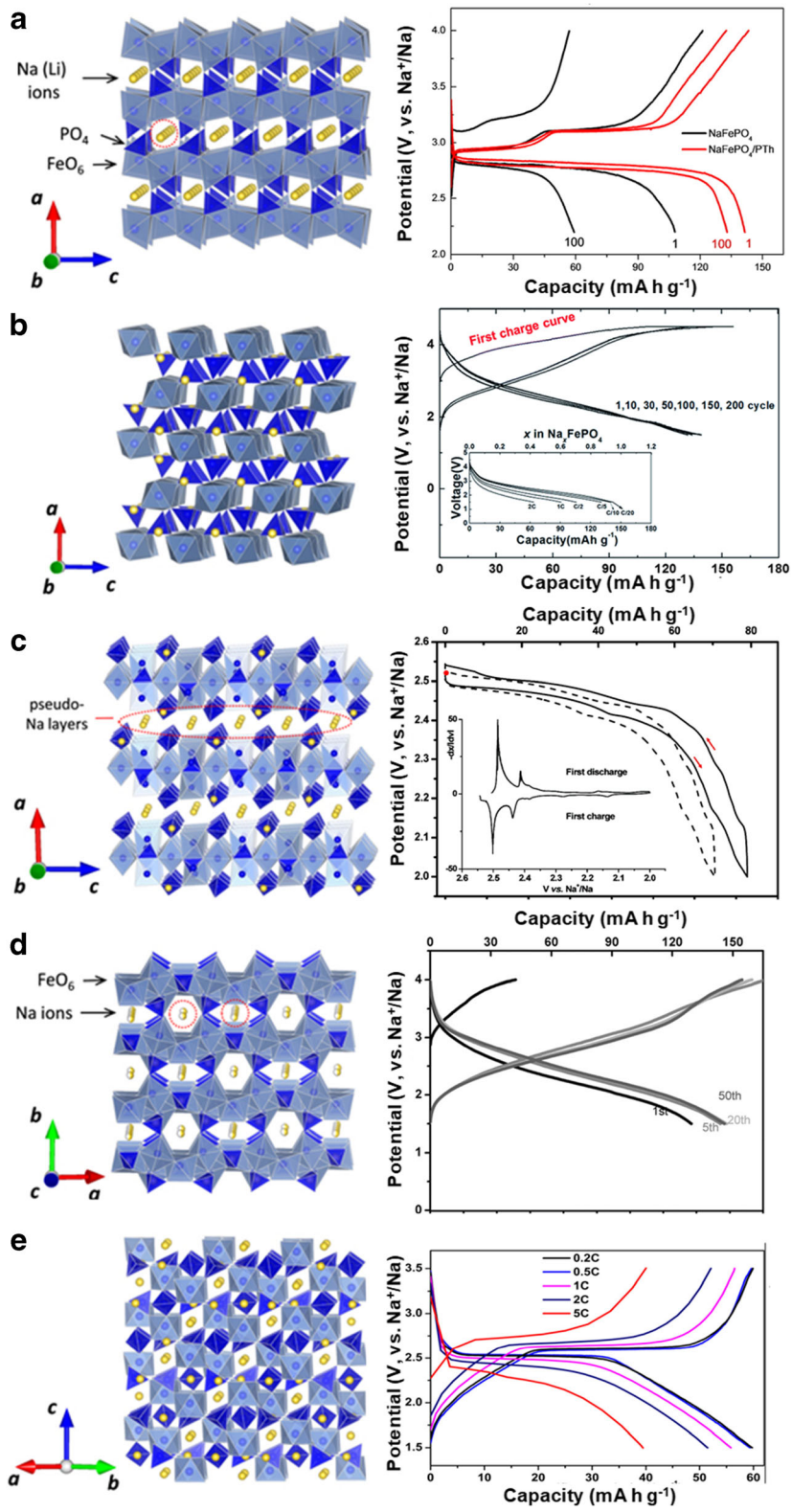

Fig. 15 **a**–**e** Crystal structures of olivine NFP, maricite NFP, NASICON-type $Na_3Fe_2(PO_4)_3$, layered $Na_3Fe_3(PO_4)_4$, alluaudite-type $Na_2Fe_3(PO_4)_3$. Reproduced from ref. (Naoaki and Shinichi 2014) with permission. Their typical charge/discharge curves are shown on the right side. Reproduced from ref. (Ali et al. 2016), (Kim et al. 2015b), (Trad et al. 2010b), (Huang et al. 2015b), and (Liu et al. 2017b) with permissions

and thermodynamically feasible (Barpanda et al. 2013b). Their further atomistic simulations disclosed low barriers for long-range Na^+ diffusion in all directions in $Na_2(Fe, Mn)P_2O_7$, theoretically proving the 3D Na^+ pathway (Clark et al. 2014) (Fig. 16).

Fe- and Mn-based sulfates and oxalates

The stronger inductive effect of the SO_4^{2-} group can elevate the redox potential when compared with common PO_4^3. In 2014, Barpanda et al. reported the use of a new $Na_2Fe_2(SO_4)_3$ with the alluaudite-type as a cathode material for SIB. The sulfate showed the highest-ever Fe^{3+}/Fe^{2+} redox potential at 3.8 V and delivered a reversible capacity of 100 mAh g^{-1} coupled with good kinetics (Barpanda et al. 2014b). Further experimental and computational studies revealed the alluaudite sulfate witnesses a reversible single-phase reaction with a small volume change (ca. 3.5%) after the initial charge (Oyama et al. 2016). The sulfate also possessed four and two orders of magnitude higher intrinsic ionic and electronic conductivity than LFP, underpinning the high kinetics (Lu and Yamada 2016). With the intrinsic merits, the cathode can undergoes 40 °C charge/discharge by constructing the additional conductive network (Meng et al. 2016; Yu et al. 2016).

Apart from alluaudite-type sulfates, Kröhnkite-type $Na_2Fe(SO_4)_2{\cdot}2H_2O$ was also explored as a 3.25 V insertion compound for SIBs, showing a reversible capacity of around 70 mAh g^{-1} (Barpanda et al. 2014a). Besides, eldfellite $NaFe(SO_4)_2$ was validated to be electrochemically active by Singh et al., with a discharge capacity of ~ 80 mAh g^{-1} at 0.1 °C with a plateau of 3.0 V (Singh et al. 2015). Density functional theory calculations suggested the low kinetics of eldfellite is due to high activation energies over 1 eV for the Na^+ ion hop (Banerjee et al. 2016).

Mn-based sulfates progressed much slower. Barpanda et al. continued to explore the sulfate-based cathode family by reporting the isostructural alluaudite-type $Na_{2+2x}Mn_{2-x}(SO_4)_3$, but no electrochemical data was presented, as they claimed that the predicted high-potential (*ca*. 4.4 V) requires the advent of suitable electrolytes (Dwibedi et al. 2015). After that, Yamada's group reported a series of Mn-substituted alluaudite solid solutions $Na_{2.5}(Fe_{1-y}Mn_y)_{1.75}(SO_4)_3$ ($y = 0$, 0.25, 0.5, 0.75, and 1.0). However, there were no Mn^{2+}/Mn^{3+} redox reactions that had taken place. The material simply showed continuous capacity decrease along with the increasing Mn content (Wei et al. 2016).

Oxalates have also been investigated as Na^+ host materials. According to the electronegativity order of

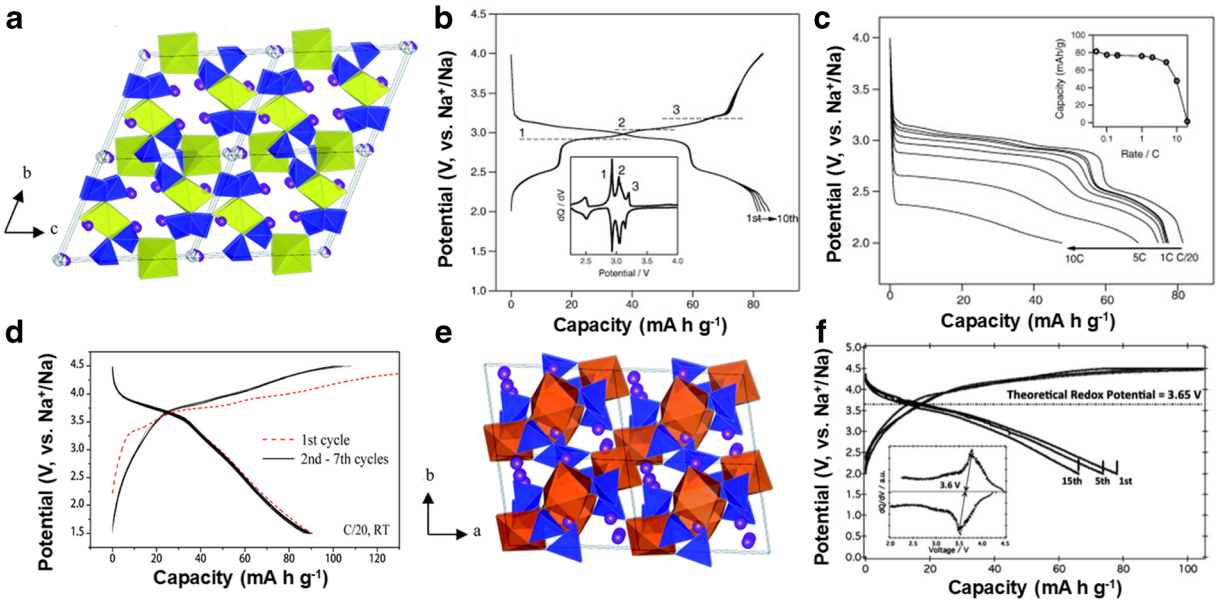

Fig. 16 **a**–**c** Triclinic structure (*P*-1) of $Na_2FeP_2O_7$ and corresponding electrochemical properties. Reproduced from ref. (Barpanda et al. 2012) with permission. **d** Voltage profiles of *P*-1 $Na_2MnP_2O_7$. Reproduced from ref. (Park et al. 2013) with permission. **e**, **f** Crystal structure of β-$Na_2MnP_2O_7$ (triclinic *P*1) and its voltage profiles. Reproduced from ref. (Barpanda et al. 2013b) with permission

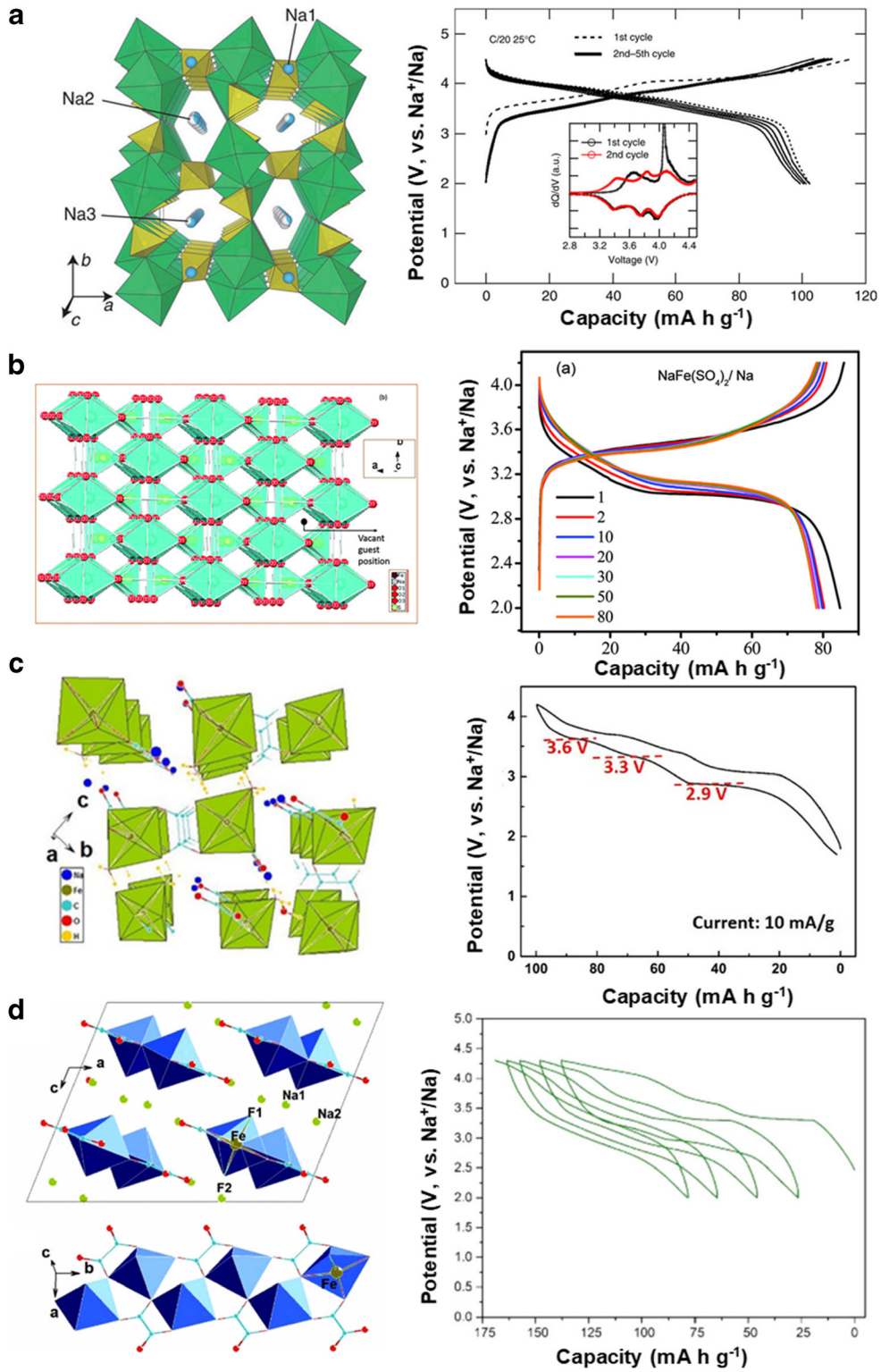

Fig. 17 Crystal structures of alluaudite-type $Na_2Fe_2(SO_4)_3$ (**a**), eldfellite $NaFe(SO_4)_2$ (**b**), $Na_2Fe_2(C_2O_4)_3{\cdot}2H_2O$ (**c**), and $Na_2Fe(C_2O_4)F_2$ with their voltage profiles are shown on the right side. Reproduced from ref. (Barpanda et al. 2014b), (Singh et al. 2015), (Yao et al. 2017b), and (Yao et al. 2017a) with permissions

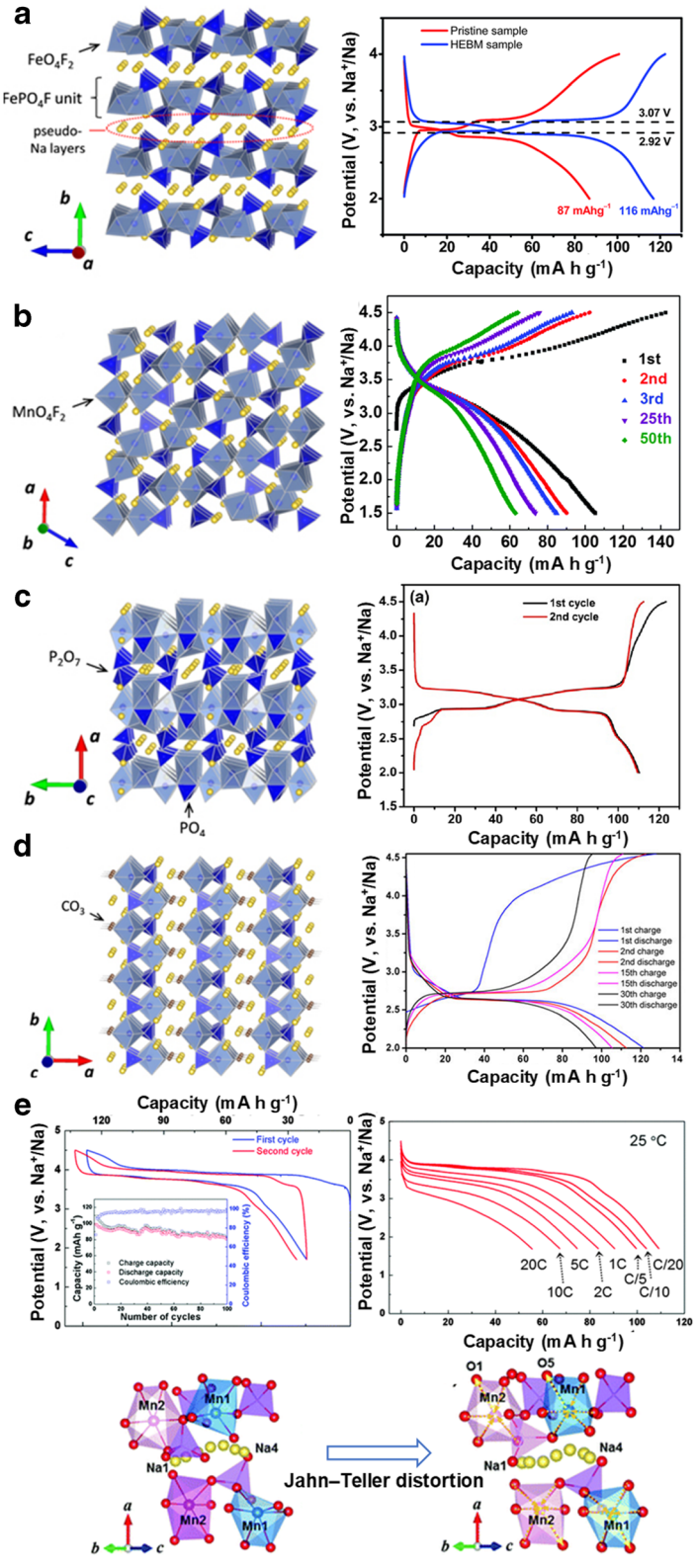

Fig. 18 **a**–**d** Crystal structures of Na_2FePO_4F (**a**), Na_2MnPO_4F (**b**), $Na_4Fe_3(PO_4)_2(P_2O_7)$ (**c**), and $Na_3MnPO_4CO_3$ (**d**). Reproduced from ref. (Naoaki and Shinichi 2014) with permission. Their representative voltage profiles are shown on the right side. Reproduced from ref. (Law et al. 2015), (Lin et al. 2014), (Wu et al. 2016), and (Huang et al. 2014) with permissions. **e** High-performance $Na_4Mn_3(PO_4)_2(P_2O_7)$, which was ascribed to the cooperative Jahn-Teller effect of Mn^{3+}. Reproduced from ref. (Kim et al. 2015a) with permission

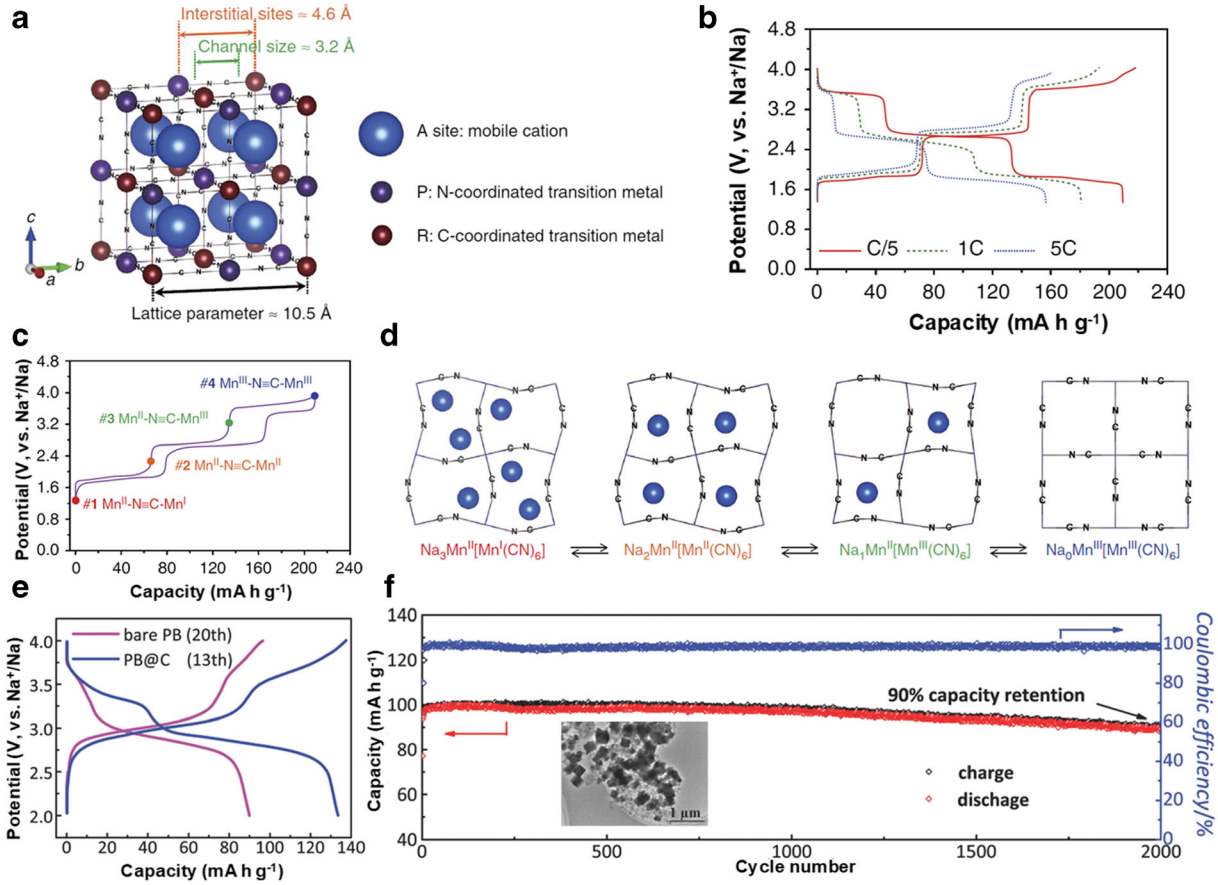

Fig. 19 **a** Crystal structure of PBAs with a face-centered cubic phase. **b** Charge and discharge curves of $Na_2MnMn(CN)_6$. **c**, **d** The schematic illustrations of the step-wise structural evolution over the extraction/insertion of Na^+ ions. Reproduced from ref. (Lee et al. 2014) with permission. **e**, **f** Voltage profile and cycling performance of a Prussian blue@C composite. Reproduced from ref. (Jiang et al. 2016) with permission

$SO_4^{2-} > C_2O_4^{2-} > PO_4^{3-}$, metal oxalates can display competitive redox potentials. In 2014, Yamada's group prepared $K_4Na_2[Fe(C_2O_4)_2]_3{\cdot}2\,H_2O$ and studied its Na storage capability (Wang et al. 2015b). The material initially discharged 54.5 mAh g^{-1} at C/50 with an average potential of 2.7 V in the subsequent 9 cycles. Yao et al. investigated the electrochemical properties of $Na_2Fe_2(C_2O_4)_3{\cdot}2H_2O$(Yao et al. 2017b) and $Na_2Fe(C_2O_4)F_2$ (Yao et al. 2017a) as SIB cathodes. The former one was suggested to be electrochemically inactive in LIBs, but they found a reversible capacity of *ca.* 100 mAh g^{-1} (10 mA g^{-1} current) with three redox plateaus at 2.9, 3.3, and 3.6 V (Yao et al. 2017b). The fluoro-oxalate showed a reversible capacity of 70 mAh g^{-1} at 10 mA g^{-1} for 50 cycles (Yao et al. 2017a). Although electrochemical activities have been demonstrated in these polyanion compounds, especially the alluaudite-type sulfates, it is worth noting that some critical issues should be addressed before their practical application, including the air (water, oxygen) sensitivity and thermal instability (decomposition) (Fig. 17).

Fe- and Mn-based mixed anion compounds (fluorophosphates and mixed polyanions)

The combination of different anion groups (F^-, PO_4^{3-}, $P_2O_7^{4-}$, CO_3^{2-}, etc.) offers new opportunities toward desirable electrode materials. The induction of highly electronegative F^- ions enables higher redox potentials due to the stronger inductive effect. Na_2FePO_4F is a representative Fe-based fluorophosphate, which was first introduced by Nazar's group in 2007 (Ellis et al. 2007). As shown in Fig. 18a, the structure is assigned to the orthorhombic *Pbcn* space group, in which the bioctahedral $Fe_2O_7F_2$ chains are connected by PO_4 tetrahedra to constitute 2D $[FePO_4F]$ layers. In this way,

Na ions can transport between the layers. The structure also favors a small volume change (3.7%) after extraction of one Na^+ ion, corresponding to a theoretical capacity of around 124 mAh g^{-1} as a cathode for SIBs. The atomistic simulations also suggested low activation energy for the Na^+ diffusion between the layers (Tripathi et al. 2013). However, the strong iconicity of fluorine reduced the inherent electrical conductivity. Unlike the pyrophosphates, iron fluorophosphates are unlikely to perform well in micron particles. With the aid of carbon coating and nanosizing (Kawabe et al. 2011; Ko et al. 2017; Law et al. 2015), the electrochemical performance experienced some improvements.

Different from the 2D-layered Na_2FePO_4F, Na_2MnPO_4F adopts a 3D tunnel structure (space group: $P2_1/n$) (Fig. 19b) (Yakubovich et al. 1997). By investigating the Mn-substituted $Na_2Fe_{1-x}Mn_xPO_4F$, the presence of 0.25 Mn is enough to trigger the 2D-3D phase transition. The Mn substitution resulted in a substantial decay of the electrochemical performances (Wu et al. 2011). In the quest of active Mn^{2+}/Mn^{3+}, Yong's group prepared a series of $Na_2Fe_{1-x}Mn_xPO_4F/C$ ($x = 0$, 0.1, 0.3, 0.7, 1) nanostructured composites. When operating at a high temperature of 60 °C, all these electrodes showed electrochemical activity. Na_2FePO_4F can even perform 1.46 electron reaction with a capacity of 182 mAh g^{-1}. The partial substitution of Fe by Mn enables higher redox potentials with limited loss of capacity. However, entirely substituted Na_2MnPO_4F was much less active (Wu et al. 2011). After that, they optimized electrode materials by utilizing spray-drying precursor, the resultant Na_2MnPO_4F/C delivered 140 mAh g^{-1} at 6.2 mA g^{-1}, when operating at 30 °C. However, the capacity retention was only around 50% after 50 cycles (Lin et al. 2014). The very low Na^+ diffusion coefficient of 10^{-17} cm^2 s^{-1} given by the GITT test suggests the formidable challenge in the use of this material.

Kim et al. first introduced the Fe-based mixed phosphate compound $Na_4Fe_3(PO_4)_2(P_2O_7)$ to SIBs. As shown in Fig. 18c, the structure belongs to the orthorhombic *Pbcn* space group, which is constructed by $[Fe_3P_2O_{13}]$ layers and P_2O_7 pillars. First-principles calculations identified feasible 3D Na^+ paths. The theoretical capacity based on one-electron reaction is 129 mAh g^{-1}. Their result showed that 88% of the theoretical value can be achieved at an extreme rate of C/40 (Kim et al. 2012b). Furthermore, they employed *ex-situ* XRD to disclose a single-phase reaction mechanism coupled with a small volumetric change of less than 4% during the (de)sodiation of the $Na_xFe_3(PO_4)_2(P_2O_7)$ (Kim et al. 2013a). Wood et al. simulated molecular dynamics for $Na_4M_3(PO_4)_2P_2O_7$ (M = Fe, Mn, Co, Ni), with the results showed a small activation barrier of 0.20–0.24 eV for 3D Na^+ migration and diffusion coefficients of 10^{-10}–10^{-11} cm^2 s^{-1} at 325 K (Wood et al. 2015). Impressive electrochemical performance was realized by $Na_4Fe_3(PO_4)_2(P_2O_7)/C$ nanocomposites synthesized by a sol-gel method, which showed capacities of 105 and 78 at 0.2 and 10 °C, respectively (Wu et al. 2016). Unexpectedly, $Na_4Mn_3(PO_4)_2(P_2O_7)$ (Kim et al. 2015a) and $Na_4Mn_xFe_{3-x}(PO_4)_2(P_2O_7)$ ($x = 1$, 2) (Kim et al. 2016a) reported by Kim et al. showed better performance. $Na_4Mn_3(PO_4)_2(P_2O_7)$ had a redox potential of 3.8 V and a reversible capacity of 109 mAh g^{-1} at C/20, and maintained 55 mAh g^{-1} at 20 °C (Fig. 18e). The $Na_4MnFe_2(PO_4)(P_2O_7)$ showed capacity retention of 83% after 3000 cycles at 1 °C.

Carbonophosphates are an emerging class of mixed polyanion compounds in SIB system. The idea of engaging carbonophosphates was proposed by Ceder's group using ab initio computations (Hautier et al. 2011). They successfully synthesized a series of carbonophosphates $Na_3M(PO_4)(CO_3)$ (M = Mg, Mn, Fe, Co, Ni, Cu, Sr) with a sidorenkite phase (space group: $P2_1/m$, Fig. 18d). Chemical desodiation performed on the $Na_3Fe(CO_3)(PO_4)$ suggested the possibility of serving as a SIB cathode (Chen et al. 2012). Then they reported the first use of $Na_3MnPO_4CO_3$ as a cathode material for SIBs (Chen et al. 2013). The electrode displayed a high discharge capacity of 125 mAh g^{-1}, indicating a two-electron intercalation reaction, which was further evidenced by ^{23}Na NMR spectroscopy. In-situ XRD suggested a single-phase reaction upon electrochemical cycling. Until now, there are only limited reports on this type of material, and the rate capability still seems unsatisfactory after nanosizing and carbon modification (Hassanzadeh et al. 2016a, b; Huang et al. 2014). Additionally, carbonophosphates show appreciable thermal stability that can withstand a temperature of 500 °C.

Fe- and Mn-based hexacyanometalates

Metal hexacyanometalates, also known as Prussian blue analogs (PBAs), have a general formula of $A_xP[R(CN)_6]_{1-y}\square_y \cdot nH_2O$ (A: removable cations, P: N-coordinated metal ion; R: C-coordinated metal ion; □: $[R(CN)_6]$ vacancy; $0 \le x \le 2$; $0 \le y < 1$).

They are crystallized into a cubic structure with the space group of *Fm-3m*. The cyanide ligands link the coordinated metal ions together to form elementary cubes that can host various cations due to the large channels and interstitial sites, and each unit cell contains eight elementary cubes (Lee et al. 2014). Goodenough's group first investigated the use of metal hexacyanometalates as cathodes for non-aqueous SIBs. Among a range of hexacyanometalates, $KFe_2(CN)_6$ exhibited a reversible capacity near 100 mAh g^{-1} at 0.05 °C. However, they showed quite a low efficiency, which was ascribed to the crystal water contained in MHCs (Lu et al. 2012). Moving forward, they reported a high-performance $Na_{1.72}MnFe(CN)_6$, where the Na displacement at higher Na concentrations reduces the crystal symmetry to a rhombohedral phase. The initial rhombohedral structure demonstrated a capacity of 134 mAh g^{-1} at 0.05 °C, and retained 45 mAh g^{-1} at 40 °C (Wang et al. 2013). In search of high-capacity PBAs, Cui et al. prepared Na-rich monoclinic $Na_2MnMn(CN)_6$, which can even host additional Na^+, resulting in a high discharge capacity of 209 mAh g^{-1} at C/5 (40 mA g^{-1}). The three-step Na^+ insertion corresponds to three plateaus with an average potential of 2.65 V (Lee et al. 2014). As the water residue and $[R(CN)_6]$ vacancies are considered to be detrimental to the coulombic efficiency, cyclic stability, and kinetics, many efforts have been to prepare high-quality PBAs for enhanced overall performance. Guo et al. developed a slow crystal growth process from $Na_4Fe(CN)_6$, with the resultant Prussian blue containing less zeolite water and $[Fe(CN)_6]$ vacancies, and showing a capacity of 170 mAh g^{-1} with no capacity loss for 150 cycles (You et al. 2014). Goodenough's (Song et al. 2015) and Ma's (Yang et al. 2015a) groups respectively reported the removal of Interstitial water by different methods, leading to much improved electrochemical performance. Recently, a Prussian blue@C composite was reported for excellent rate and cycling performance (Jiang et al. 2016), which maintained 77.5 mAh g^{-1} at 90 °C, and received 90% capacity retention after 2000 cycles at 20 °C, indicating a promising future for this type of material. It is worth mentioning that metal hexacyanometalates are subject to thermal decomposition at temperatures over 300 °C (Zhang et al. 2012).

Table 1 Electrochemical properties of representative Fe- and Mn-based cathode materials for LIBs

Electrode material (code in Fig. 20)	Average potential (V *vs.* Li^+/Li)	Discharge capacity (current density)	Discharge capacity at high current densities (current density)	Capacity retention (cycles, current density)	Ref.
α-$LiFeO_2$ (1)	~ 2	287 (141 mA g^{-1})	153 (846 mA g^{-1})	80% (100, 141 mA g^{-1})	Rahman et al. 2011
$LiMnO_2$ (orthorhombic) (2)	~ 3	235 (10 mA g^{-1})	–	81% (20, 10 mA g^{-1})	He et al. 2010
$LiMn_2O_4$ (3)	4.05	120 (60 mA g^{-1})	93 (60,000 mA g^{-1})	84.5% (200, 3600 mA g^{-1})	Lee et al. 2017
$LiNi_{0.5}Mn_{1.5}O_4$ (4)	4.7	140 (147 mA g^{-1})	109 (2940 mA g^{-1})	91% (500, 730 mA g^{-1})	Zhang et al. 2013a
$Li_{1.2}Mn_{0.52}Ni_{0.2}Co_{0.08}O_2$ (5)	3.5	303 (25 mA g^{-1})	180 (1250 mA g^{-1})	92% (200, 250 mA g^{-1})	Xu et al. 2017a
$LiFePO_4$ (6)	3.4	155 (34 mA g^{-1})	78 (17,000 mA g^{-1})	89% (1000, 1700 mA g^{-1})	Wang et al. 2015a
$LiMnPO_4$ (7)	4.1	168 (8.5 mA g^{-1})	110 (1700 mA g^{-1})	94% (100, 85 mA g^{-1})	Hong et al. 2015
$LiMn_{0.75}Fe_{0.25}PO_4$ (8)	3.75	155 (85 mA g^{-1})	65 (17,000 mA g^{-1})	~ 90% (100, 85 mA g^{-1})	Wang et al. 2011a
Li_2FeSiO_4 (9)	~ 3	317 (16.6 mA g^{-1})	~ 125 (1660 mA g^{-1})	75% (2000, 1600 mA g^{-1})	Yang et al. 2016
Li_2MnSiO_4 (10)	~ 3	200 (160 mA g^{-1})	119 (160 mA g^{-1})	78% (100, 160 mA g^{-1})	He and Manthiram 2014
$LiFeBO_3$ (11)	2.7	190 (10 mA g^{-1})	70 (1600 mA g^{-1})	77% (100, 10 mA g^{-1})	Chen et al. 2015

Table 2 Electrochemical properties of representative Fe- and Mn-based cathode materials for SIBs

Electrode material (code in Fig. 20)	Average potential (V *vs.* Na^+/Na)	Discharge capacity [mAh g^{-1} (current density)]	Rate capacity [mAh g^{-1} (current density)]	Capacity retention (cycles, current density)	Ref.
$NaFeO_2$ (1)	3.3	90 (12 mA g^{-1})	–	50% (30, 12 mA g^{-1})	Yabuuchi et al. 2012b
$NaMnO_2$ (2)	2.6	190 (10 mA g^{-1})	90 (2000 mA g^{-1})	ca. 68% (50, 10 mA g^{-1})	Billaud et al. 2014a
$Na_{2/3}Mn_{0.95}Mg_{0.05}O_2$ (3)	2.7	170 (100 mA g^{-1})	106 (5000 mA g^{-1})	84% (100, 100 mA g^{-1})	Clement et al. 2016
$Na_{0.44}MnO_2$ (4)	2.8	101.3 (12 mA g^{-1})	54.7 (1200 mA g^{-1})	ca. 100% (2000, 1000 mA g^{-1})	Liu et al. 2017a
$Na_{2/3}Fe_{1/2}Mn_{1/2}O_2$ (5)	2.75	190 (12 mA g^{-1})	60 (1040 mA g^{-1})	ca. 82% (30, 12 mA g^{-1})	Yabuuchi et al. 2012a
$NaFePO_4$ (amorphous) (6)	2.32	152 (15.5 mA g^{-1})	67.4 (1550 mA g^{-1})	95% (300, 15.5 mA g^{-1})	Li et al. 2015a
$Na_2FeP_2O_7$ (7)	3.0	95 (9.7 mA g^{-1})	55 (5820 mA g^{-1})	83% (10,000, 970 mA g^{-1})	(Song et al. 2017a)
$Na_2Fe_2(SO_4)_3$ (8)	3.8	102 (6 mA g^{-1})	71 (1200 mA g^{-1})		Barpanda et al. 2014b
Na_2FePO_4F (9)	~2.75	110 (12.4 mA g^{-1})	45 (2480 mA g^{-1})	70% (5000, 1240 mA g^{-1})	Ko et al. 2017
$Na_4Fe_3(PO_4)_2(P_2O_7)$ (10)	~3	110 (6 mA g^{-1})	80 (1290 mA g^{-1})	89% (300, 64.5 mA g^{-1})	Wu et al. 2016
$Na_4Mn_3(PO_4)_2(P_2O_7)$ (11)	3.84	109 (6 mA g^{-1})	56 (1290 mA g^{-1})	82% (100, 26 mA g^{-1})	Kim et al. 2015a
$Na_4MnFe_2(PO_4)(P_2O_7)$ (12)	~3.3	110 (6 mA g^{-1})	77 (1290 mA g^{-1})	83% (3000, 129 mA g^{-1})	Kim et al. 2016a
$Na_2MnMn(CN)_6$ (13)	2.65	209 (40 mA g^{-1})	160 (1000 mA g^{-1})	75% (100, 400 mA g^{-1})	Lee et al. 2014
$Na_{0.647}Fe[Fe(CN)_6]_{0.93}$ (14)	~3.0	116 (50 mA g^{-1})	77.5 (9000 mA g^{-1})	90% (2000, 2000 mA g^{-1})	Jiang et al. 2016

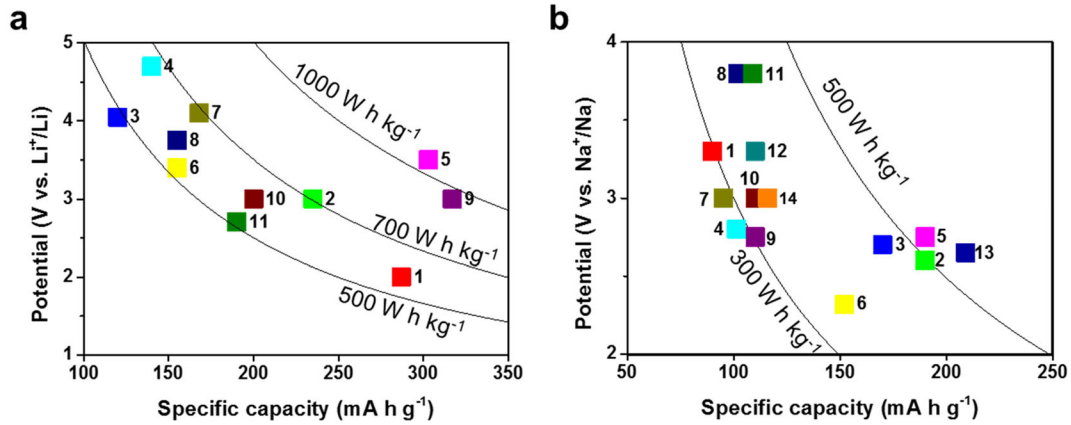

Fig. 20 Illustration of the energy densities of those Fe- and Mn-based cathode materials for LIBs (**a**) and SIBs (**b**)

Therefore, the practical difficulties regarding sulfates also exist here.

Summary and outlook

Considering the technology advances achieved on energy conversion and storage and the pressing concerns of carbon emission and environmental pollution, the transitions to clean, green, and sustainable development are practically logical and urgent. LIBs, as the state-of-the-art energy storage system, are starting to support green vehicles and residential energy storage. To meet the enlarging market, batteries themselves should adopt green and low-cost chemistries. As the costliest sector of a LIB, cathode materials involve removable Li ions as charge carriers, and transition metal ions serving as redox centers, which account for most of the cost. Given their elemental abundance, Mn- and Fe-based cathode materials are therefore preferable choices, and their sodium analogs are also attracting much attention, as they might enable the future of Li-free SIBs, which would be ideal choices for large-scale applications.

This review involves the discussion of most of the Fe- and Mn-based cathode materials for LIBs and SIBs, including oxides, polyanion compounds, and hexacyanometalates (for SIBs). We especially emphasize their merits, drawbacks, and up-to-date advances. To gain a direct view of the recently achieved electrochemical properties of those materials, we list their average operating potentials, discharge capacities (at low and high rates), and cycling performances in Table 1 (LIBs) and Table 2 (SIBs). The energy densities of those Fe- and Mn-based cathode materials are plotted in Fig. 20. From the straightforward comparison, it is easy to understand the different development phases and goals of cathode materials for LIBs and SIBs. To meet the requirement of practical applications, significant challenges in this field remain in:

1) The extensively investigated strategies of constructing conductive composites and tailoring particle size easily cause insufficient gravimetric and volumetric energy densities as well as additional materials and processing costs.
2) Due to the large size of the Na ion, conventional host structures do not favor efficient and repeatable Na ion (de)intercalation. A critical step to realizing large-scale SIB applications is to search stable and kinetic SIB cathode materials.
3) Instead of emphasizing the electrode performance of a cathode material in a half cell, the practical performance should be demonstrated in full battery level, which requires innovation in the design and optimization of both the cathode and the anode materials.

As discussed above, nanostructuring is used to boost the reactivity for many electrode materials, given that it reduce the diffusion lengths of mobile ions and electrons, which also have been reviewed intensively (Armstrong et al. 2014; Lu et al. 2016; Mahmood and Hou 2014; Myung et al. 2015; Wang et al. 2016; Zhang et al. 2015a). In the case of cathodes for LIBs, many electrode materials have been reported for outstanding rate capability (over 50 °C) and cycling performance by forming conductive composites and tailoring particle shape and size.

However, to compete with the benchmark LCO and NMC, efforts should be made to improving the gravimetric and volumetric energy densities at reduced cost. In comparison to the "external" modifications, governing the crystal and electronic structures of the host materials can alter the fundamental ionic and electronic conductivities, which can be considered as a research focus toward more practical cathode materials. Concerning SIB cathodes, which are experiencing even quicker advances with a range of candidatures being proposed, instead of simply mimicking the host structures of Li^+ during synthesis, some new complex structures have been introduced to cope with the challenges due to the distinct ionic size and electron configuration of Na^+. Although the kinetics are reduced when compared with their LIB counterparts, there are some exciting results identified during the investigation of SIB cathodes. For example, the reversible high-energy Fe^{3+}/Fe^{4+} redox couple is observed in Fe-contained layered oxides for SIBs, which is absent for LIBs. The Jahn–Teller effect of Mn^{3+}, which is always blamed for issues in LIB cathodes, is found to be "cooperative" in some SIB cathodes. These phenomena are worthwhile to be further studied, and the outputs may, in turn, stimulate the advances of LIBs. In addition, the development of a low-cost and high-performance battery requires the advance of the anode part. Current graphite anode suffers from poor ionic conductivity and poses safety concerns due to its low lithiation potential. Zero-strain hosts and dendrite-free anodes are promising candidates. We believe better understanding and development of Fe- and Mn-based cathode materials will help to make rechargeable Li-ion and Na-ion batteries cheaper, greener, and better.

Acknowledgments Funding support from ARC through its LP and DP programs is acknowledged.

Compliance with ethical standards

Conflict of interest The authors declare that they have no conflict of interest.

References

Adamczyk E, Pralong V (2017) Na2Mn3O7: a suitable electrode material for Na-Ion batteries? Chem Mater 29:4645–4648. https://doi.org/10.1021/acs.chemmater.7b01390

Ali G, Lee J-H, Susanto D, Choi S-W, Cho BW, Nam K-W, Chung KY (2016) Polythiophene-wrapped olivine NaFePO4 as a cathode for Na-Ion batteries. ACS Appl Mater Interfaces 8: 15422–15429. https://doi.org/10.1021/acsami.6b04014

Amalraj F et al (2013) Study of the lithium-rich integrated compound xLi2MnO3·(1-x)LiMO2 (x around 0.5; M = Mn, Ni, Co; 2:2:1) and its electrochemical activity as positive electrode in lithium cells. J Electrochem Soc 160:A324–A337. https://doi.org/10.1149/2.070302jes

Amine K, Tukamoto H, Yasuda H, Fujita Y (1997) Preparation and electrochemical investigation of LiMn2 − xMexO4 (Me: Ni, Fe, and x = 0.5, 1) cathode materials for secondary lithium batteries. J Power Sources 68:604–608. https://doi.org/10.1016/S0378-7753(96)02590-6

Armstrong AR, Bruce PG (1996) Synthesis of layered LiMnO2 as an electrode for rechargeable lithium batteries. Nature 381: 499–500. https://doi.org/10.1038/381499a0

Armstrong AR, Holzapfel M, Novák P, Johnson CS, Kang S-H, Thackeray MM, Bruce PG (2006) Demonstrating oxygen loss and associated structural reorganization in the lithium battery cathode Li[Ni0.2Li0.2Mn0.6]O2. J Am Chem Soc 128:8694–8698. https://doi.org/10.1021/ja062027+

Armstrong AR, Tee DW, La Mantia F, Novák P, Bruce PG (2008) Synthesis of tetrahedral LiFeO2 and Its behavior as a cathode in rechargeable lithium batteries. J Am Chem Soc 130:3554–3559. https://doi.org/10.1021/ja077651g

Armstrong AR, Kuganathan N, Islam MS, Bruce PG (2011) Structure and lithium transport pathways in Li2FeSiO4 cathodes for lithium batteries. J Am Chem Soc 133:13031–13035. https://doi.org/10.1021/ja2018543

Armstrong MJ, O'Dwyer C, Macklin WJ, Holmes JD (2014) Evaluating the performance of nanostructured materials as lithium-ion battery electrodes. Nano Res 7:1–62. https://doi.org/10.1007/s12274-013-0375-x

Arroyo-de Dompablo ME, Armand M, Tarascon JM, Amador U (2006) On-demand design of polyoxianionic cathode materials based on electronegativity correlations: an exploration of the Li2MSiO4 system (M=Fe, Mn, Co, Ni). Electrochem Commun 8:1292–1298. https://doi.org/10.1016/j.elecom.2006.06.003

Banerjee A, Araujo RB, Ahuja R (2016) Unveiling the thermodynamic and kinetic properties of NaxFe(SO4)2 (x = 0-2): toward a high-capacity and low-cost cathode material. J Mater Chem A 4:17960–17969. https://doi.org/10.1039/C6TA05330K

Banerjee A, Shilina Y, Ziv B, Ziegelbauer JM, Luski S, Aurbach D, Halalay IC (2017) On the oxidation state of manganese ions in Li-Ion battery electrolyte solutions. J Am Chem Soc 139:1738–1741. https://doi.org/10.1021/jacs.6b10781

Barpanda P, Djellab K, Recham N, Armand M, Tarascon J-M (2011) Direct and modified ionothermal synthesis of LiMnPO4 with tunable morphology for rechargeable Li-ion batteries. J Mater Chem 21:10143–10152. https://doi.org/10.1039/C0JM04423G

Barpanda P et al (2012) Sodium iron pyrophosphate: a novel 3.0V iron-based cathode for sodium-ion batteries. Electrochem Commun 24:116–119. https://doi.org/10.1016/j.elecom.2012.08.028

Barpanda P et al (2013a) Na2FeP2O7: a safe cathode for rechargeable sodium-ion batteries. Chem Mater 25:3480–3487. https://doi.org/10.1021/cm401657c

Barpanda P, Ye T, Avdeev M, Chung S-C, Yamada A (2013b) A new polymorph of Na2MnP2O7 as a 3.6 V cathode material for sodium-ion batteries. J Mater Chem A 1:4194–4197. https://doi.org/10.1039/C3TA10210F

Barpanda P, Oyama G, Ling CD, Yamada A (2014a) Kröhnkite-Type Na2Fe(SO4)2·2H2O as a novel 3.25 V insertion compound for Na-Ion batteries. Chem Mater 26:1297–1299. https://doi.org/10.1021/cm4033226

Barpanda P, Oyama G, Nishimura S-i, Chung S-C, Yamada A (2014b) A 3.8-V earth-abundant sodium battery electrode. Nat Commun 5:4358. https://doi.org/10.1038/ncomms5358 https://www.nature.com/articles/ncomms5358#supplementary-information

Berthelot R, Carlier D, Delmas C (2010) Electrochemical investigation of the P2–NaxCoO2 phase diagram. Nat Mater 10:74. https://doi.org/10.1038/nmat2920 https://www.nature.com/articles/nmat2920#supplementary-information

Billaud J, Clément RJ, Armstrong AR, Canales-Vázquez J, Rozier P, Grey CP, Bruce PG (2014a) β-NaMnO2: a high-performance cathode for sodium-ion batteries. J Am Chem Soc 136:17243–17248. https://doi.org/10.1021/ja509704t

Billaud J et al (2014b) Na0.67Mn1-xMgxO2 (0 [less-than-or-equal] x [less-than-or-equal] 0.2): a high capacity cathode for sodium-ion batteries. Energy Environ Sci 7:1387–1391. https://doi.org/10.1039/C4EE00465E

Bo S-H et al (2014) Structures of delithiated and degraded LiFeBO3, and their distinct changes upon electrochemical cycling. Inorg Chem 53:6585–6595. https://doi.org/10.1021/ic500169g

Boyadzhieva T, Koleva V, Zhecheva E, Nihtianova D, Mihaylov L, Stoyanova R (2015) Competitive lithium and sodium intercalation into sodium manganese phospho-olivine NaMnPO4 covered with carbon black. RSC Adv 5:87694–87705. https://doi.org/10.1039/C5RA17299C

Bridson JN, Quinlan SE, Tremaine PR (1998) Synthesis and crystal structure of maricite and sodium iron(III) hydroxyphosphate. Chem Mater 10:763–768. https://doi.org/10.1021/cm9704847

Cao Y et al (2011) Reversible sodium ion insertion in single crystalline manganese oxide nanowires with long cycle life. Adv Mater 23:3155–3160. https://doi.org/10.1002/adma.201100904

Catti M, Montero-Campillo M (2011) First-principles modelling of lithium iron oxides as battery cathode materials. J Power Sources 196:3955–3961. https://doi.org/10.1016/j.jpowsour.2010.11.062

Chen G, Shukla AK, Song X, Richardson TJ (2011) Improved kinetics and stabilities in Mg-substituted LiMnPO4. J Mater Chem 21:10126–10133. https://doi.org/10.1039/C0JM04230G

Chen H, Hautier G, Ceder G (2012) Synthesis, computed stability, and crystal structure of a new family of inorganic compounds: carbonophosphates. J Am Chem Soc 134:19619–19627. https://doi.org/10.1021/ja3040834

Chen H et al (2013) Sidorenkite (Na3MnPO4CO3): a new intercalation cathode material for Na-Ion batteries. Chem Mater 25:2777–2786. https://doi.org/10.1021/cm400805q

Chen H, Dawson JA, Harding JH (2014) Effects of cationic substitution on structural defects in layered cathode materials LiNiO2. J Mater Chem A 2:7988–7996. https://doi.org/10.1039/C4TA00637B

Chen Z, Cao L, Chen L, Zhou H, Zheng C, Xie K, Kuang Y (2015) Mesoporous LiFeBO3/C hollow spheres for improved stability lithium-ion battery cathodes. J Power Sources 298:355–362. https://doi.org/10.1016/j.jpowsour.2015.08.073

Chen R, Zhao T, Zhang X, Li L, Wu F (2016) Advanced cathode materials for lithium-ion batteries using nanoarchitectonics. Nanoscale Horiz 1:423–444. https://doi.org/10.1039/C6NH00016A

Cheng Q, He W, Zhang X, Li M, Wang L (2017) Modification of Li2MnSiO4 cathode materials for lithium-ion batteries: a review. J Mater Chem A 5:10772–10797. https://doi.org/10.1039/C7TA00034K

Chung SY, Bloking JT, Chiang YM (2002) Electronically conductive phospho-olivines as lithium storage electrodes. Nat Mater 1:123–128. https://doi.org/10.1038/nmat732

Clark JM, Barpanda P, Yamada A, Islam MS (2014) Sodium-ion battery cathodes Na2FeP2O7 and Na2MnP2O7: diffusion behaviour for high rate performance. J Mater Chem A 2:11807–11812. https://doi.org/10.1039/C4TA02383H

Clément RJ, Bruce PG, Grey CP (2015) Review—manganese-based P2-type transition metal oxides as sodium-ion battery cathode materials. J Electrochem Soc 162:A2589–A2604. https://doi.org/10.1149/2.0201514jes

Clement RJ, Billaud J, Robert Armstrong A, Singh G, Rojo T, Bruce PG, Grey CP (2016) Structurally stable Mg-doped P2-Na2/3Mn1-yMgyO2 sodium-ion battery cathodes with high rate performance: insights from electrochemical, NMR and diffraction studies. Energy Environ Sci 9:3240–3251. https://doi.org/10.1039/C6EE01750A

Croguennec L, Deniard P, Brec R (1997a) Electrochemical cyclability of orthorhombic LiMnO2 : characterization of cycled materials. J Electrochem Soc 144:3323–3330. https://doi.org/10.1149/1.1838013

Croguennec L, Deniard P, Brec R, Lecerf A (1997b) Nature of the stacking faults in orthorhombic LiMnO2. J Mater Chem 7:511–516. https://doi.org/10.1039/A604947H

Dai K, Mao J, Song X, Battaglia V, Liu G (2015) Na0.44MnO2 with very fast sodium diffusion and stable cycling synthesized via polyvinylpyrrolidone-combustion method. J Power Sources 285:161–168. https://doi.org/10.1016/j.jpowsour.2015.03.087

Dai Z, Mani U, Tan HT, Yan Q (2017) Advanced Cathode Materials for Sodium-Ion Batteries: What Determines Our Choices? Small Methods 1:1700098. https://doi.org/10.1002/smtd.201700098

Davidson IJ, McMillan RS, Murray JJ, Greedan JE (1995) Lithium-ion cell based on orthorhombic LiMnO2. J Power Sources 54:232–235. https://doi.org/10.1016/0378-7753(94)02074-D

de la Llave E et al (2016) Improving energy density and structural stability of manganese oxide cathodes for Na-Ion batteries by structural lithium substitution. Chem Mater 28:9064–9076. https://doi.org/10.1021/acs.chemmater.6b04078

Delacourt C, Poizot P, Morcrette M, Tarascon JM, Masquelier C (2004) One-step low-temperature route for the preparation of electrochemically active LiMnPO4 powders. Chem Mater 16:93–99. https://doi.org/10.1021/cm030347b

Delacourt C et al (2005) Toward understanding of electrical limitations (Electronic, Ionic) in LiMPO4 (M = Fe , Mn) electrode materials. J Electrochem Soc 152:A913–A921. https://doi.org/10.1149/1.1884787

Delmas C, Fouassier C, Hagenmuller P (1980) Structural classification and properties of the layered oxides. Physica B+C 99: 81–85. https://doi.org/10.1016/0378-4363(80)90214-4

Ding Z et al (2016) Three-dimensionally ordered macroporous Li2FeSiO4/C composite as a high performance cathode for advanced lithium ion batteries. J Power Sources 329:297–304. https://doi.org/10.1016/j.jpowsour.2016.08.091

Dominko R (2008) Li2MSiO4 (M=Fe and/or Mn) cathode materials. J Power Sources 184:462–468. https://doi.org/10.1016/j.jpowsour.2008.02.089

Dong XX, Huang CY, Jin Q, Zhou J, Feng P, Shi FY, Zhang DY (2017) Enhancing the rate performance of spherical LiFeBO3/C via Cr doping. RSC Adv 7:33745–33750. https://doi.org/10.1039/C7RA03028B

Dwibedi D, Araujo RB, Chakraborty S, Shanbogh PP, Sundaram NG, Ahuja R, Barpanda P (2015) Na2.44Mn1.79(SO4)3: a new member of the alluaudite family of insertion compounds for sodium ion batteries. J Mater Chem A 3:18564–18571. https://doi.org/10.1039/C5TA04527D

Ein-Eli Y, Howard WF, Lu SH, Mukerjee S, McBreen J, Vaughey JT, Thackeray MM (1998) LiMn2 − x Cu x O 4 Spinels (0.1 ⩽ x ⩽ 0.5): a new class of 5 V cathode materials for Li batteries: I. Electrochemical, Structural, and Spectroscopic Studies. J Electrochem Soc 145:1238–1244. https://doi.org/10.1149/1.1838445

Ellis BL, Makahnouk WRM, Makimura Y, Toghill K, Nazar LF (2007) A multifunctional 3.5 V iron-based phosphate cathode for rechargeable batteries. Nat Mater 6:749–753 http://www.nature.com/nmat/journal/v6/n10/suppinfo/nmat2007_S1.html

Erickson EM et al (2017) Review—recent advances and remaining challenges for lithium Ion battery cathodes: II. lithium-rich, xLi2MnO3·(1-x)LiNiaCobMncO2. J Electrochem Soc 164:A6341–A6348. https://doi.org/10.1149/2.0461701jes

Fang Y, Xiao L, Qian J, Ai X, Yang H, Cao Y (2014) Mesoporous amorphous FePO4 nanospheres as high-performance cathode material for sodium-ion batteries. Nano Lett 14:3539–3543. https://doi.org/10.1021/nl501152f

Fang Y, Liu Q, Xiao L, Ai X, Yang H, Cao Y (2015) High-performance olivine NaFePO4 microsphere cathode synthesized by aqueous electrochemical displacement method for sodium ion batteries. ACS Appl Mater Interfaces 7:17977–17984. https://doi.org/10.1021/acsami.5b04691

Fisher CAJ, Kuganathan N, Islam MS (2013) Defect chemistry and lithium-ion migration in polymorphs of the cathode material Li2MnSiO4. J Mater Chem A 1:4207–4214. https://doi.org/10.1039/C3TA00111C

Fuchs B, Kemmler-Sack S (1994) Synthesis of LiMnO2 and LiFeO2 in molten Li halides. Solid State Ionics 68:279–285. https://doi.org/10.1016/0167-2738(94)90186-4

Furuta N, Nishimura S-i, Barpanda P, Yamada A (2012) Fe3+/Fe2+ redox couple approaching 4 V in Li2–x(Fe1–yMny)P2O7 pyrophosphate cathodes. Chem Mater 24: 1055–1061. https://doi.org/10.1021/cm2032465

Gent WE et al (2017) Coupling between oxygen redox and cation migration explains unusual electrochemistry in lithium-rich layered oxides. Nat Commun 8:2091. https://doi.org/10.1038/s41467-017-02041-x

Gong Z, Yang Y (2011) Recent advances in the research of polyanion-type cathode materials for Li-ion batteries. Energy Environ Sci 4:3223–3242. https://doi.org/10.1039/C0EE00713G

Gonzalo E, Han MH, Lopez del Amo JM, Acebedo B, Casas-Cabanas M, Rojo T (2014) Synthesis and characterization of pure P2- and O3-Na2/3Fe2/3Mn1/3O2 as cathode materials for Na ion batteries. J Mater Chem A 2:18523–18530. https://doi.org/10.1039/C4TA03991B

Gu M et al (2013) Formation of the spinel phase in the layered composite cathode used in Li-Ion batteries. ACS Nano 7: 760–767. https://doi.org/10.1021/nn305065u

Gummow RJ, Dekock A, Thackeray MM (1994) Improved capacity retention in rechargeable 4v lithium lithium manganese oxide (spinel) cells. Solid State Ionics 69:59–67. https://doi.org/10.1016/0167-2738(94)90450-2

Guo H, Wu C, Xie J, Zhang S, Cao G, Zhao X (2014a) Controllable synthesis of high-performance LiMnPO4 nanocrystals by a facile one-spot solvothermal process. J Mater Chem A 2:10581–10588. https://doi.org/10.1039/C4TA01365D

Guo S et al (2014b) A high-capacity, low-cost layered sodium manganese oxide material as cathode for sodium-ion batteries. ChemSusChem 7:2115–2119. https://doi.org/10.1002/cssc.201402138

Han MH, Gonzalo E, Casas-Cabanas M, Rojo T (2014) Structural evolution and electrochemistry of monoclinic NaNiO2 upon the first cycling process. J Power Sources 258:266–271. https://doi.org/10.1016/j.jpowsour.2014.02.048

Han MH, Acebedo B, Gonzalo E, Fontecoba PS, Clarke S, Saurel D, Rojo T (2015) Synthesis and Electrochemistry Study of P2- and O3-phase Na2/3Fe1/2Mn1/2O2. Electrochim Acta 182:1029–1036. https://doi.org/10.1016/j.electacta.2015.10.003

Hasa I, Buchholz D, Passerini S, Scrosati B, Hassoun J (2014) High Performance Na0.5[Ni0.23Fe0.13Mn0.63]O2 Cathode for Sodium-Ion Batteries. Adv Energy Mater 4:1400083. https://doi.org/10.1002/aenm.201400083

Hassanzadeh N, Sadrnezhaad SK, Chen G (2016a) Ball mill assisted synthesis of Na3MnCO3PO4 nanoparticles anchored on reduced graphene oxide for sodium ion battery cathodes. Electrochim Acta 220:683–689. https://doi.org/10.1016/j.electacta.2016.10.160

Hassanzadeh N, Sadrnezhaad SK, Chen G (2016b) In-situ hydrothermal synthesis of Na3MnCO3PO4/rGO hybrid as a cathode for Na-ion battery. Electrochim Acta 208:188–194. https://doi.org/10.1016/j.electacta.2016.05.028

Hautier G, Jain A, Chen H, Moore C, Ong SP, Ceder G (2011) Novel mixed polyanions lithium-ion battery cathode materials predicted by high-throughput ab initio computations. J Mater Chem 21:17147–17153. https://doi.org/10.1039/C1JM12216A

He G, Manthiram A (2014) Nanostructured Li2MnSiO4/C cathodes with hierarchical macro-/mesoporosity for lithium-ion batteries. Adv Funct Mater 24:5277–5283. https://doi.org/10.1002/adfm.201400610

He Y, Li R, Ding X, Jiang L, Wei M (2010) Hydrothermal synthesis and electrochemical properties of orthorhombic LiMnO2 nanoplates. J Alloys Compd 492:601–604. https://doi.org/10.1016/j.jallcom.2009.11.191

He X et al (2016) Durable high-rate capability Na0.44MnO2 cathode material for sodium-ion batteries. Nano Energy 27: 602–610. https://doi.org/10.1016/j.nanoen.2016.07.021

Hirayama M, Tomita H, Kubota K, Kanno R (2011) Structure and electrode reactions of layered rocksalt LiFeO2 nanoparticles for lithium battery cathode. J Power Sources 196:6809–6814. https://doi.org/10.1016/j.jpowsour.2010.10.009

Hong Y, Tang Z, Wang S, Quan W, Zhang Z (2015) High-performance LiMnPO4 nanorods synthesized via a facile EG-assisted solvothermal approach. J Mater Chem A 3: 10267–10274. https://doi.org/10.1039/C5TA01218J

Hu J et al (2017) Tuning Li-Ion diffusion in α-LiMn1–xFexPO4 nanocrystals by antisite defects and embedded β-phase for advanced Li-Ion batteries. Nano Lett 17:4934–4940. https://doi.org/10.1021/acs.nanolett.7b01978

Huang W et al (2014) Detailed investigation of Na2.24FePO4CO3 as a cathode material for Na-ion batteries. Sci Rep 4:4188. https://doi.org/10.1038/srep04188 https://www.nature.com/articles/srep04188#supplementary-information

Huang W et al (2015a) Self-assembled alluaudite Na2Fe3−xMnx(PO4)3 micro/nanocompounds for sodium-ion battery electrodes: a new insight into their electronic and geometric structure. Chem Eur J 21:851–860. https://doi.org/10.1002/chem.201403062

Huang W et al (2015b) A new route toward improved sodium ion batteries: a multifunctional fluffy Na0.67FePO4/CNT nanocactus. Small 11:2170–2176. https://doi.org/10.1002/smll.201402246

Hy S, Liu H, Zhang M, Qian D, Hwang B-J, Meng YS (2016) Performance and design considerations for lithium excess layered oxide positive electrode materials for lithium ion batteries. Energy Environ Sci 9:1931–1954. https://doi.org/10.1039/C5EE03573B

Islam MS, Dominko R, Masquelier C, Sirisopanaporn C, Armstrong AR, Bruce PG (2011) Silicate cathodes for lithium batteries: alternatives to phosphates? J Mater Chem 21: 9811–9818. https://doi.org/10.1039/C1JM10312A

Jang DH, Shin YJ, Oh SM (1996) Dissolution of Spinel Oxides and Capacity Losses in 4 V Li / Li x Mn2 O 4 Cells. J Electrochem Soc 143:2204–2211. https://doi.org/10.1149/1.1836981

Jarry A et al (2015) The formation mechanism of fluorescent metal complexes at the LixNi0.5Mn1.5O4−δ/carbonate ester electrolyte interface. J Am Chem Soc 137:3533–3539. https://doi.org/10.1021/ja5116698

Jarvis K, Deng Z, Manthiram A, Ferreira P (2012) Understanding the role of lithium content on the structure and capacity of lithium-rich layered oxides by aberration-corrected STEM, D-STEM, and EDS. Microsc Microanal 18:1484–1485. https://doi.org/10.1017/S1431927612009270

Jiang Y et al (2016) Prussian Blue@C composite as an ultrahigh-rate and long-life sodium-ion battery cathode. Adv Funct Mater 26:5315–5321. https://doi.org/10.1002/adfm.201600747

Jin Y-C, Lin C-Y, Duh J-G (2012) Improving rate capability of high potential LiNi0.5Mn1.5O4-x cathode materials via increasing oxygen non-stoichiometries. Electrochim Acta 69: 45–50. https://doi.org/10.1016/j.electacta.2012.02.022

Kang B, Ceder G (2009) Battery materials for ultrafast charging and discharging. Nature 458:190–193. https://doi.org/10.1038/nature07853

Kang K, Meng YS, Bréger J, Grey CP, Ceder G (2006) Electrodes with high power and high capacity for rechargeable lithium batteries. Science 311:977–980. https://doi.org/10.1126/science.1122152

Kawabe Y et al (2011) Synthesis and electrode performance of carbon coated Na2FePO4F for rechargeable Na batteries. Electrochem Commun 13:1225–1228. https://doi.org/10.1016/j.elecom.2011.08.038

Kawai H, Nagata M, Tukamoto H, Westa AR (1998) A new lithium cathode LiCoMnO4: toward practical 5 V lithium batteries. Electrochem Solid-State Lett 1:212–214. https://doi.org/10.1149/1.1390688

Kikkawa S, Miyazaki S, Koizumi M (1985) Sodium deintercalation from α-NaFeO2. Mater Res Bull 20:373–377. https://doi.org/10.1016/0025-5408(85)90003-0

Kim JH, Myung ST, Yoon CS, Kang SG, Sun YK (2004) Comparative study of LiNi0.5Mn1.5O4-delta and LiNi0.5Mn1.5O4 cathodes having two crystallographic structures: Fd(3)over-barm and P4(3)32. Chem Mater 16: 906–914. https://doi.org/10.1021/cm035050s

Kim JC, Moore CJ, Kang B, Hautier G, Jain A, Ceder G (2011) Synthesis and electrochemical properties of monoclinic LiMnBO3 as a Li intercalation material. J Electrochem Soc 158:A309–A315. https://doi.org/10.1149/1.3536532

Kim D, Lee E, Slater M, Lu W, Rood S, Johnson CS (2012a) Layered Na[Ni1/3Fe1/3Mn1/3]O2 cathodes for Na-ion battery application. Electrochem Commun 18:66–69. https://doi.org/10.1016/j.elecom.2012.02.020

Kim H et al (2012b) New iron-based mixed-polyanion cathodes for lithium and sodium rechargeable batteries: combined first principles calculations and experimental study. J Am Chem Soc 134:10369–10372. https://doi.org/10.1021/ja3038646

Kim H et al (2013a) Understanding the electrochemical mechanism of the new iron-based mixed-phosphate Na4Fe3(PO4)2(P2O7) in a Na rechargeable battery. Chem Mater 25:3614–3622. https://doi.org/10.1021/cm4013816

Kim H et al (2013b) Na2FeP2O7 as a promising iron-based pyrophosphate cathode for sodium rechargeable batteries: a combined experimental and theoretical study. Adv Funct Mater 23:1147–1155. https://doi.org/10.1002/adfm.201201589

Kim Y, Ha K-H, Oh SM, Lee KT (2014) High-capacity anode materials for sodium-ion batteries. Chem Eur J 20:11980–11992. https://doi.org/10.1002/chem.201402511

Kim H et al (2015a) Anomalous Jahn-Teller behavior in a manganese-based mixed-phosphate cathode for sodium ion batteries. Energy Environ Sci 8:3325–3335. https://doi.org/10.1039/C5EE01876E

Kim J et al (2015b) Unexpected discovery of low-cost maricite NaFePO4 as a high-performance electrode for Na-ion batteries. Energy Environ Sci 8:540–545. https://doi.org/10.1039/C4EE03215B

Kim JC, Seo D-H, Chen H, Ceder G (2015c) The effect of antisite disorder and particle size on Li intercalation kinetics in monoclinic LiMnBO3. Adv Energy Mater 5:1401916. https://doi.org/10.1002/aenm.201401916

Kim H et al (2016a) Highly stable iron- and manganese-based cathodes for long-lasting sodium rechargeable batteries. Chem Mater 28:7241–7249. https://doi.org/10.1021/acs.chemmater.6b01766

Kim M-S et al (2016b) Synthesis of reduced graphene oxide-modified LiMn0.75Fe0.25PO4 microspheres by salt-assisted spray drying for high-performance lithium-ion

batteries. Sci Rep 6:26686. https://doi.org/10.1038/srep26686 https://www.nature.com/articles/srep26686#supplementary-information

Ko JS et al (2017) High-rate capability of Na2FePO4F nanoparticles by enhancing surface carbon functionality for Na-ion batteries. J Mater Chem A 5:18707–18715. https://doi.org/10.1039/C7TA05680J

Koga H et al (2012) Li1.20Mn0.54Co0.13Ni0.13O2 with different particle sizes as attractive positive electrode materials for lithium-ion batteries: insights into their structure. J Phys Chem C 116:13497–13506. https://doi.org/10.1021/jp301879x

Kokalj A, Dominko R, Mali G, Meden A, Gaberscek M, Jamnik J (2007) Beyond one-electron reaction in Li cathode materials: designing Li2MnxFe1-xSiO4. Chem Mater 19:3633–3640. https://doi.org/10.1021/cm0630111

Komaba S, Takei C, Nakayama T, Ogata A, Yabuuchi N (2010) Electrochemical intercalation activity of layered NaCrO2 vs. LiCrO2. Electrochem Commun 12:355–358. https://doi.org/10.1016/j.elecom.2009.12.033

Kumakura S, Tahara Y, Kubota K, Chihara K, Komaba S (2016) Sodium and manganese stoichiometry of P2-Type Na2/3MnO2. Angew Chem Int Ed 55:12760–12763. https://doi.org/10.1002/anie.201606415

Kumakura S, Tahara Y, Sato S, Kubota K, Komaba S (2017) P′2-Na2/3Mn0.9Me0.1O2 (Me = Mg, Ti, Co, Ni, Cu, and Zn): correlation between orthorhombic distortion and electrochemical property. Chem Mater 29:8958–8962. https://doi.org/10.1021/acs.chemmater.7b02772

Kwon M-S, Lim SG, Park Y, Lee S-M, Chung KY, Shin TJ, Lee KT (2017) P2 Orthorhombic Na0.7[Mn1–xLix]O2+y as cathode materials for Na-Ion batteries. ACS Appl Mater Interfaces 9:14758–14768. https://doi.org/10.1021/acsami.7b00058

Larcher D, Tarascon JM (2015) Towards greener and more sustainable batteries for electrical energy storage. Nat Chem 7:19–29. https://doi.org/10.1038/nchem.2085

Law M, Ramar V, Balaya P (2015) Synthesis, characterisation and enhanced electrochemical performance of nanostructured Na2FePO4F for sodium batteries. RSC Adv 5:50155–50164. https://doi.org/10.1039/C5RA07583A

Lee KT, Ramesh TN, Nan F, Botton G, Nazar LF (2011) Topochemical synthesis of sodium metal phosphate olivines for sodium-ion batteries. Chem Mater 23:3593–3600. https://doi.org/10.1021/cm200450y

Lee H-W, Wang RY, Pasta M, Woo Lee S, Liu N, Cui Y (2014) Manganese hexacyanomanganate open framework as a high-capacity positive electrode material for sodium-ion batteries. Nat Commun 5:5280. https://doi.org/10.1038/ncomms6280 https://www.nature.com/articles/ncomms6280#supplementary-information

Lee E, Brown DE, Alp EE, Ren Y, Lu J, Woo J-J, Johnson CS (2015) New insights into the performance degradation of Fe-Based layered oxides in sodium-ion batteries: instability of Fe3+/Fe4+ redox in α-NaFeO2. Chem Mater 27:6755–6764. https://doi.org/10.1021/acs.chemmater.5b02918

Lee M-J, Lho E, Bai P, Chae S, Li J, Cho J (2017) Low-temperature carbon coating of nanosized Li1.015Al0.06Mn1.925O4 and high-density electrode for high-power Li-Ion batteries. Nano Lett 17:3744–3751. https://doi.org/10.1021/acs.nanolett.7b01076

Legagneur V et al (2001) LiMBO3 (M=Mn, Fe, Co):: synthesis, crystal structure and lithium deinsertion/insertion properties. Solid State Ionics 139:37–46. https://doi.org/10.1016/S0167-2738(00)00813-4

Lei Y, Li X, Liu L, Ceder G (2014) Synthesis and stoichiometry of different layered sodium cobalt oxides. Chem Mater 26:5288–5296. https://doi.org/10.1021/cm5021788

Li G, Azuma H, Tohda M (2002) LiMnPO4 as the cathode for lithium batteries. Electrochem Solid-State Lett 5:A135–A137. https://doi.org/10.1149/1.1475195

Li J, Li J, Luo J, Wang L, He X (2011) Recent advances in the LiFeO2-based materials for Li-ion batteries. Int J Electrochem Sci 6:1550–1561

Li BZ, Wang Y, Xue L, Li XP, Li WS (2013) Acetylene black-embedded LiMn0.8Fe0.2PO4/C composite as cathode for lithium ion battery. J Power Sources 232:12–16. https://doi.org/10.1016/j.jpowsour.2013.01.019

Li C, Miao X, Chu W, Wu P, Tong DG (2015a) Hollow amorphous NaFePO4 nanospheres as a high-capacity and high-rate cathode for sodium-ion batteries. J Mater Chem A 3:8265–8271. https://doi.org/10.1039/C5TA01191D

Li J, Ma C, Chi M, Liang C, Dudney NJ (2015b) Solid Electrolyte: the Key for High-Voltage Lithium Batteries. Adv Energy Mater 5:1401408. https://doi.org/10.1002/aenm.201401408

Li Y et al (2015c) Air-Stable Copper-Based P2-Na7/9Cu2/9Fe1/9Mn2/3O2 as a New Positive Electrode Material for Sodium-Ion Batteries. Adv Sci 2:1500031. https://doi.org/10.1002/advs.201500031

Li D et al (2016) Soft-template construction of three-dimensionally ordered inverse opal structure from Li2FeSiO4/C composite nanofibers for high-rate lithium-ion batteries. Nanoscale 8:12202–12214. https://doi.org/10.1039/C5NR07783D

Lin X, Hou X, Wu X, Wang S, Gao M, Yang Y (2014) Exploiting Na2MnPO4F as a high-capacity and well-reversible cathode material for Na-ion batteries. RSC Adv 4:40985–40993. https://doi.org/10.1039/C4RA05336B

Liu Q, Mao D, Chang C, Huang F (2007) Phase conversion and morphology evolution during hydrothermal preparation of orthorhombic LiMnO2 nanorods for lithium ion battery application. J Power Sources 173:538–544. https://doi.org/10.1016/j.jpowsour.2007.03.077

Liu D et al (2012a) Synthesis of pure phase disordered LiMn1.45Cr0.1Ni0.45O4 by a post-annealing method. J Power Sources 217:400–406. https://doi.org/10.1016/j.jpowsour.2012.06.063

Liu Y et al (2012b) Porous amorphous FePO4 nanoparticles connected by single-wall carbon nanotubes for sodium ion battery cathodes. Nano Lett 12:5664–5668. https://doi.org/10.1021/nl302819f

Liu X, Wang X, Iyo A, Yu H, Li D, Zhou H (2014) High stable post-spinel NaMn2O4 cathode of sodium ion battery. J Mater Chem A 2:14822–14826. https://doi.org/10.1039/C4TA03349C

Liu L et al (2015a) High-Performance P2-Type Na2/3(Mn1/2Fe1/4Co1/4)O2 Cathode Material with Superior Rate Capability for Na-Ion Batteries. Adv Energy Mater 5:1500944. https://doi.org/10.1002/aenm.201500944

Liu Y, Xu S, Zhang S, Zhang J, Fan J, Zhou Y (2015b) Direct growth of FePO4/reduced graphene oxide nanosheet

composites for the sodium-ion battery. J Mater Chem A 3: 5501–5508. https://doi.org/10.1039/C5TA00199D

Liu C, Neale ZG, Cao G (2016a) Understanding electrochemical potentials of cathode materials in rechargeable batteries. Mater Today 19:109–123. https://doi.org/10.1016/j.mattod.2015.10.009

Liu H, Ji P, Han X (2016b) Rheological phase synthesis of nanosized α-LiFeO2 with higher crystallinity degree for cathode material of lithium-ion batteries. Mater Chem Phys 183:152–157. https://doi.org/10.1016/j.matchemphys.2016.08.013

Liu Q et al (2017a) Multiangular rod-shaped Na0.44MnO2 as cathode materials with high rate and long life for sodium-ion batteries. ACS Appl Mater Interfaces 9:3644–3652. https://doi.org/10.1021/acsami.6b13830

Liu Y, Zhou Y, Zhang J, Xia Y, Chen T, Zhang S (2017b) Monoclinic phase Na3Fe2(PO4)3: synthesis, structure, and electrochemical performance as cathode material in sodium-ion batteries. ACS Sustain Chem Eng 5:1306–1314. https://doi.org/10.1021/acssuschemeng.6b01536

Lu J, Yamada A (2016) Ionic and electronic transport in alluaudite Na2+2xFe2−x(SO4)3. ChemElectroChem 3:902–905. https://doi.org/10.1002/celc.201500535

Lu Y, Wang L, Cheng J, Goodenough JB (2012) Prussian blue: a new framework of electrode materials for sodium batteries. Chem Commun 48:6544–6546. https://doi.org/10.1039/C2CC31777J

Lu J, Chen Z, Ma Z, Pan F, Curtiss LA, Amine K (2016) The role of nanotechnology in the development of battery materials for electric vehicles. Nat Nanotechnol 11:1031. https://doi.org/10.1038/nnano.2016.207

Luo C, Langrock A, Fan X, Liang Y, Wang C (2017) P2-type transition metal oxides for high performance Na-ion battery cathodes. J Mater Chem A 5:18214–18220. https://doi.org/10.1039/C7TA04515H

Ma X, Kang B, Ceder G (2010) High rate micron-sized ordered LiNi0.5Mn1.5O4. J Electrochem Soc 157:A925–A931. https://doi.org/10.1149/1.3439678

Ma X, Chen H, Ceder G (2011) Electrochemical properties of monoclinic NaMnO2. J Electrochem Soc 158:A1307–A1312. https://doi.org/10.1149/2.035112jes

MacNeil DD, Lu Z, Chen Z, Dahn JR (2002) A comparison of the electrode/electrolyte reaction at elevated temperatures for various Li-ion battery cathodes. J Power Sources 108:8–14. https://doi.org/10.1016/S0378-7753(01)01013-8

Mahmood N, Hou Y (2014) Electrode nanostructures in lithium-based Batteries. Adv Sci 1:1400012. https://doi.org/10.1002/advs.201400012

Manthiram A, Knight JC, Myung S-T, Oh S-M, Sun Y-K (2016) Nickel-Rich and lithium-rich layered oxide cathodes: progress and perspectives. Adv Energy Mater 6:1501010. https://doi.org/10.1002/aenm.201501010

Martha SK et al (2009a) LiMn0.8Fe0.2PO4: an advanced cathode material for rechargeable lithium batteries. Angew Chem Int Ed 48:8559–8563. https://doi.org/10.1002/anie.200903587

Martha SK et al (2009b) LiMnPO4 as an advanced cathode material for rechargeable lithium batteries. J Electrochem Soc 156:A541–A552. https://doi.org/10.1149/1.3125765

Masquelier C, Croguennec L (2013) Polyanionic (Phosphates, Silicates, Sulfates) frameworks as electrode materials for rechargeable Li (or Na) batteries. Chem Rev 113:6552–6591

Matsumura T, Kanno R, Inaba Y, Kawamoto Y, Takano M (2002) Synthesis, structure, and electrochemical properties of a new cathode material, LiFeO2, with a tunnel structure. J Electrochem Soc 149:A1509–A1513. https://doi.org/10.1149/1.1516769

Meethong N, Kao Y-H, Tang M, Huang H-Y, Carter WC, Chiang Y-M (2008) Electrochemically induced phase transformation in nanoscale olivines Li1−xMPO4 (M = Fe, Mn). Chem Mater 20:6189–6198. https://doi.org/10.1021/cm801722f

Meng Y, Yu T, Zhang S, Deng C (2016) Top-down synthesis of muscle-inspired alluaudite Na2+2xFe2-x(SO4)3/SWNT spindle as a high-rate and high-potential cathode for sodium-ion batteries. J Mater Chem A 4:1624–1631. https://doi.org/10.1039/C5TA07696J

Mizushima K, Jones PC, Wiseman PJ, Goodenough JB (1980) Lixcoo2 (oless-thanxless-than-or-equal-to1)—a new cathode material for batteries of high-energy density. Mater Res Bull 15:783–789. https://doi.org/10.1016/0025-5408(80)90012-4

Mohanty D et al (2013) Structural transformation of a lithium-rich Li1.2Co0.1Mn0.55Ni0.15O2 cathode during high voltage cycling resolved by in situ X-ray diffraction. J Power Sources 229:239–248. https://doi.org/10.1016/j.jpowsour.2012.11.144

Morales J, Santos-Peña J (2007) Highly electroactive nanosized α-LiFeO2. Electrochem Commun 9:2116–2120. https://doi.org/10.1016/j.elecom.2007.06.013

Moreau P, Guyomard D, Gaubicher J, Boucher F (2010) Structure and stability of sodium intercalated phases in olivine FePO4. Chem Mater 22:4126–4128. https://doi.org/10.1021/cm101377h

Mortemard de Boisse B, Carlier D, Guignard M, Bourgeois L, Delmas C (2014) P2-NaxMn1/2Fe1/2O2 phase used as positive electrode in na batteries: structural changes induced by the electrochemical (De)intercalation process. Inorg Chem 53:11197–11205. https://doi.org/10.1021/ic5017802

Muraliganth T, Stroukoff KR, Manthiram A (2010) Microwave-solvothermal synthesis of nanostructured Li2MSiO4/C (M = Mn and Fe) cathodes for lithium-ion batteries. Chem Mater 22:5754–5761. https://doi.org/10.1021/cm102058n

Myung S-T, Amine K, Sun Y-K (2015) Nanostructured cathode materials for rechargeable lithium batteries. J Power Sources 283:219–236. https://doi.org/10.1016/j.jpowsour.2015.02.119

Naoaki Y, Shinichi K (2014) Recent research progress on iron- and manganese-based positive electrode materials for rechargeable sodium batteries. Sci Technol Adv Mater 15:043501

Naoi K et al (2016) Ultrafast charge-discharge characteristics of a nanosized core-shell structured LiFePO4 material for hybrid supercapacitor applications. Energy Environ Sci 9:2143–2151. https://doi.org/10.1039/C6EE00829A

Ni J, Jiang Y, Bi X, Li L, Lu J (2017) Lithium iron orthosilicate cathode: progress and perspectives. ACS Energy Lett 2: 1771–1781. https://doi.org/10.1021/acsenergylett.7b00452

Nie ZX et al (2010) First principles study of Jahn–Teller effects in LixMnPO4. Solid State Commun 150:40–44. https://doi.org/10.1016/j.ssc.2009.10.010

Nishimura S-i, Nakamura M, Natsui R, Yamada A (2010) New lithium iron pyrophosphate as 3.5 V class cathode material for lithium ion battery. J Am Chem Soc 132:13596–13597. https://doi.org/10.1021/ja106297a

Nitta Y, Okamura K, Haraguchi K, Kobayashi S, Ohata A (1995) Crystal structure study of LiNi1−xMnxO2. J Power Sources 54:511–515. https://doi.org/10.1016/0378-7753(94)02137-R

Nitta N, Wu F, Lee JT, Yushin G (2015) Li-ion battery materials: present and future. Mater Today 18:252–264. https://doi.org/10.1016/j.mattod.2014.10.040

Norberg NS, Kostecki R (2012) The degradation mechanism of a composite LiMnPO4 cathode. J Electrochem Soc 159: A1431–A1434. https://doi.org/10.1149/2.018209jes

Nytén A, Abouimrane A, Armand M, Gustafsson T, Thomas JO (2005) Electrochemical performance of Li2FeSiO4 as a new Li-battery cathode material. Electrochem Commun 7:156–160. https://doi.org/10.1016/j.elecom.2004.11.008

Oh S-M, Oh S-W, Yoon C-S, Scrosati B, Amine K, Sun Y-K (2010) High-performance carbon-LiMnPO4 nanocomposite cathode for lithium batteries. Adv Funct Mater 20:3260–3265. https://doi.org/10.1002/adfm.201000469

Oh S-M, Myung S-T, Hassoun J, Scrosati B, Sun Y-K (2012) Reversible NaFePO4 electrode for sodium secondary batteries. Electrochem Commun 22:149–152. https://doi.org/10.1016/j.elecom.2012.06.014

Ohzuku T, Ueda A, Nagayama M (1993) Electrochemistry and structural chemistry of LiNiO2 ($R\bar{3}m$) for 4 volt secondary lithium cells. J Electrochem Soc 140:1862–1870. https://doi.org/10.1149/1.2220730

Ohzuku T, Takeda S, Iwanaga M (1999) Solid-state redox potentials for Li [Me1/2Mn3/2] O4 (Me: 3d-transition metal) having spinel-framework structures: a series of 5 volt materials for advanced lithium-ion batteries. J Power Sources 81:90–94

Okada S, Takahashi Y, Kiyabu T, Doi T, Yamaki J-I, Nishida T (2006) Layered transition metal oxides as cathodes for sodium secondary battery meeting abstracts MA2006-02:201

Ong SP, Chevrier VL, Ceder G (2011) Comparison of small polaron migration and phase separation in olivine LiMnPO${}_{4}$ and LiFePO${}_{4}$ using hybrid density functional theory. Phys Rev B 83:075112

Oyama G, Pecher O, Griffith KJ, Nishimura S-i, Pigliapochi R, Grey CP, Yamada A (2016) Sodium intercalation mechanism of 3.8 V class alluaudite sodium iron sulfate. Chem Mater 28: 5321–5328. https://doi.org/10.1021/acs.chemmater.6b01091

Palomares V, Serras P, Villaluenga I, Hueso KB, Carretero-Gonzalez J, Rojo T (2012) Na-ion batteries, recent advances and present challenges to become low cost energy storage systems. Energy Environ Sci 5:5884–5901. https://doi.org/10.1039/c2ee02781j

Paolella A et al (2014) Etched colloidal LiFePO4 nanoplatelets toward high-rate capable Li-Ion battery electrodes. Nano Lett 14:6828–6835. https://doi.org/10.1021/nl504093w

Parant J-P, Olazcuaga R, Devalette M, Fouassier C, Hagenmuller P (1971) Sur quelques nouvelles phases de formule NaxMnO2 ($x \leqslant 1$). J Solid State Chem 3:1–11. https://doi.org/10.1016/0022-4596(71)90001-6

Park CS et al (2013) Anomalous manganese activation of a pyrophosphate cathode in sodium ion batteries: a combined experimental and theoretical study. J Am Chem Soc 135:2787–2792. https://doi.org/10.1021/ja312044k

Paulsen JM, Dahn JR (1999) Studies of the layered manganese bronzes, Na2/3[Mn1−xMx]O2 with M=Co, Ni, Li, and Li2/3[Mn1−xMx]O2 prepared by ion-exchange. Solid State Ionics 126:3–24. https://doi.org/10.1016/S0167-2738(99)00147-2

Pei Y et al (2016) Chelate-induced formation of Li2MnSiO4 nanorods as a high capacity cathode material for Li-ion batteries. J Mater Chem A 4:9447–9454. https://doi.org/10.1039/C6TA01269H

Pivko M, Bele M, Tchernychova E, Logar NZ, Dominko R, Gaberscek M (2012) Synthesis of nanometric LiMnPO4 via a two-step technique. Chem Mater 24:1041–1047. https://doi.org/10.1021/cm203095d

Qin Z, Zhou X, Xia Y, Tang C, Liu Z (2012) Morphology controlled synthesis and modification of high-performance LiMnPO4 cathode materials for Li-ion batteries. J Mater Chem 22:21144–21153. https://doi.org/10.1039/C2JM30821E

Rahman MM, Wang J-Z, Hassan MF, Chou S, Chen Z, Liu HK (2011) Nanocrystalline porous α-LiFeO2-C composite-an environmentally friendly cathode for the lithium-ion battery. Energ Environ Sci 4:952–957. https://doi.org/10.1039/C0EE00527D

Ramar V, Balaya P (2016) The effect of polymorphism on the lithium storage performance of Li2MnSiO4. J Power Sources 306:552–558. https://doi.org/10.1016/j.jpowsour.2015.12.033

Rangappa D, Murukanahally KD, Tomai T, Unemoto A, Honma I (2012) Ultrathin nanosheets of Li2MSiO4 (M = Fe, Mn) as high-capacity Li-Ion battery electrode. Nano Lett 12:1146–1151. https://doi.org/10.1021/nl202681b

Ravnsbæk DB et al (2014) Extended solid solutions and coherent transformations in nanoscale olivine cathodes. Nano Lett 14: 1484–1491. https://doi.org/10.1021/nl404679t

Ravnsbæk DB et al (2016) Engineering the transformation strain in LiMnyFe1–yPO4 olivines for ultrahigh rate battery cathodes. Nano Lett 16:2375–2380. https://doi.org/10.1021/acs.nanolett.5b05146

Rossen E, Jones CDW, Dahn JR (1992) Structure and electrochemistry of LixMnyNi1−yO2. Solid State Ionics 57:311–318. https://doi.org/10.1016/0167-2738(92)90164-K

Rossouw MH, Liles DC, Thackeray MM (1993) Synthesis and structural characterization of a novel layered lithium manganese oxide, Li0.36Mn0.91O2, and its lithiated derivative, Li1.09Mn0.91O2. J Solid State Chem 104:464–466. https://doi.org/10.1006/jssc.1993.1182

Sakurai Y, Arai H, Okada S, Yamaki J-i (1997) Low temperature synthesis and electrochemical characteristics of LiFeO2 cathodes. J Power Sources 68:711–715. https://doi.org/10.1016/S0378-7753(96)02579-7

Sauvage F, Laffont L, Tarascon JM, Baudrin E (2007) Study of the insertion/deinsertion mechanism of sodium into Na0.44MnO2. Inorg Chem 46:3289–3294. https://doi.org/10.1021/ic0700250

Seo D-H, Park Y-U, Kim S-W, Park I, Shakoor RA, Kang K (2011) First-principles study on lithium metal borate cathodes for lithium rechargeable batteries. Phys Rev B 83: 205127

Shaju KM, Subba Rao GV, Chowdari BVR (2002) Performance of layered Li(Ni1/3Co1/3Mn1/3)O2 as cathode for Li-ion batteries. Electrochim Acta 48:145–151. https://doi.org/10.1016/S0013-4686(02)00593-5

Sharma N et al (2015) Rate dependent performance related to crystal structure evolution of Na0.67Mn0.8Mg0.2O2 in a

sodium-ion battery. Chem Mater 27:6976–6986. https://doi.org/10.1021/acs.chemmater.5b02142

Sharma N, Bahri OKA, Han MH, Gonzalo E, Pramudita JC, Rojo T (2016) Comparison of the structural evolution of the O3 and P2 phases of Na2/3Fe2/3Mn1/3O2 during electrochemical cycling. Electrochim Acta 203:189–197. https://doi.org/10.1016/j.electacta.2016.04.008

Shirane T, Kanno R, Kawamoto Y, Takeda Y, Takano M, Kamiyama T, Izumi F (1995) Structure and physical properties of lithium iron oxide, LiFeO2, synthesized by ionic exchange reaction. Solid State Ionics 79:227–233. https://doi.org/10.1016/0167-2738(95)00066-F

Shukla AK, Ramasse QM, Ophus C, Duncan H, Hage F, Chen G (2015) Unravelling structural ambiguities in lithium- and manganese-rich transition metal oxides. Nat Commun 6:8711. https://doi.org/10.1038/ncomms9711 https://www.nature.com/articles/ncomms9711#supplementary-information

Sigala C, Guyomard D, Verbaere A, Piffard Y, Tournoux M (1995) Positive electrode materials with high operating voltage for lithium batteries: LiCryMn2 − yO4 ($0 \le y \le 1$). Solid State Ionics 81:167–170. https://doi.org/10.1016/0167-2738(95)00163-Z

Singh P, Shiva K, Celio H, Goodenough JB (2015) Eldfellite, NaFe(SO4)2: an intercalation cathode host for low-cost Na-ion batteries. Energ Environ Sci 8:3000–3005. https://doi.org/10.1039/C5EE02274F

Slater MD, Kim D, Lee E, Johnson CS (2013) Sodium-ion batteries. Adv Funct Mater 23:947–958. https://doi.org/10.1002/adfm.201200691

Song J et al (2015) Removal of interstitial H2O in hexacyanometallates for a superior cathode of a sodium-ion battery. J Am Chem Soc 137:2658–2664. https://doi.org/10.1021/ja512383b

Song HJ, Kim D-S, Kim J-C, Hong S-H, Kim D-W (2017a) An approach to flexible Na-ion batteries with exceptional rate capability and long lifespan using Na2FeP2O7 nanoparticles on porous carbon cloth. J Mater Chem A 5:5502–5510. https://doi.org/10.1039/C7TA00727B

Song HJ, Kim K-H, Kim J-C, Hong S-H, Kim D-W (2017b) Superior sodium storage performance of reduced graphene oxide-supported Na3.12Fe2.44(P2O7)2/C nanocomposites. Chem Commun 53:9316–9319. https://doi.org/10.1039/C7CC01812F

Sun Y, Lu X, Xiao R, Li H, Huang X (2012) Kinetically controlled lithium-staging in delithiated LiFePO4 driven by the Fe center mediated interlayer Li–Li interactions. Chem Mater 24:4693–4703. https://doi.org/10.1021/cm3028324

Tabuchi M, Ado K, Sakaebe H, Masquelier C, Kageyama H, Nakamura O (1995) Preparation of AFeO2 (A = Li, Na) by hydrothermal method. Solid State Ionics 79:220–226. https://doi.org/10.1016/0167-2738(95)00065-E

Tabuchi M, Nabeshima Y, Takeuchi T, Tatsumi K, Imaizumi J, Nitta Y (2010) Fe content effects on electrochemical properties of Fe-substituted Li2MnO3 positive electrode material. J Power Sources 195:834–844. https://doi.org/10.1016/j.jpowsour.2009.08.059

Takeda Y, Nakahara K, Nishijima M, Imanishi N, Yamamoto O, Takano M, Kanno R (1994) Sodium deintercalation from sodium iron oxide. Mater Res Bull 29:659–666. https://doi.org/10.1016/0025-5408(94)90122-8

Talaie E, Duffort V, Smith HL, Fultz B, Nazar LF (2015) Structure of the high voltage phase of layered P2-Na2/3-z[Mn1/2Fe1/2]O2 and the positive effect of Ni substitution on its stability. Energy Environ Sci 8:2512–2523. https://doi.org/10.1039/C5EE01365H

Talyosef Y, Markovsky B, Salitra G, Aurbach D, Kim HJ, Choi S (2005) The study of LiNi0.5Mn1.5O4 5-V cathodes for Li-ion batteries. J Power Sources 146:664–669. https://doi.org/10.1016/j.jpowsour.2005.03.064

Tao L et al (2014) Preparation, structure and electrochemistry of LiFeBO3: a cathode material for Li-ion batteries. J Mater Chem A 2:2060–2070. https://doi.org/10.1039/C3TA13021E

Thackeray MM, David WIF, Bruce PG, Goodenough JB (1983) Lithium insertion into manganese spinels. Mater Res Bull 18:461–472. https://doi.org/10.1016/0025-5408(83)90138-1

Thackeray MM, Johnson PJ, de Picciotto LA, Bruce PG, Goodenough JB (1984) Electrochemical extraction of lithium from LiMn2O4. Mater Res Bull 19:179–187. https://doi.org/10.1016/0025-5408(84)90088-6

Thackeray MM, Kang S-H, Johnson CS, Vaughey JT, Benedek R, Hackney SA (2007) Li2MnO3-stabilized LiMO2 (M = Mn, Ni, Co) electrodes for lithium-ion batteries. J Mater Chem 17:3112–3125. https://doi.org/10.1039/B702425H

Thackeray MM, Wolverton C, Isaacs ED (2012) Electrical energy storage for transportation-approaching the limits of, and going beyond, lithium-ion batteries. Energ Environ Sci 5:7854–7863. https://doi.org/10.1039/C2EE21892E

Thorne JS, Dunlap RA, Obrovac MN (2013) Structure and electrochemistry of NaxFexMn1-xO2 ($1.0 \le x \le 0.5$) for Na-Ion battery positive electrodes. J Electrochem Soc 160:A361–A367. https://doi.org/10.1149/2.058302jes

Trad K, Carlier D, Croguennec L, Wattiaux A, Ben Amara M, Delmas C (2010a) NaMnFe2(PO4)3 alluaudite phase: synthesis, structure, and electrochemical properties as positive electrode in lithium and sodium batteries. Chem Mater 22:5554–5562. https://doi.org/10.1021/cm1015614

Trad K, Carlier D, Croguennec L, Wattiaux A, Lajmi B, Ben Amara M, Delmas C (2010b) A layered iron(III) phosphate phase, Na3Fe3(PO4)4: synthesis, structure, and electrochemical properties as positive electrode in sodium batteries. J Phys Chem C 114:10034–10044. https://doi.org/10.1021/jp100751b

Tripathi R, Wood SM, Islam MS, Nazar LF (2013) Na-ion mobility in layered Na2FePO4F and olivine Na[Fe,Mn]PO4. Energy Environ Sci 6:2257–2264. https://doi.org/10.1039/C3EE40914G

Tsutomu O, Yoshinari M (2001) Layered lithium insertion material of LiCo1/3Ni1/3Mn1/3O2 for lithium-ion batteries. Chem Lett 30:642–643. https://doi.org/10.1246/cl.2001.642

Wang H et al (2011a) LiMn1−xFexPO4 nanorods grown on graphene sheets for ultrahigh-rate-performance lithium ion batteries. Angew Chem Int Ed 50:7364–7368. https://doi.org/10.1002/anie.201103163

Wang L, Li H, Huang X, Baudrin E (2011b) A comparative study of Fd-3m and P4332 "LiNi0.5Mn1.5O4". Solid State Ionics 193:32–38. https://doi.org/10.1016/j.ssi.2011.04.007

Wang L, Lu Y, Liu J, Xu M, Cheng J, Zhang D, Goodenough JB (2013) A superior low-cost cathode for a Na-Ion battery. Angew Chem Int Ed 52:1964–1967. https://doi.org/10.1002/anie.201206854

Wang B, Al Abdulla W, Wang D, Zhao XS (2015a) A three-dimensional porous LiFePO4 cathode material modified with a nitrogen-doped graphene aerogel for high-power lithium ion batteries. Energy Environ Sci 8:869–875. https://doi.org/10.1039/C4EE03825H

Wang X, Kurono R, Nishimura S-i, Okubo M, Yamada A (2015b) Iron–oxalato framework with one-dimensional open channels for electrochemical sodium-ion intercalation. Chem Eur J 21:1096–1101. https://doi.org/10.1002/chem.201404929

Wang F, Wu X, Li C, Zhu Y, Fu L, Wu Y, Liu X (2016) Nanostructured positive electrode materials for post-lithium ion batteries. Energy Environ Sci 9:3570–3611. https://doi.org/10.1039/C6EE02070D

Wang C, Li S, Han Y, Lu Z (2017) Assembly of LiMnPO4 Nanoplates into microclusters as a high-performance cathode in lithium-ion batteries. ACS Appl Mater Interfaces 9:27618–27624. https://doi.org/10.1021/acsami.7b05868

Wei S, Mortemard de Boisse B, Oyama G, Nishimura S-i, Yamada A (2016) Synthesis and electrochemistry of Na2.5(Fe1−yMny)1.75(SO4)3 Solid solutions for Na-Ion batteries. ChemElectroChem 3:209–213. https://doi.org/10.1002/celc.201500455

Wi S et al (2017a) Synchrotron-based x-ray absorption spectroscopy for the electronic structure of LixMn0.8Fe0.2PO4 mesocrystal in Li+ batteries. Nano Energy 31:495–503. https://doi.org/10.1016/j.nanoen.2016.11.044

Wi S et al (2017b) Insights on the delithiation/lithiation reactions of LixMn0.8Fe0.2PO4 mesocrystals in Li+ batteries by in situ techniques. Nano Energy 39:371–379. https://doi.org/10.1016/j.nanoen.2017.07.016

Wood SM, Eames C, Kendrick E, Islam MS (2015) Sodium ion diffusion and voltage trends in phosphates Na4M3(PO4)2P2O7 (M = Fe, Mn, Co, Ni) for possible high-rate cathodes. J Phys Chem C 119:15935–15941. https://doi.org/10.1021/acs.jpcc.5b04648

Wu X, Zheng J, Gong Z, Yang Y (2011) Sol-gel synthesis and electrochemical properties of fluorophosphates Na2Fe1-xMnxPO4F/C (x = 0, 0.1, 0.3, 0.7, 1) composite as cathode materials for lithium ion battery. J Mater Chem 21:18630–18637. https://doi.org/10.1039/C1JM13578C

Wu X, Guo J, Wang D, Zhong G, McDonald MJ, Yang Y (2015) P2-type Na0.66Ni0.33–xZnxMn0.67O2 as new high-voltage cathode materials for sodium-ion batteries. J Power Sources 281:18–26. https://doi.org/10.1016/j.jpowsour.2014.12.083

Wu X, Zhong G, Yang Y (2016) Sol-gel synthesis of Na4Fe3(PO4)2(P2O7)/C nanocomposite for sodium ion batteries and new insights into microstructural evolution during sodium extraction. J Power Sources 327:666–674. https://doi.org/10.1016/j.jpowsour.2016.07.061

Xia Y, Zhou Y, Yoshio M (1997) Capacity fading on cycling of 4 V Li / LiMn2 O 4 Cells. J Electrochem Soc 144:2593–2600. https://doi.org/10.1149/1.1837870

Xia H, Lu L, Meng YS, Ceder G (2007) Phase transitions and high-voltage electrochemical behavior of LiCoO2 thin films grown by pulsed laser deposition. J Electrochem Soc 154:A337–A342. https://doi.org/10.1149/1.2509021

Xiao X, Wang L, Wang D, He X, Peng Q, Li Y (2009) Hydrothermal synthesis of orthorhombic LiMnO2 nanoparticles and LiMnO2 nanorods and comparison of their electrochemical performances. Nano Res 2:923–930. https://doi.org/10.1007/s12274-009-9094-8

Xiao J et al (2012) High-performance LiNi0.5Mn1.5O4 spinel controlled by Mn3+concentration and site disorder. Adv Mater 24:2109–2116. https://doi.org/10.1002/adma.201104767

Xu M et al (2017a) Tailoring anisotropic Li-Ion transport tunnels on orthogonally arranged Li-rich layered oxide nanoplates toward high-performance Li-Ion batteries. Nano Lett 17:1670–1677. https://doi.org/10.1021/acs.nanolett.6b04951

Xu X, Deng S, Wang H, Liu J, Yan H (2017b) Research progress in improving the cycling stability of high-voltage LiNi0.5Mn1.5O4 cathode in lithium-ion battery. Nano-Micro Lett 9:22. https://doi.org/10.1007/s40820-016-0123-3

Yabuuchi N, Yoshii K, Myung S-T, Nakai I, Komaba S (2011) Detailed studies of a high-capacity electrode material for rechargeable batteries, Li2MnO3−LiCo1/3Ni1/3Mn1/3O2. J Am Chem Soc 133:4404–4419. https://doi.org/10.1021/ja108588y

Yabuuchi N et al (2012a) P2-type Nax[Fe1/2Mn1/2]O2 made from earth-abundant elements for rechargeable Na batteries. Nat Mater 11:512–517 http://www.nature.com/nmat/journal/v11/n6/abs/nmat3309.html#supplementary-information

Yabuuchi N, Yoshida H, Komaba S (2012b) Crystal Structures and Electrode Performance of Alpha-NaFeO₂ for Rechargeable Sodium Batteries. Electrochemistry 80:716–719. https://doi.org/10.5796/electrochemistry.80.716

Yabuuchi N, Hara R, Kubota K, Paulsen J, Kumakura S, Komaba S (2014a) A new electrode material for rechargeable sodium batteries: P2-type Na2/3[Mg0.28Mn0.72]O2 with anomalously high reversible capacity. J Mater Chem A 2:16851–16855. https://doi.org/10.1039/C4TA04351K

Yabuuchi N, Kubota K, Dahbi M, Komaba S (2014b) Research development on sodium-ion batteries. Chem Rev 114:11636–11682. https://doi.org/10.1021/cr500192f

Yakubovich OV, Karimova OV, Mel'nikov OK (1997) The mixed anionic framework in the structure of Na2{MnF[PO4]}. Acta Crystallogr C 53:395–397. https://doi.org/10.1107/S0108270196014102

Yamada A, Kudo Y, Liu K-Y (2001) Reaction mechanism of the olivine-type Li x (Mn0.6Fe0.4) PO 4 (0 ⩽ x ⩽ 1). J Electrochem Soc 148:A747–A754. https://doi.org/10.1149/1.1375167

Yamada A, Iwane N, Harada Y, Nishimura S-i, Koyama Y, Tanaka I (2010) Lithium iron borates as high-capacity battery electrodes. Adv Mater 22:3583–3587. https://doi.org/10.1002/adma.201001039

Yan S-Y, Wang C-Y, Gu R-M, Li M-W (2015) Enhanced kinetic behaviors of LiMn0.5Fe0.5PO4/C cathode material by Fe substitution and carbon coating. J Solid State Electrochem 19:2943–2950. https://doi.org/10.1007/s10008-015-2905-9

Yang J, Han X, Zhang X, Cheng F, Chen J (2013) Spinel LiNi0.5Mn1.5O4 cathode for rechargeable lithiumion batteries: nano vs micro, ordered phase (P4332) vs disordered phase (Fd $\bar 3$ m). Nano Res. https://doi.org/10.1007/s12274-013-0343-5

Yang D, Xu J, Liao X-Z, Wang H, He Y-S, Ma Z-F (2015a) Prussian blue without coordinated water as a superior cathode for sodium-ion batteries. Chem Commun 51:8181–8184. https://doi.org/10.1039/C5CC01180A

Yang J, Hu L, Zheng J, He D, Tian L, Mu S, Pan F (2015b) Li2FeSiO4 nanorods bonded with graphene for high performance batteries. J Mater Chem A 3:9601–9608. https://doi.org/10.1039/C5TA01529D

Yang W et al (2015c) LiMn0.8Fe0.2PO4/C cathode material synthesized via co-precipitation method with superior high-rate and low-temperature performances for lithium-ion batteries. J Power Sources 275:785–791. https://doi.org/10.1016/j.jpowsour.2014.11.063

Yang J et al (2016) Tuning structural stability and lithium-storage properties by d-orbital hybridization substitution in full tetrahedron Li2FeSiO4 nanocrystal. Nano Energy 20:117–125. https://doi.org/10.1016/j.nanoen.2015.12.004

Yao W, Sougrati M-T, Hoang K, Hui J, Lightfoot P, Armstrong AR (2017a) Na2Fe(C2O4)F2: a new iron-based polyoxyanion cathode for Li/Na ion batteries. Chem Mater 29:2167–2172. https://doi.org/10.1021/acs.chemmater.6b04859

Yao W, Sougrati M-T, Hoang K, Hui J, Lightfoot P, Armstrong AR (2017b) Reinvestigation of Na2Fe2(C2O4)3·2H2O: an iron-based positive electrode for secondary batteries. Chem Mater 29:9095–9101. https://doi.org/10.1021/acs.chemmater.7b02764

Ye DL, Ozawa K, Wang B, Hulicova-Jurcakova D, Zou J, Sun CH, Wang LZ (2014a) Capacity-controllable Li-rich cathode materials for lithium-ion batteries. Nano Energy 6:92–102. https://doi.org/10.1016/j.nanoen.2014.03.013

Ye DL et al (2014b) Understanding the stepwise capacity increase of high energy low-Co Li-rich cathode materials for lithium ion batteries. J Mater Chem A 2:18767–18774. https://doi.org/10.1039/c4ta03692a

Ye D, Zeng G, Nogita K, Ozawa K, Hankel M, Searles DJ, Wang L (2015a) Understanding the origin of Li2MnO3 activation in Li-rich cathode materials for lithium-ion batteries. Adv Funct Mater 25:7488–7496. https://doi.org/10.1002/adfm.201503276

Ye DL, Sun CH, Chen Y, Ozawa K, Hulicova-Jurcakova D, Zou J, Wang LZ (2015b) Ni-induced stepwise capacity increase in Ni-poor Li-rich cathode materials for high performance lithium ion batteries. Nano Res 8:808–820. https://doi.org/10.1007/s12274-014-0563-3

Yi T-F, Xie Y, Ye M-F, Jiang L-J, Zhu R-S, Zhu Y-R (2011) Recent developments in the doping of LiNi0.5Mn1.5O4 cathode material for 5 V lithium-ion batteries. Ionics 17:383–389. https://doi.org/10.1007/s11581-011-0550-6

Yi T-F, Mei J, Zhu Y-R (2016) Key strategies for enhancing the cycling stability and rate capacity of LiNi0.5Mn1.5O4 as high-voltage cathode materials for high power lithium-ion batteries. J Power Sources 316:85–105. https://doi.org/10.1016/j.jpowsour.2016.03.070

Yoo H, Jo M, Jin B-S, Kim H-S, Cho J (2011) Flexible morphology design of 3D-macroporous LiMnPO4 cathode materials for Li secondary batteries: ball to flake. Adv Energy Mater 1:347–351. https://doi.org/10.1002/aenm.201000049

You Y, Wu X-L, Yin Y-X, Guo Y-G (2014) High-quality Prussian blue crystals as superior cathode materials for room-temperature sodium-ion batteries. Energ Environ Sci 7:1643–1647. https://doi.org/10.1039/C3EE44004D

Yu H, Ishikawa R, So Y-G, Shibata N, Kudo T, Zhou H, Ikuhara Y (2013) Direct atomic-resolution observation of two phases in the Li1.2Mn0.567Ni0.166Co0.067O2 cathode material for lithium-ion batteries. Angew Chem Int Ed 52:5969–5973. https://doi.org/10.1002/anie.201301236

Yu T, Lin B, Li Q, Wang X, Qu W, Zhang S, Deng C (2016) First exploration of freestanding and flexible Na2+2xFe2-x(SO4)3@porous carbon nanofiber hybrid films with superior sodium intercalation for sodium ion batteries. PCCP 18:26933–26941. https://doi.org/10.1039/C6CP04958C

Zaghib K, Trottier J, Hovington P, Brochu F, Guerfi A, Mauger A, Julien CM (2011) Characterization of Na-based phosphate as electrode materials for electrochemical cells. J Power Sources 196:9612–9617. https://doi.org/10.1016/j.jpowsour.2011.06.061

Zhang L, Wu HB, Madhavi S, Hng HH, Lou XW (2012) Formation of Fe2O3 microboxes with hierarchical shell structures from metal–organic frameworks and their lithium storage properties. J Am Chem Soc 134:17388–17391. https://doi.org/10.1021/ja307475c

Zhang X, Cheng F, Yang J, Chen J (2013a) LiNi0.5Mn1.5O4 porous nanorods as high-rate and long-life cathodes for Li-ion batteries. Nano Lett 13:2822–2825. https://doi.org/10.1021/nl401072x

Zhang X, Cheng F, Yang J, Chen J (2013b) LiNi(0.5)Mn(1.5)O4 porous nanorods as high-rate and long-life cathodes for Li-ion batteries. Nano Lett 13:2822–2825. https://doi.org/10.1021/nl401072x

Zhang K, Han X, Hu Z, Zhang X, Tao Z, Chen J (2015a) Nanostructured Mn-based oxides for electrochemical energy storage and conversion. Chem Soc Rev 44:699–728. https://doi.org/10.1039/C4CS00218K

Zhang L, Ni J, Wang W, Guo J, Li L (2015b) 3D porous hierarchical Li2FeSiO4/C for rechargeable lithium batteries. J Mater Chem A 3:11782–11786. https://doi.org/10.1039/C5TA02433A

Zhang Z et al (2017) First-principles computational studies on layered Na2Mn3O7 as a high-rate cathode material for sodium ion batteries. J Mater Chem A 5:12752–12756. https://doi.org/10.1039/C7TA02609A

Zhao J, Zhao L, Dimov N, Okada S, Nishida T (2013) Electrochemical and thermal properties of α-NaFeO2 cathode for Na-ion batteries. J Electrochem Soc 160:A3077–A3081. https://doi.org/10.1149/2.007305jes

Zhao Y, Peng L, Liu B, Yu G (2014) Single-crystalline LiFePO4 nanosheets for high-rate Li-Ion batteries. Nano Lett 14:2849–2853. https://doi.org/10.1021/nl5008568

Zheng J et al (2017) Li- and Mn-Rich Cathode Materials: Challenges to Commercialization. Adv Energy Mater 7:1601284. https://doi.org/10.1002/aenm.201601284

Zhong QM, Bonakdarpour A, Zhang MJ, Gao Y, Dahn JR (1997) Synthesis and electrochemistry of LiNixMn2-xO4. J Electrochem Soc 144:205–213. https://doi.org/10.1149/1.1837386

Zhou F, Kang K, Maxisch T, Ceder G, Morgan D (2004) The electronic structure and band gap of LiFePO4 and LiMnPO4. Solid State Commun 132:181–186. https://doi.org/10.1016/j.ssc.2004.07.055

Zhou L, Zhao D, Lou X (2012) LiNi0.5Mn1.5O4 hollow structures as high-performance cathodes for lithium-ion batteries. Angew Chem Int Ed 51:239–241. https://doi.org/10.1002/anie.201106998

Zhou L et al (2017) Recent Developments on and prospects for electrode materials with hierarchical structures for lithium-

ion batteries. Adv Energy Mater 8(6):1701415. https://doi.org/10.1002/aenm.201701415

Zhu Y, Xu Y, Liu Y, Luo C, Wang C (2013) Comparison of electrochemical performances of olivine NaFePO4 in sodium-ion batteries and olivine LiFePO4 in lithium-ion batteries. Nanoscale 5:780–787. https://doi.org/10.1039/C2NR32758A

Zhu X, Li X, Zhu Y, Jin S, Wang Y, Qian Y (2014a) LiNi0.5Mn1.5O4 nanostructures with two-phase intergrowth as enhanced cathodes for lithium-ion batteries. Electrochim Acta 121:253–257. https://doi.org/10.1016/j.electacta.2013.12.176

Zhu X, Li X, Zhu Y, Jin S, Wang Y, Qian Y (2014b) Porous LiNi0.5Mn1.5O4 microspheres with different pore conditions: preparation and application as cathode materials for lithium-ion batteries. J Power Sources 261:93–100. https://doi.org/10.1016/j.jpowsour.2014.03.047